Chapter 4

Polar Stratospheric Ozone: Past, Present, and Future

Lead Authors
U. Langematz
M. Tully

Coauthors
N. Calvo
M. Dameris
A.T.J. de Laat
A. Klekociuk
R. Müller
P. Young

Contributors
S. Alexander
S. Dhomse
B. Funke
J.-U. Grooß
S. Kremser
G.L. Manney
S. Molleker
E. Nash
M.C. Pitts
A. Saiz-Lopez
F. Schmidt
M. Sinnhuber
R. Spang
I. Tritscher
P. von der Gathen
M. Weber

Review Editors
W. Randel
S. Solomon

Cover photo: An ozonesonde launch on a small balloon from Davis Station in Antarctica. Ozonesondes provide high-resolution measurements of the vertical profile of ozone concentrations in the atmosphere. Long-term monitoring, conducted at a small number of stations in the Arctic and Antarctic as part of the WMO Global Atmosphere Watch Programme, provides essential data for understanding the processes that affect polar ozone and ozone changes over time. Photo: Courtesy of V. Heinrich, Bureau of Meteorology, Australia

Chapter 4

Polar Stratospheric Ozone: Past, Present, and Future

CONTENTS

Chapter 4

Update on Polar Ozone: Past, Present, and Future

SCIENTIFIC SUMMARY

The chemical and dynamical processes controlling polar ozone are well understood. Polar ozone depletion is fundamentally driven by anthropogenic chlorine and bromine, with the severity of the chemical loss each year in both hemispheres strongly modulated by meteorological conditions (temperatures and winds), and, to a lesser extent, by the stratospheric aerosol loading and the solar cycle. As noted in prior Assessments, the stratospheric halogen concentration resulting from the emission of ozone-depleting substances (ODSs) reached its peak in the polar regions around the turn of the century and has been gradually declining since then in response to actions taken under the Montreal Protocol and its Amendments and adjustments. Early signs of ozone recovery are now beginning to appear in the Antarctic; as the observational record lengthens, clearer ozone hole recovery trends are expected to emerge against the background of natural variability. Nevertheless, the Antarctic ozone hole will continue to be a recurring phenomenon until the middle of the century. The Arctic is more dynamically variable, precluding identification of a significant increase in Arctic ozone, and cold conditions conducive to substantial ozone loss may still occur in a particular year in the coming decades. New chemistry–climate model (CCM) projections largely confirm previous studies that in both hemispheres, spring polar total column ozone will return to 1980 historical levels in the coming decades, albeit with a delay of a few years due to updated future ODS and greenhouse gas (GHG) emissions scenarios.

OBSERVED CHANGES IN POLAR OZONE

- **The characteristics of the October Antarctic ozone hole in the years since 2014 have generally been within the range observed since the early 1990s.** In 2015, however, the ozone hole was particularly large and long-lasting, as a result of a cold and undisturbed polar stratospheric vortex. Aerosols from the Calbuco volcanic eruption in April 2015 are also believed to have contributed to the large ozone hole observed that year. Conversely, in 2017, the Antarctic ozone hole was very small due to a warm and unusually disturbed polar vortex.

- **Several lines of evidence have started to emerge indicating an increase in Antarctic stratospheric ozone during September.** Statistically significant trends since the year 2000 have now been identified showing an increase in observed ozone and a decrease in ozone hole size and depth. Although accounting for the large degree of natural variability is challenging, the weight of evidence from statistical analyses and modeling studies suggests that the decline in ODSs made a substantial contribution to these trends.

- **In the Arctic, the exceptionally low ozone abundances of spring 2011 have not been observed again in the last four years.** Arctic stratospheric springtime ozone is dominated by large year-to-year dynamically induced variability of the polar vortex, with severe ozone loss occurring in very cold years, such as 2011. Extreme meteorological conditions in the early 2015/2016 winter led to rapid ozone loss, but a sudden stratospheric warming (SSW) at the beginning of March 2016 curtailed the chemical processes which lead to ozone destruction about a month earlier than in 2011, keeping ozone above record low levels. Arctic ozone trends are small compared to the dynamical variability, and thus a recovery trend remains undetectable in observations over the 2000–2016 period.

UNDERSTANDING OF FACTORS CONTROLLING POLAR OZONE

- **Observations in the Arctic winter have demonstrated that large nitric acid trihydrate (NAT) particles are a regularly occurring phenomenon in the lower stratosphere.** This knowledge improves our understanding of polar stratospheric cloud (PSC) formation and denitrification, which is important for catalytic ozone loss cycles.

- **Bromine-containing very short-lived substances (VSLSs) of natural origin have an important impact on the stratospheric halogen loading and consequently on stratospheric ozone loss in the polar regions.** The inclusion of additional stratospheric bromine from VSLSs is necessary for models to produce a realistic simulation of polar ozone loss.

- **The effects of tropospheric dynamical forcing in winter on Arctic polar ozone are now better quantified.** Ozone depletion in northern winters with SSWs is on average two-thirds less than in winters without SSWs, with depletion ending about one month earlier in the year. Such an SSW was a major influence on ozone levels observed in the Arctic winter of 2015/16.

- **Polar ozone in the middle and upper stratosphere varies by 10–15% from year to year due to energetic particle precipitation (EPP) related to solar variability.** Satellite observations and model results show that NO_y produced in the aurora is transported from the thermosphere down into the stratosphere in each winter, leading to stratospheric ozone decreases modulated by geomagnetic activity. The resulting variation in total column ozone is small (a few percent) but can persist for 2–3 years. Full EPP-effects were not included in current assessment models.

- **Model simulations show that the Montreal Protocol and its Amendments and adjustments have already brought about substantial ozone benefits.** In the polar regions of both hemispheres, much larger ozone depletion than currently observed has been avoided through implementation of the Protocol.

FUTURE EVOLUTION OF POLAR OZONE

- **Updated CCM projections based on full compliance with the Montreal Protocol and assuming the baseline estimate of the future evolution of GHGs (RCP-6.0) have confirmed that the Antarctic ozone hole is expected to gradually close, with springtime total column ozone returning to 1980 values shortly after mid-century (about 2060).** The timing of the recovery of the ozone hole will not be significantly affected by increases in GHG concentrations. There are no substantial differences between Antarctic total ozone columns at the end of this century for the various GHG scenarios (Representative Concentration Pathways [RCPs]).

- **The timing of the recovery of Arctic total ozone in spring will be affected by anthropogenic climate change. Based on full compliance with the Montreal Protocol and assuming the baseline estimate of the future evolution of GHGs (RCP-6.0), Arctic springtime total ozone is expected to return to 1980 values before mid-century (2030s).** New model simulations confirm that in the Arctic, enhanced GHG concentrations cause an earlier return of total column ozone to historical values than a reduction of ODSs alone.

- **In the second half of the 21st century CO_2, CH_4, and N_2O will be the dominant drivers of Arctic ozone changes, assuming full compliance with the Montreal Protocol.** These gases impact both chemical cycles and the stratospheric overturning circulation, with a larger response in stratospheric ozone associated with stronger climate forcing. By 2100, the stratospheric ozone column is expected to not only recover but to exceed 1960–1980 average values in the Arctic, with springtime Arctic ozone being higher by about 35 DU for RCP-4.5 and about 50 DU for RCP-8.5.

- **In the coming decades, substantial Arctic ozone loss will remain possible in cold winters as long as ODS concentrations are well above natural levels.** Increasing GHG concentrations may cool the lower stratosphere and lead to enhanced formation of polar stratospheric clouds (PSCs) early in the Arctic winter. However, one recent study indicates that no corresponding cooling is expected in March, which is the month when persistent low temperatures lead to large chemical ozone losses.

Chapter 4

Polar Stratospheric Ozone: Past, Present, and Future

4.1 INTRODUCTION

This chapter builds on the long sequence of chapters in most of the previous Assessments that have specifically considered stratospheric ozone in the polar regions of the earth. This history reflects the large scientific effort that has been dedicated to observing and understanding polar ozone changes, as well as the great long-standing interest in polar ozone among policymakers and the general public.

4.1.1 Summary of Findings from the Previous Ozone Assessment

WMO (2014) reported that the Antarctic ozone hole had continued to appear each spring, with year-to-year changes in the depth and area of the hole predominantly controlled by temperature variations, given the slow rate of decrease of equivalent effective stratospheric chlorine (EESC; see **Chapter 1**) expected in Antarctica since its peak value around the year 2000. Somewhat reduced ozone depletion was observed in the years 2010, 2012, and 2013, but not in 2011. These observations of less severe ozone depletion were broadly consistent with the anticipated effects of the declining levels of ozone-depleting substances (ODSs) due to the Montreal Protocol and its Amendments and adjustments. However, a definitive conclusion that the observed changes were due to EESC decline could not yet be reached. Nonetheless, WMO (2014) stated that an estimate of the increase of springtime Antarctic total ozone of 10 to 25 Dobson Units (DU) could be made over the years 2000 to 2010 by attempting to remove the effects of natural variability.

In the Arctic, exceptionally low ozone concentrations were observed in the winter and spring of 2010/2011 between 15 and 23 km, but importantly, WMO (2014) reported that chemistry transport models (CTMs) were able to successfully reproduce the measured depletion, given the observed meteorological conditions. This was seen as providing confidence that the understanding of Arctic ozone depletion processes was largely correct.

Continued observations from satellites and aircraft campaigns had further refined knowledge of PSC formation and polar chemical processes. Although several important scientific questions had not been resolved, these uncertainties did not hinder the successful simulation of polar ozone destruction, which is ultimately driven by temperatures falling below threshold values for the activation of chlorine. Previous issues surrounding conflicting values of the ClOOCl absorption cross-section were considered by WMO (2014) to be resolved, with more recent observational studies and laboratory investigations confirming the role of the catalytic ozone destruction cycle initiated by the ClO+ClO reaction, with a significant contribution also from the cycle initiated by BrO+ClO.

Additionally, WMO (2014) stated the apparent trend towards Arctic cold winters becoming colder, as expressed through the V_{PSC} diagnostic, had become less certain, as subsequent research found statistically weaker results.

While WMO (2011) made extensive use of model results from the SPARC Chemistry-Climate Model Validation-2 (CCMVal-2) initiative, no such large suite of results was available for WMO (2014). However, it was reported that no work subsequent to CCMVal-2 had significantly challenged the previous findings pointing to an earlier recovery of ozone to 1980 levels in the Arctic than the Antarctic (2030 and 2050, respectively), with future levels of Arctic ozone also showing a greater sensitivity to the greenhouse gas (GHG) scenario used in model projections.

4.1.2 Scope of Chapter

This chapter updates the state of our knowledge about stratospheric ozone in the polar regions of both hemispheres, taking advantage of systematic observational programs and special measurement campaigns, laboratory studies, and a wide array of computer

modeling. The long-term record of meteorological conditions and ozone depletion in the polar vortex of both hemispheres is presented, updated for the years following the last Assessment. The particular winter–spring seasons of 2015 and 2017 in the Antarctic and 2015/2016 in the Arctic are considered in more detail. Progress in the understanding of the many chemical and physical processes underlying and influencing polar ozone depletion is then reported. Recent studies seeking to identify a statistically significant trend due to declining anthropogenic halogen levels (known as the second stage of Antarctic ozone recovery as set out in WMO (2007)) are discussed, before the chapter concludes with the presentation of results from the SPARC/IGAC Chemistry-Climate Model Initiative (CCMI) and the latest projections of polar ozone over the coming decades.

4.2 RECENT POLAR OZONE CHANGES

4.2.1 Measurements of Ozone and Related Constituents

Scientific study of polar ozone is made possible by the continuation of long-term measurements of ozone made by ground-based, balloon, aircraft, and satellite instruments, supplemented by measurements of related chemical constituents and meteorological parameters. In general, these measurement programs have largely been maintained since WMO (2014).

Long-standing ground-based and balloon measurements of both total column and vertically resolved ozone have continued under the WMO Global Atmosphere Watch and its contributing network NDACC (Network for the Detection of Atmospheric Composition Change). Observational data from these networks are freely available from the World Ozone and Ultraviolet Radiation Data Centre (www.woudc.org). A summary of available satellite measurements relevant to polar ozone was provided in Table 3A-1 of WMO (2014). Many satellite missions launched in the early 2000s have continued to collect data well beyond their expected lifetimes. A number of specific measurement campaigns have also been conducted in addition to long-term monitoring programs. The understanding that these missions and campaigns have contributed to will be discussed in **Section 4.3**.

It is also important to note the contribution of recent work that has combined observational ozone data from different instruments into single homogeneous long-term data sets (**Sections 4.2.3, 4.2.4,** and **4.4**) and the extra insight and usefulness obtained by assimilating meteorological observations and producing reanalysis products (discussed more fully in **Section 4.2.2**).

4.2.2 Evolution of Polar Temperatures and Vortex Characteristics

4.2.2.1 Temperatures and PSC Volume

Polar ozone depletion is highly dependent on stratospheric temperature, as this acts as a strong control on the potential for polar stratospheric cloud (PSC) formation and thus the rate of heterogeneous reactions. **Figure 4-1** shows the annual climatological cycle (1979–2017) of 50 hPa polar minimum temperature for both the Arctic and Antarctic, with four recent years highlighted.

As is well established, winter and spring temperatures show a far higher degree of interannual variability over the Arctic than over Antarctica, indicative of the large year-to-year variability in dynamics and the more frequent disturbances to the Arctic vortex in the form of sudden stratospheric warmings (SSWs) (Labitzke and van Loon, 1999). Since the last Assessment (WMO, 2014), Arctic minimum temperatures have been in the 10–90% envelope about the climatological mean, except for winter/spring of 2015/2016. This period was characterized by December and January minimum temperatures that were close to, or at, the lowest minimum values for the whole period, with a strong and undisturbed vortex (Manney and Lawrence, 2016; Matthias et al., 2016). However, a major final SSW occurred on 5–6 March 2016 and the vortex broke up in early April (Manney and Lawrence, 2016). After the SSW, the polar minimum temperatures were then near, or at, their highest for the 1979–2017 period. The effects of these conditions on Arctic ozone levels will be further discussed in **Section 4.2.4.1**.

The less dynamically disturbed Antarctic vortex shows much lower interannual temperature variability. Recent winter/spring temperatures over Antarctica have typically been within 30–70% of the long-term climatological mean, with the exception of the 2015 spring where they were close to, or at, the lowest

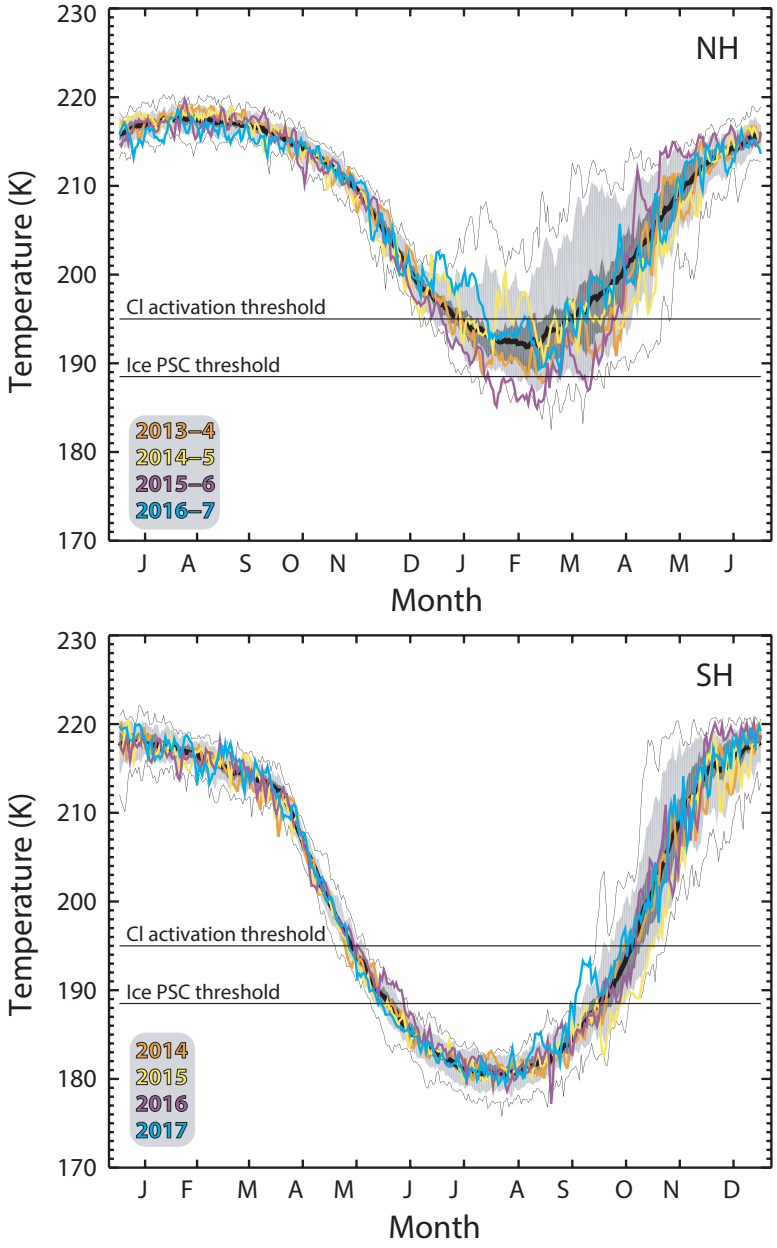

Figure 4-1. Annual cycle and variability at 50 hPa (~20 km) of minimum temperature for the Northern Hemisphere (50°N–90°N, *top*) and the Southern Hemisphere (50°S–90°S, *bottom*) from ERA-Interim reanalysis data (Dee et al., 2011). The thick black line shows the climatological mean annual cycle, with the dark and light gray shaded areas to indicate the 30–70% and 10–90% probabilities, respectively; the thin gray lines indicate the record maximum and minimum values for the period; and the colored lines show the annual cycle of temperatures for recent years. The data cover the periods 1978/1979 to 2016/2017 for the Northern Hemisphere and 1979–2017 for the Southern Hemisphere. Also indicated are the threshold temperatures for chlorine activation and ice PSC formation. Updated from Figure 3-1 in WMO (2014).

minimum temperatures during October and early November, and 2017, when they were above the previous maximum during September. The effects on ozone of the 2015 low temperature in combination with the volcanic eruption of Calbuco in southern Chile are discussed in **Section 4.2.3.1**.

A vortex-wide and season-long picture of the potential for ozone depletion in a winter/spring period is given by a measure of the time-integrated volume of air within the vortex, between the 400 K and 700 K isentropic surfaces, where heterogeneous ozone loss can occur. This metric, hereafter integrated V_{PSC}, is defined using height-resolved temperature data from radiosondes or reanalyses, together with a standard, non-denitrified profile of nitric acid, in order to estimate the temperature threshold for existence of nitric acid trihydrate (NAT) PSCs (Rex et al., 2002). (Due to the use of a non-denitrified nitric acid profile, this does not strictly define threshold temperatures for NAT existence, but rather is a proxy for low temperatures.)

Figure 4-2 shows the long-term evolution of Arctic integrated V_{PSC}, updating the similar figure from WMO (2014), which used V_{PSC}, rather than integrated V_{PSC}. The addition of the time integration emphasizes the importance of duration of the low temperatures (see

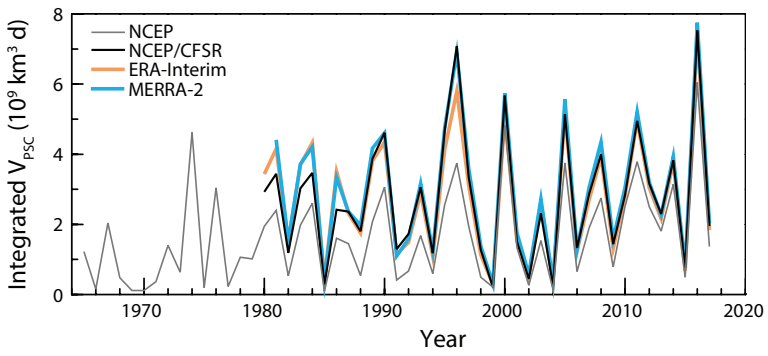

Figure 4-2. Time-integrated Arctic V_{PSC}, integrated by day (d) from 1 November to 30 April for each winter/spring, on isentropic surfaces from 400 to 700 K. Results are shown for different meteorological reanalyses: NCEP (Kalnay et al., 1996), NCEP/CFSR (Saha et al., 2010), MERRA-2 (Gelaro et al., 2017), and ERA-Interim (Dee et al., 2011). The figure is an update from WMO (2014) with the refinement of time integrating V_{PSC} and the addition of new reanalysis products. The V_{PSC} metric is calculated based on the method described by Rex et al. (2006) and estimates the volume within the vortex in which the temperature is low enough for NAT PSCs to exist, based on a standardized non-denitrified nitric acid profile.

also Strahan et al., 2016). The figure shows integrated V_{PSC} calculated from several reanalysis products to provide an idea about structural uncertainty arising from the different reanalysis systems. The three more recent reanalyses (NCEP/CFSR, ERA-Interim, and MERRA-2) are in closer agreement with each other than they are with the earlier NCEP reanalysis (see the figure caption for references). NCEP is shown for comparison with earlier reports but is no longer recommended for stratospheric analyses due to the availability of more recent reanalyses that have been shown to be more suitable (Lawrence et al., 2015; Long et al., 2017).

Apparent from **Figure 4-2** is the large integrated V_{PSC} value for the 2015/2016 winter/spring, driven by the particularly cold December and January in 2015/2016 (Manney and Lawrence, 2016). It exceeds the corresponding value associated with the stronger Arctic ozone depletion of 2011, even though March total ozone values were not anomalously low (**Figure 4-4**). This suggests an instance where the integrated V_{PSC} metric alone is insufficient as an ozone depletion proxy. Arctic ozone depletion in the winter and spring of 2015/2016 is discussed in **Section 4.2.4.1**. In the last Assessment, the evidence for a significant climate change-driven trend towards larger V_{PSC} values occurring in the coldest winters (Rex et al., 2004; 2006) was challenged by studies using extreme value statistics (Rieder and Polvani, 2013) or sunlit vortex volumes (Pommereau et al., 2013). Since then, there have been no in-depth analyses of the V_{PSC} metric and despite the large (integrated) V_{PSC} value for 2015/2016, due to the large year-to-year variability no significant trend can be detected. More recent studies have explored the drivers of polar stratospheric trends using observations and model simulations; these are discussed in **Section 4.5.3**.

4.2.2.2 Polar Vortex Breakup Dates

Figure 4-3 shows the date at which the Arctic and Antarctic polar vortices breakup each spring, due to strong planetary wave breaking and the returning sun resulting in a warming of the polar stratosphere. As in **Figure 4-2**, the dates are calculated from a range of different reanalysis products, using wind data along the vortex edge (Nash et al., 1996). Similar to polar temperature variability, there is a higher degree of interannual variability of the vortex breakup date for the Arctic, compared to the Antarctic. As noted in the previous Assessment, this Arctic variability is greater since 2000 (average standard deviation across the reanalyses: 30.7 days) compared to the 1990s (average standard deviation: 18.8 days), although the amount depends on the reanalysis product. Breakup dates over Antarctica also show a degree of interannual variability, which is more marked after the first decade of the record shown, although again this varies between the reanalysis products. Overall, there is evidence of decadal variability in both hemispheres.

In general, there is better agreement between the different reanalyses for the Antarctic vortex breakup dates (average max–min range between the reanalyses of 5.6 days) than the Arctic (average max–min range of 16.7 days), with the Arctic having some years where the range between different reanalyses exceeds one month. Differences in the simulation of stratospheric

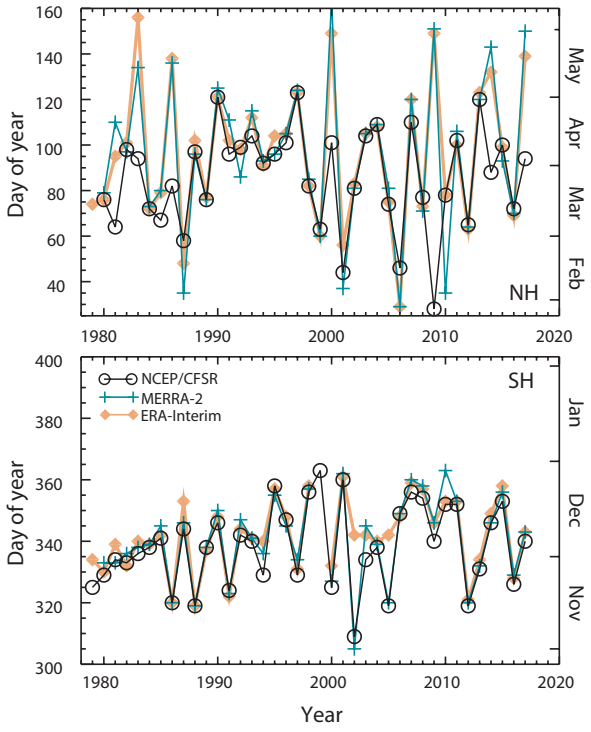

Figure 4-3. Breakup dates for the Arctic (*top*) and Antarctic (*bottom*) polar vortices, defined as when the wind speed on the 500 K isentropic surface falls below 15.2 m s^{-1}, as per Nash et al. (1996). Dates are determined using reanalysis data from NCEP/CFSR (Saha et al., 2010), MERRA-2 (Gelaro et al., 2017), and ERA-Interim (Dee et al., 2011). Note that the Nash et al. (1996) definition does not yield a breakup date in all reanalyses for certain years. Updated from Figure 3-2 of WMO (2014).

winds between the reanalysis products (e.g., Butler et al., 2017; Long et al., 2017) explain the differences between the lines in **Figure 4-3**. There are a range of definitions for breakup date, but no systematic comparison exists in the literature. Other definitions, such as a temperature-based metric (e.g., Haigh and Roscoe, 2009) or computer image analysis techniques (Lawrence and Manney, 2017) may yield better agreement between reanalyses.

4.2.3 Ozone Depletion in Antarctic Springs (2014–2017)

Figures 4-4 and **4-5**, updates to figures that have been used in previous Assessments, represent the evolution of polar ozone loss in both hemispheres. **Figure 4-4** shows mean polar cap (63°–90° latitude) total column ozone averaged for the months of March (for the Arctic) and October (for the Antarctic) compiled from various satellite datasets since 1970. For the Antarctic, generally reliable and well-sampled satellite measurements of total ozone have been available for October since 1979 from the TOMS/OMI/OMPS series of instruments, with some gaps in 1993 and 1995 where alternate instruments were used.

In **Figure 4-5**, rather than mean ozone, the minimum of the daily mean ozone is shown, and further, an attempt is made to confine the averaging region to within the polar vortex through use of a threshold for equivalent latitude on the 475 K isentrope (Müller et al., 2008).

In the Antarctic, both metrics share the general

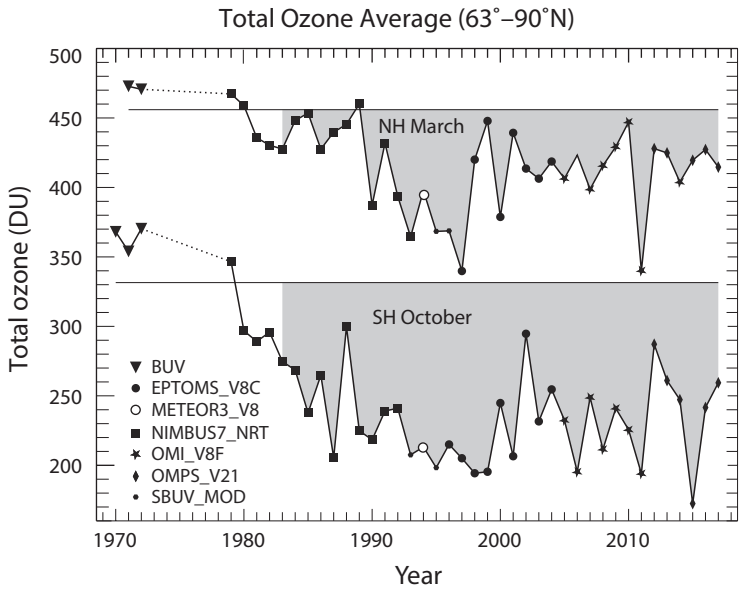

Figure 4-4. Total ozone average (Dobson units) over 63°–90° latitude in March (Northern Hemisphere, NH) and October (Southern Hemisphere, SH). Symbols indicate the satellite data that have been used in different years. The horizontal gray lines represent the average total ozone for the years prior to 1983 in March for the NH and in October for the SH. Updated from Figure 3-4, WMO (2014).

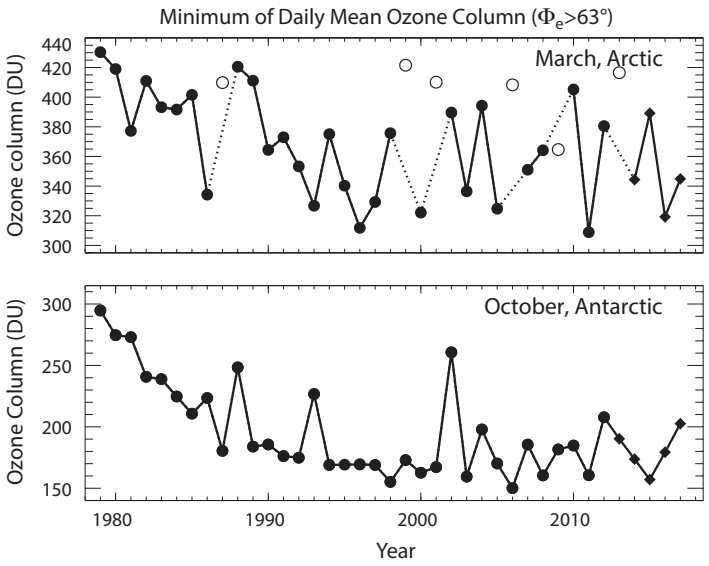

Figure 4-5. Time series of the minimum of the daily average column ozone (Dobson units) within the 63° contour of equivalent latitude (Φ_e) in (*top*) March in the Arctic and (*bottom*) October in the Antarctic. Arctic winters in which the polar vortex broke up before March (1987, 1999, 2001, 2006, 2009, and 2013) are shown by open symbols; dotted lines connect surrounding years. Adapted from WMO (2014), updated using the Bodeker Scientific combined total column ozone data base (version 3.0; circles; Müller et al., 2008) through March 2013 and Aura OMI measurements thereafter (diamonds).

features of a clear decline over the 1980s and 1990s, followed by a period without a clear trend but showing increased year-to-year variability, with the variability reduced in **Figure 4-5** relative to **Figure 4-4** due to the use of equivalent latitude. For 1988, 2002, and 2012, relatively high temperatures in the winter stratosphere limited the severity of ozone loss in the following spring (Klekociuk et al., 2015); in the case of 2002, an unprecedented major sudden stratospheric warming in September disrupted the polar vortex and allowed unusually strong transport of ozone-rich air into the polar cap (Newman and Nash, 2005; WMO, 2007).

Mean October ozone values for three of the last four years since the last Assessment—2014, 2016, and 2017—were all at the higher end of the range of values observed since the year 2000, as were the two preceding years 2012 and 2013. In contrast, the October mean value for 2015 was the lowest on record. The relative positions are similar for minimum daily vortex-averaged ozone **(Figure 4-5)**, although 2014 and 2016 are closer to the middle of the range, and the 2015 minimum is not as low as 2006, which is the record low value for this metric.

The evolution of Antarctic ozone has also been represented in previous Assessments by the time series of three standard metrics: area of the ozone hole, minimum ozone within the ozone hole and ozone hole mass deficit (**Figure 4-6**—refer to the caption for the specific definitions and time periods of the metrics shown). For ozone hole area, the last four years have varied within the general range observed since the early 1990s, with 2015 being among the largest recorded and 2017 the second smallest since the late 1980s. Ozone hole minimum is similar in **Figure 4-6** to the minimum vortex average shown in **Figure 4-5** but shows a greater general increase since 2000. Several years from the period 2000–2013 had lower ozone hole minimum values than all four years 2014–2017. Ozone hole mass deficit (OMD) shows the most evident change since 2000, with the 2017 value being the smallest since 1988. To illustrate the development of the Antarctic ozone hole over winter and spring in the four years, **Figure 4-7** shows the estimated daily ozone mass deficit for July to December in years 2014 to 2017 and also the extreme years of 2002 and 2006 for comparison. This metric is the difference in column ozone from 220 DU expressed as a mass integrated over the area of the ozone hole. A similar figure was last presented in WMO (2007). The onset of significant ozone depletion in the Antarctic normally occurs between the beginning and middle of August, when total column abundances usually begin to drop below the 220 DU threshold that was introduced by Stolarski et al. (1990) as a definition of the Antarctic ozone hole (see Uchino et al. (1999), Bodeker et al. (2005), and Huck et al. (2007) for additional definitions, and Pazmiño et al. (2018) for different thresholds). Ozone loss typically maximizes at the beginning of October after which ozone concentrations tend to increase through the remainder of

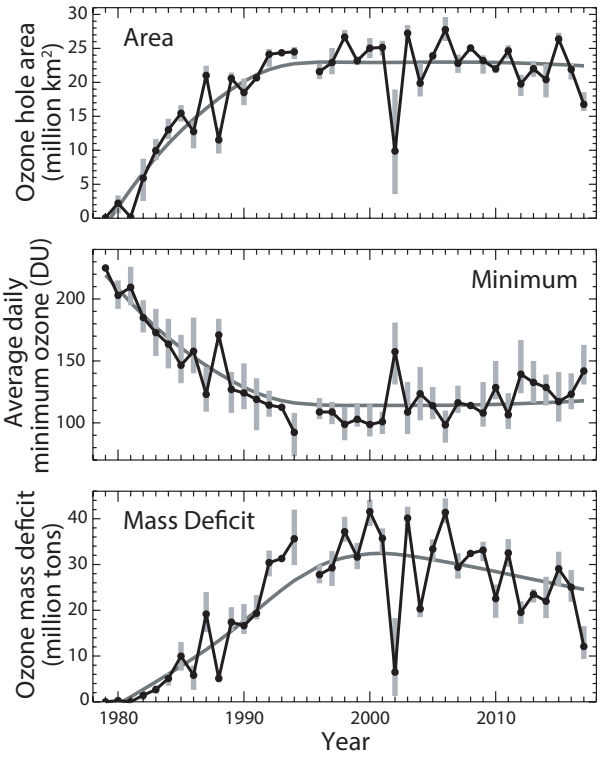

Figure 4-6. (*top*) Area of the Antarctic ozone hole for 1979–2017, averaged from daily total ozone area values contained by the 220 DU contour for 21–30 September. (*middle*) An average of daily minimum ozone values over Antarctica during the period from 21 September to 16 October. (*bottom*) Ozone mass deficit (OMD) averaged over the 21–30 September period. For all three panels, the vertical gray bars indicate the range of values over the same time period. The dark gray curves show the fits to each quantity as was shown in Newman et al. (2004) using EESC, as derived in Newman et al. (2006), updated with the current baseline A1 scenario. The EESC has a mean age of 5.5 years, an age spectrum width of 2.75 years, and a bromine-scaling factor of 65. The fit is quadratic in EESC. This figure was generated from TOMS (1979–2004), Aura OMI (2005–2015), and Suomi NPP OMPS (2016–2017) data. Updated from Figure 4-8 from WMO (2007).

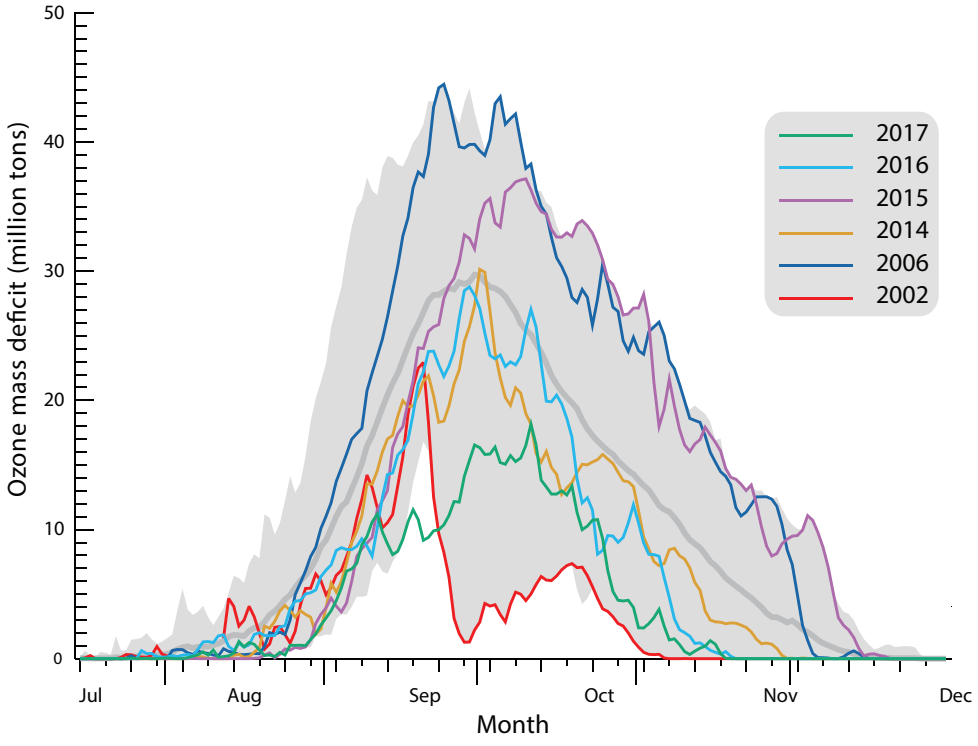

Figure 4-7. Daily ozone mass deficit over Antarctica for various years compared with the range of values over the period 1990–2016 (gray shaded area). The thick dark gray line shows daily values averaged over the 1990–2016 period. Values have been computed using data from TOMS, Aura OMI, and Suomi NPP OMPS. Updated from Figure 4-9 from WMO (2007).

the year, but do often show significant variability on timescales of days to weeks due to disturbance of the polar vortex by Rossby wave activity.

The growth and decline of daily ozone mass deficit in 2014 and 2016 were generally similar to each other, and took place over a somewhat contracted period relative to the long-term mean, with a 1-2 weeks slower development in early September and an earlier zero-crossing in November (**Figure 4-7**). In terms of the broad features of the daily time series of deficit and area, these specific ozone holes exhibited behavior similar to some years in the early 1990s, although their total ozone mass deficits were generally greater than pre-1990 levels (**Figure 4-6**; Newman et al., 2015; Weber et al., 2015; Newman et. al., 2017; Weber et al., 2017). In 2016, the latest date for which total column ozone values were below 220 DU was November 20 (**Figure 4-7**), which was the earliest such date for the period 2014-2017. This early elevation of levels above the 220 DU threshold was brought about by an episode of strong warming in the polar cap during late November of that year (**Figure 4-1**). Some evidence of a shift in the timing of the formation and growth of the ozone hole towards a later date since 2000 has also been presented (Solomon et al., 2016). The evolution of the ozone mass deficit in years 2015 and 2017, which were distinctly different to 2014 and 2016, are discussed in **Sections 4.2.3.1** and **4.2.3.2**, respectively.

4.2.3.1 Antarctic Spring 2015: Volcanic and Dynamical Influence on Ozone

In terms of total annual ozone mass deficit, the 2015 Antarctic ozone hole was the largest of the period 2014–2017 (**Figure 4-7**). The 2015 ozone hole was notable in achieving a large maximum area, being comparable to the largest values observed for 2003 and 2006 (**Figure 4-6**). Through much of the period from early October to mid-December, the Antarctic ozone hole of 2015 set records in daily area and mass deficit and had unusually low minimum column abundances (Nash et al., 2016; Weber et al., 2016). Additionally, its onset was approximately two weeks later than typical (Nash et al., 2016).

The large area of the 2015 Antarctic ozone hole was influenced in part by the chemical effects in the lowermost stratosphere (particularly around the 100–150 hPa pressure level) of aerosols that were entrained in the polar vortex from the eruption of the Calbuco volcano in southern Chile in April 2015 (Solomon et al., 2016; Ivy et al., 2017; Stone et al., 2017). Studies comparing ozone hole metrics with and without the inclusion of prescribed aerosol loading derived from observed volcanic SO_2 emissions found simulations with prescribed aerosols provide an ozone hole area that closely matches observations, and concluded that chemical ozone depletion enhanced by heterogeneous processes associated with the volcanic aerosols was the primary factor behind the ozone hole achieving record size. Dynamical and temperature feedbacks from the ozone loss were less important (Solomon et al., 2016; Ivy et al., 2017). Measurements by ozonesondes and the Aura MLS satellite instrument are consistent with the model results and indicate that the aerosol-influenced ozone loss was most significant in the lowermost stratosphere (Stone et al., 2017).

It should be noted that the contribution of volcanic aerosol particles took place in the setting of a notably cold and stable Antarctic vortex in 2015 (**Figures 4-1** and **4-12**). The level of disturbance to the Antarctic vortex was relatively low in the winter and spring. The eddy heat flux at 100 hPa was generally below the long-term average from July to October, and particularly in October, which favored the ozone hole having greater persistence than on average (Nash et al., 2016). Much of 2015 was marked by a positive value for the Southern Annular Mode index, which did not favor Rossby wave propagation to high (> 60°S) southern latitudes (Fogt, 2016).

4.2.3.2 Antarctic Spring 2017: Dynamical Influences on Ozone

Antarctic ozone loss in the spring of 2017 was unusually low and comparable in some metrics, particularly mass deficit, with that for 2002 (when the stratospheric vortex exhibited an unprecedented major warming as noted earlier) and most years prior to 1989. The small size of the ozone hole in terms of its maximum area and total mass deficit compared with other years can be seen in **Figure 4-6**. The rate of increase of ozone mass deficit in 2017 was notably below average throughout September (**Figure 4-7**), during the majority of which time stratospheric temperatures were the warmest in the 1979–2017 record (**Figure 4-1**). Unusually for the Southern Hemisphere, the ratio of September to March ozone from 50° to 90°S

was greater than one, consistent with the high value of poleward eddy heat flux integrated over winter (**Figure 4-12**).

4.2.4 Ozone Depletion in Arctic Springs (2014–2017)

The annual time series of polar cap mean and minimum ozone in March for the Arctic are shown in the upper panels of **Figures 4-4** and **4-5.** Some issues around the interpretation of these figures in the Arctic are discussed in Section 3.2.3 of WMO (2014). These averages have been used to assess the long-term behavior of Arctic stratospheric ozone as chemical depletion normally peaks in March, unless the polar vortex dissipates earlier. In the Arctic polar cap, ozone concentrations in the lower stratosphere are more strongly influenced by horizontal transport than in the Antarctic, owing to the relatively weak and disturbed nature of the northern polar vortex. The Arctic vortex is smaller and more spatially variable than the Antarctic vortex, and variability in the amount of ozone transported to the polar cap can complicate the interpretation of total column measurements. In spite of these limitations, which can be minimized by considering partial columns (e.g., Strahan et al., 2016), these metrics have been used to highlight years where ozone concentrations in the Arctic are notably low. However, as discussed in detail in WMO (2014), years of particularly low Arctic ozone in March, such as 1997 and 2011, can show distinctly different behavior in chemical ozone loss (which was strong in 2011 but only moderate in 1997) and dynamical influences (which reduced ozone levels in the latter part of the 1997 winter). More recently, chemical depletion of ozone has been shown to account for one-third of the difference from the pre-1983 mean (the gray shaded area in **Figure 4-4**) in most years, with the remainder being due to variations in dynamical resupply of ozone (Strahan et al., 2016; see also WMO, 2010 Figure 2-15).

As for the Antarctic, **Figures 4-4** and **4-5** display an evident negative trend in ozone in the 1980s which did not continue past the late 1990s. In terms of March mean ozone across the geographic polar cap **(Figure 4-4)**, the four years since the last Assessment have all been well within the range of typical values observed since 2000, with only small differences between each of the years and significantly above the value for 2011 which experienced very large ozone depletion. The differences between the four years are much larger in **Figure 4-5** however, with minimum ozone in March 2015 now at the higher end of the range of values since 1990 and March 2016 being one of the lowest values.

To consider the development of Arctic ozone in winter and spring over these four recent years, **Figure 4-8** shows time series of the daily average concentration of specific species relevant to ozone chemistry at a height of approximately 18 km—representative for the lower stratosphere within the Arctic polar vortex. The 2013/2014 Arctic vortex was large, cold (see also **Figure 4-1**), and relatively strong throughout the winter; temperatures near 18-km altitude were below chlorine activation thresholds until approximately mid-March. The observed decrease in ozone was slightly more than the average up until April 2014 (Bernhard et al., 2015). Over the period December 2014 to April 2015, ozone concentrations in the Arctic lower stratosphere near 18 km altitude were the highest in the Aura MLS record (which started in August 2004; **Figure 4-8**) (Manney et al., 2015b; Bernhard et al., 2016). A minor sudden stratospheric warming (SSW) event in early January 2015 (**Figure 4-1**) raised temperatures and limited further development of ozone-depleting chemistry within the polar vortex. Additionally, Aura MLS data showed evidence for above average transport of ozone-rich air into the polar cap through the upper branch of the Brewer-Dobson circulation (Manney et al., 2015b), which also elevated HNO_3 concentrations to levels in the lower stratosphere not previously observed in the Aura MLS record. The enhanced temperatures and transport were both the result of increased high-latitude wave activity (Manney et al., 2015b).

The early part of the 2016/2017 Arctic winter was unusually warm in the lower stratosphere with a weak vortex, although with a cold and strong vortex in the middle and upper stratosphere. Several minor SSWs occurred, with two of them near the threshold to be defined as "major" (according to definitions by Butler et al., 2015). Temperatures below chlorine activation thresholds in the lower stratosphere did not appear until late December. However, cold conditions were consistently present thereafter until early March, and significant chlorine activation and ozone loss were observed. As indicated by relatively high levels of HNO_3 in the lower stratosphere (top panel of **Figure**

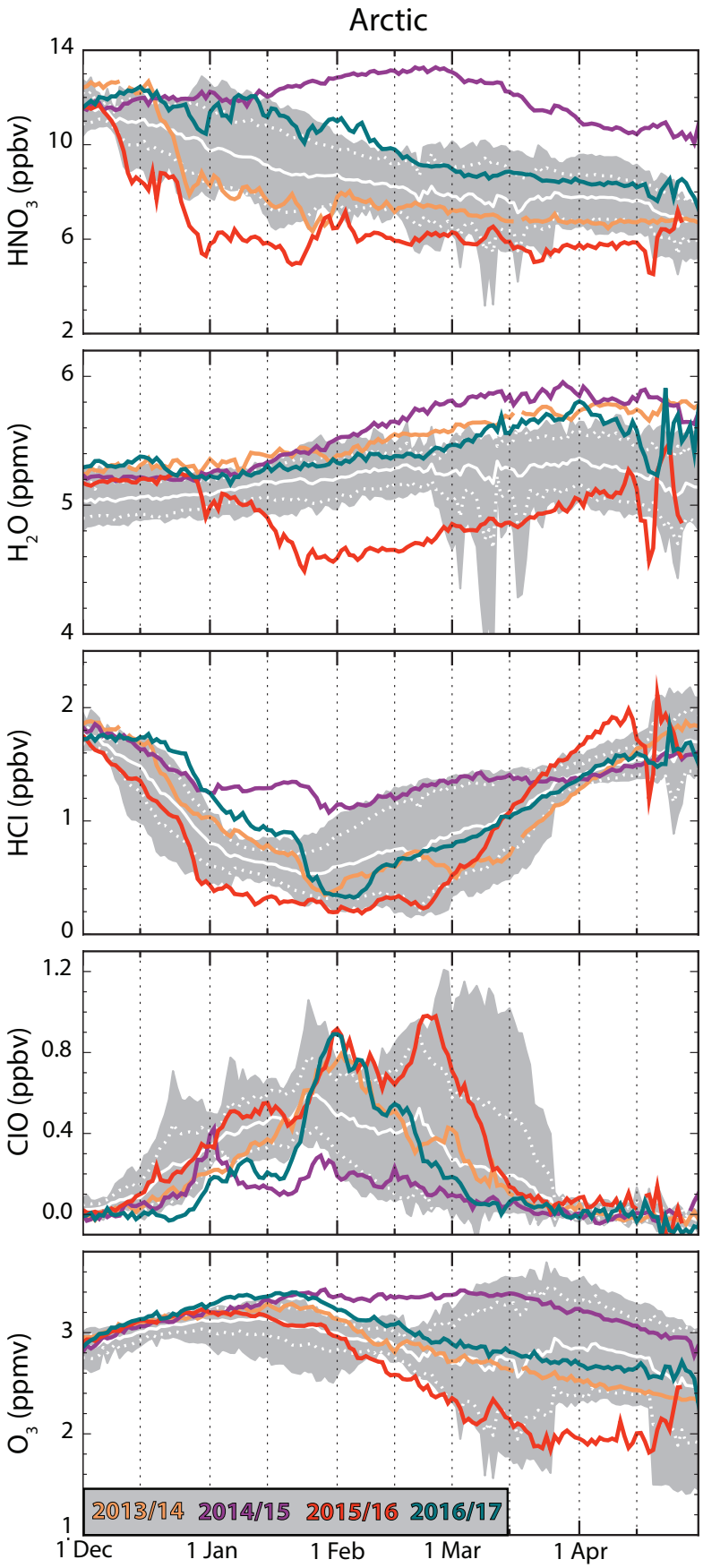

Figure 4-8. Time series of vortex-averaged HNO_3, H_2O, HCl, ClO, and O_3 from Aura Microwave Limb Sounder (MLS) on the 480 K potential temperature surface (~18 km, ~50 hPa) for winters and spring in the Arctic. Gray shading shows the envelope of behavior observed by Aura MLS over the 2005–2013 period. A data gap from 27 March to 18 April 2011 has produced a noticeable artefact in the envelope of some panels. The last four winters are highlighted by colored lines as indicated in the legend, for which the given year refers to January to April. Updated from Figure 3-6 from WMO (2014).

4-8), denitrification was not particularly pronounced within the vortex during 2016/2017.

4.2.4.1 Arctic Spring 2016: Record Ozone Depletion Halted by Major Warming

The 2015/2016 Arctic winter had significant potential for large ozone loss (Manney and Lawrence, 2016). Exceptionally low temperatures occurred throughout the period from December 2015 to February 2016, which were the lowest in the 68-year observational record (Matthias et al., 2016). Strong denitrification and dehydration occurred (Manney and Lawrence, 2016; **Figure 4-8**), which were associated with extensive PSC formation (Khosrawi et al., 2017; Bernhard et al., 2017). The low stratospheric temperatures, particularly in November and December of 2015, were linked with weak planetary wave-1 activity associated with the prevailing enhanced tropospheric meridional temperature gradient that appears to have increased the vertical wind shear at northern mid-latitudes and reduced the ability of the planetary waves to propagate upward (Matthias et al., 2016).

The cold conditions led to very strong chlorine activation within the polar vortex in 2015/2016 until the end of February. Levels of HCl at the 480 K surface in the vortex in January were the lowest in the Aura MLS record, below those of 2010/2011 when ozone loss was exceptional and levels of ClO were correspondingly high (**Figure 4-8**). The amount of ozone depletion was enhanced by the strong level of denitrification (Manney and Lawrence, 2016). However, the overall ozone loss in this season was halted by a major final SSW in early March, which terminated stratospheric chlorine activation approximately a month earlier than was the case for the 2010/2011 season (Bernhard et al., 2017). From this point on, ClO levels dropped rapidly (**Figure 4-8**). As a result of the warming, record Arctic ozone depletion that might have occurred with such high levels of chlorine activation earlier in the season, did not take place.

4.3 UNDERSTANDING OF POLAR OZONE PROCESSES

4.3.1 Polar Stratospheric Clouds

Polar stratospheric clouds (PSCs) and cold sulfate aerosols impact polar ozone and chlorine chemistry by converting chlorine from inactive reservoir species (mainly hydrochloric acid (HCl) and chlorine nitrate ($ClONO_2$)) to active ozone-destroying species. Furthermore, PSCs can both temporarily sequester HNO_3 from the gas phase (substantially reducing gas-phase concentrations of HNO_3 as long as the PSCs exist) and irreversibly redistribute HNO_3 by gravitational sedimentation of large nitric acid trihydrate (NAT) particles (referred to as "denitrification"; WMO (2014), Box 3-1). These impacts on polar ozone and chlorine chemistry are now considered to be well understood. However, many aspects of the microphysics of PSCs and their formation still remain unclear, such as the nucleation mechanism for NAT particles (in particular, large NAT particles), the impact of rapid cooling rates (gravity waves), and the origin and nature of refractory (that is, non-volatile) particles in the polar vortex. As well, the substantial uncertainties in the reactivity on NAT surfaces (particularly the heterogeneous reaction HCl + $ClONO_2$) identified many years ago (WMO, 1998; Carslaw and Peter, 1997) remain unresolved. Most results, such as comparisons of chemical transport models to observations, are generally robust to the details of the assumptions employed regarding PSCs and heterogeneous chemistry (e.g., Kirner et al., 2015a; Wohltmann et al., 2013). Nonetheless, there are conditions where the exact rates of heterogeneous chlorine activation reactions and thus also PSC composition will be significant; for example, when chlorine activation occurs in the Arctic within a limited spatial or temporal region (Wegner et al., 2016) or in the Antarctic under conditions of a direct competition of the rate of gas-phase deactivation and heterogeneous activation of chlorine (Solomon et al., 2015). Further, an accurate representation of PSC processes in models is required to ensure the reliability of projections of the future development of polar ozone under conditions of changed atmospheric concentrations of key species. The contribution of the latest observational, laboratory, and modeling studies to addressing these questions is described in the following sections.

4.3.1.1 Observations of PSC Extent and Composition

Long-term data sets of the occurrence of different types of PSC particles over the polar regions are now available from both satellite and ground-based observations. The MIPAS instrument, which was carried by the ENVISAT satellite, was an infrared limb

sounder providing a pole-covering day and night time climatology of PSC distributions and their composition from July 2002 until April 2012. The CALIOP instrument onboard CALIPSO is a two-wavelength polarization-sensitive lidar that provides night-time high-resolution vertical profiles of PSCs with data collection beginning in mid-June 2006 and lasting until the present day. In addition, ground-based lidar systems provide important long-term information on PSC properties; measurements are available since 1997 at Esrange, Sweden (Achtert and Tesche, 2014) and for 1995–2001 and 2006–2010 at McMurdo, Antarctica (Di Liberto et al., 2014). Data from these ground-based systems are compared with satellite-based measurements and are used to test and develop PSC classification schemes.

The most recent data products from MIPAS and CALIOP (Spang et al., 2016; Lambert et al., 2016) show a very good agreement regarding PSC classification and occurrence as seen in the daily altitude-resolved time series of three PSC classes in 2009 for the two instruments **(Figure 4-9)** (Spang et al., 2018). Given the very different measurement principles used by CALIOP and MIPAS, the agreement between the two data sets is encouraging and will allow analyses on the temporal and spatial development of PSCs over multiple winters to be performed with the potential for the validation and improvement of PSC schemes in CTMs and CCMs (e.g., Zhu et al., 2017a).

WMO (2014) reported on the detection of unusually large particles (up to 35 μm), so-called "NAT-rocks", in synoptic-scale PSC fields during aircraft campaigns in the Arctic in 2010 and 2011 (von Hobe et al., 2013). It has been argued for a long time that the sequestering of major amounts of nitric acid in relatively large particles leads to efficient denitrification (Salawitch et al., 1989). Further analysis of these observations (Molleker et al., 2014) showed that the optically measured size distribution (**Figure 4-10**) could only be explained by either strong asphericity of the particles or an alternate composition (e.g., water ice coated with NAT). While there has been previous evidence (Fahey et al., 2001; Brooks et al., 2003) for NAT-rocks, their observational basis has been expanded by these measurements and the occurrence of large NAT particles now appears to be a regular feature of synoptic-scale PSCs in the Arctic.

Further, analysis of the spectral signature of the PSC field over northern Scandinavia obtained by airborne passive infrared limb emission measurements in December 2011 revealed a distinctive "shoulder-like" signature in the spectral region around 820 cm^{-1} (Woiwode et al., 2016). This observed signature is best explained by the combination of the absorption, emission, and scattering characteristics of large (log-normal distribution with a mode radius of 4.8 μm) highly aspherical (aspect ratios of 0.1 or 10) NAT particles. The measurement of excess gas-phase HNO_3 observed in a nitrification layer directly below the observed PSCs further supports the role of such large aspherical particles in denitrification.

Comparison of CALIOP observations for the Antarctic in winter 2010 with model simulations suggests that two major NAT particle formation mechanisms must exist. Homogeneous nucleation from supercooled ternary solution (STS; see WMO (2014), Box 3-1) droplets produces large NAT particles which are needed to reproduce the observed rates of denitrification, while heterogeneous nucleation of NAT on ice produces small particles which account for the large backscattering ratio from NAT observed by CALIOP (Zhu et al., 2017a; 2017b).

It has also previously been proposed that refractory particles of meteoric origin could serve as condensation nuclei of NAT-rocks (Curtius et al., 2005). Laboratory experiments using analogues of meteoric materials show that such surfaces have the capacity to nucleate nitric acid hydrates (James et al., 2018). As reported in WMO (2014), aircraft measurements made in the Arctic in late winter 2010 detected a large number of refractory particles with diameters above 500 nm (von Hobe et al., 2013). The abundance of refractory aerosols in the lower stratosphere during late winter in the Arctic vortex appears to be a regular feature rather than an exception (Weigel et al., 2014). At the time of these measurements, the air mass subsidence inside the Arctic winter vortex from the upper stratosphere and mesosphere was well-advanced, leading to the conclusion that the refractory particles had been transported from higher altitudes into the lower stratosphere. In contrast, in the flight samples collected in an early winter situation (December 2011, and therefore a young vortex in which the air masses had seen much less descent), no large refractory particles were observed (Ebert et al., 2016). The observed general

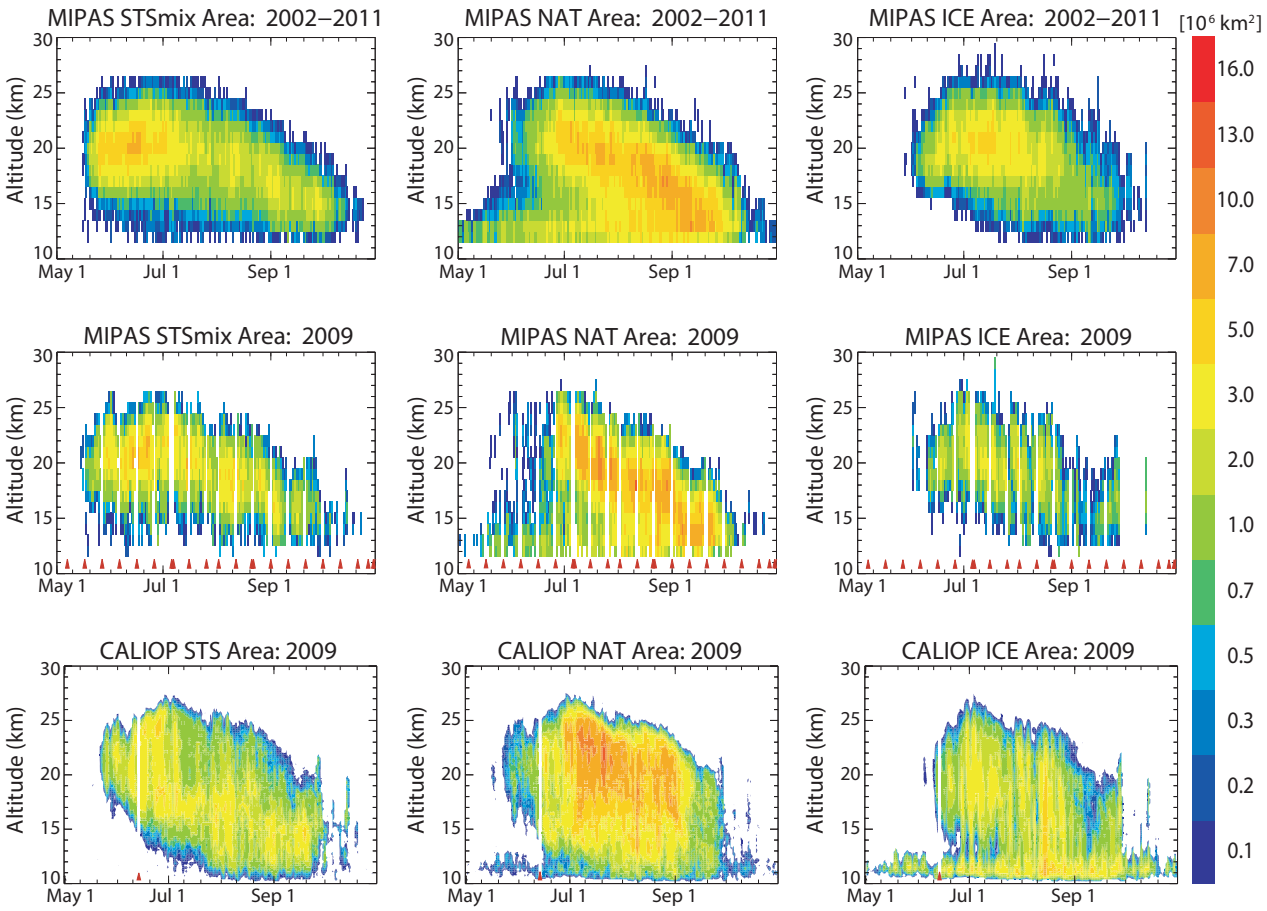

Figure 4-9. Time series of the daily Antarctic PSC areas (*top row*) from MIPAS climatology (10-year mean [2002, 2003, and 2005–2011]; MIPAS data weighted by the area of the applied latitude bins south of 55°S in the altitude range 12–30 km), (*middle row*) from MIPAS for the year 2009, and (*bottom row*) CALIOP V2 for the year 2009, based on the identical computation of PSC area for each data set. Presented are all relevant PSC classes for the MIPAS and CALIOP satellite retrievals (ice, NAT, and STSmix). For better comparability with CALIOP, MIPAS observations in the middle row are restricted to latitudes north of 82°S, the latitude coverage of CALIOP. Red triangles at 10.5 km altitude in the MIPAS and CALIOP time series (*middle and bottom rows*) mark data gaps caused by the measurement mode. Adapted from Spang et al. (2018).

tendency of a lower abundance of refractory particles during PSC events compared to non-PSC situations supports the hypothesis that such particles can provide a surface for heterogeneous nucleation during PSC formation. Further, recent analysis of particles originally collected in the Arctic stratosphere from January until March 2000 found a high abundance of carbonaceous refractory particles. Based on their chemistry and nanostructure, many non-meteoric sources for these carbonaceous particles can be excluded (Schütze et al., 2017). However, the exact source of the large refractory particles in the stratosphere and their impact on PSC formation remain to be accurately determined.

4.3.1.2 Gravity Waves and Orographic Forcing

Atmospheric gravity waves yield substantial small-scale temperature fluctuations that can trigger the formation of PSCs (e.g., Murphy and Gary, 1995). Orr et al. (2015), based on case studies over the Antarctic Peninsula, investigated the representation of stratospheric mountain-wave-induced temperature fluctuations by the UK Met Office Unified Model (UM) at climate scale and mesoscale, compared to observations. They found that, at high horizontal resolution (4 km), the regional mesoscale configuration of the UM is able to correctly simulate the magnitude, timing,

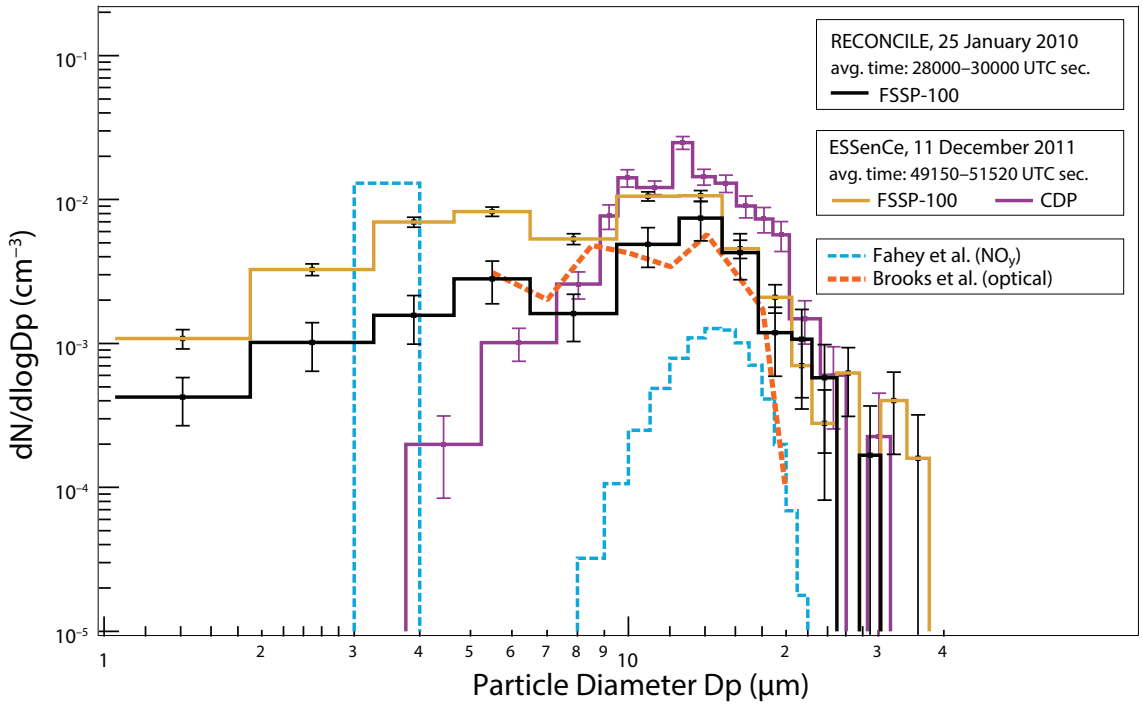

Figure 4-10. Size distributions of large HNO_3-containing PSC particles with high number densities from in situ airborne measurements in 2010 and 2011. These measurements are compared to previous measurements by Fahey et al. (2001) (retrieved from total NO_y) and Brooks et al. (2003) (optical measurements). Adapted from Molleker et al. (2014).

and location of the measured temperature fluctuations. While a climate configuration of the model with lower horizontal resolution was not able to resolve the fluctuations, in this case, the use of a mountain wave parameterization scheme gave reasonable agreement with observations. A 10-year satellite record of gravity wave activity in the polar lower stratosphere based on AIRS indicates that orography as well as jet and storm sources are the main causes of the observed gravity waves. There is a strong seasonal cycle in wave activity with wintertime maxima at high latitudes, the cycle lasting 2–6 months in the Northern Hemisphere and 5–9 months in the Southern Hemisphere (Hoffmann et al., 2017). A comparison of the satellite observations with temperature fluctuations in the ECMWF operational analysis (16-km horizontal resolution) showed that gravity wave patterns occur in the right locations, but that wave amplitudes were typically underestimated by a factor of 2–3 (Hoffmann et al., 2017). Further, Lambert and Santee (2018) find that the potential to form ice PSCs in model studies driven by various reanalyses varies significantly because of the underlying differences in the representation of mountain wave activity. Moreover, CALIOP data indicate that simulations are missing clouds containing small NAT particles with large number densities; such particles are most likely to form from ice clouds or STS in gravity waves (Zhu et al., 2017b).

These recent findings emphasize the importance of high spatial resolution, state-of-the-art meteorological reanalyses, and high-quality schemes for the representation of gravity waves in model studies aimed at PSC formation and existence.

4.3.2 Polar Chemistry

4.3.2.1 Observations of Polar Chemistry

Measurements taken with balloon-borne MIPAS-B and TELIS instruments in northern Sweden on 31 March 2011 inside the polar vortex provided vertical profiles of inorganic and organic chlorine species over the whole altitude range in which chlorine had been undergoing activation and deactivation (Wetzel et al., 2015). A total chlorine (Cl_y) concentration of 3.41 ± 0.30 ppbv is inferred above 24 km from the

measurements. This value is consistent with the slightly reduced chlorine loading of the stratosphere in 2011 compared to its peak value a decade earlier (see **Chapter 1**).

Strahan et al. (2014) reported Aura MLS-inferred Cl_y showed large variations from year to year due to the variability of transport to the Antarctic vortex. The mean expected annual Cl_y decline due to the Montreal Protocol is estimated to be –20 ppt yr^{-1}; however, fluctuations of the concentration in a given year have varied up to 200 ppt below and 150 ppt above the mean. (The concentration of Cl_y in 2013 at 450 K in the vortex was estimated by this method to have been 2650 ppt.) Because of this large interannual variability of Cl_y, it requires at least 10 years of chlorine decline after the chlorine maximum for an Antarctic ozone recovery (in the sense of an ozone increase caused by halocarbon reductions) to be attributable to a decline of stratospheric chlorine in a statistically significant manner (Strahan et al., 2014).

In the Arctic vortex of the 2009/2010 winter, satellite observations showed the initial activation of chlorine occurred in association with the formation of PSCs over the eastern coast of Greenland at the beginning of January 2010 (Wegner et al., 2016). Although this area of PSCs covered only a small fraction of the vortex, it was responsible for almost the entire initial chlorine activation throughout the vortex. Observations show that HCl mixing ratios decreased rapidly in and downstream of this region. Simulations of heterogeneous reaction rates along trajectories intersecting with the PSCs indicate that the initial phase of chlorine activation occurred in just a few hours. These calculations further suggest that the very rapid chlorine activation in Arctic winter 2009/2010 can only be explained by an increase in surface area density due to PSC formation (Wegner et al., 2016), as reactions on the background binary aerosol would have been too slow.

4.3.2.2 Laboratory Studies, Theoretical Basis, and Models

Laboratory, PSCs

New experiments on the heterogeneous kinetics of H_2O, HNO_3, and HCl on HNO_3 hydrates have been performed using a multidiagnostic stirred-flow reactor in which the gas phase as well as the condensed phase have been simultaneously investigated for stratospheric temperatures in the range 175–200 K (Iannarelli and Rossi, 2016). In these experiments, NAT was investigated in two phases; α-NAT, which exists at temperatures below 185 K and is metastable and β-NAT, which exists above this temperature and is the form predominantly found in PSCs (see also the following section). In the laboratory experiments, initial spontaneous formation of α-NAT was found, followed by the gradual transformation of α- to β-NAT at $T > 185$ K; further nitric acid dihydrate (NAD) was spontaneously formed at somewhat larger partial pressures of HNO_3 deposited on pure H_2O ice (Iannarelli and Rossi, 2016). The improved experimental instrumentation suggests, in contrast to previous studies, the formation of α-NAT proceeds without prior formation of an amorphous HNO_3/H_2O layer and always results in the formation of β-NAT.

Chlorine Chemistry and Heterogeneous Reactions

Chlorine activation and subsequent ozone depletion only occur because of heterogeneous reactions (Solomon et al., 1986); chlorine activation rates are mainly controlled by temperature, with only a limited dependence on PSC type (e.g., Salawitch et al., 1988; Kawa et al., 1997; WMO, 2014). Beyond heterogeneous chemistry, NAT particles have an impact on gas-phase chemistry through removal of HNO_3 (denitrification). Initial chlorine activation is not directly related to chemical ozone loss and chlorine activation is often saturated because of the lack of available $ClONO_2$, so that gas-phase chemistry becomes important (Solomon et al., 2015; Müller et al. 2018). However, strong polar ozone loss requires both a nearly complete activation of chlorine and the maintenance of high levels of active chlorine for an extended period (e.g., Solomon et al., 2015; Müller et al., 2018). Recent work has focused on the sensitivity of simulated ozone loss on PSC types, temperature thresholds and the maintenance of high levels of activated chlorine, and the chemical processes responsible for chlorine activation (Solomon et al., 2015; Kirner et al., 2015a; Wegner et al., 2016; Wohltmann et al., 2017; Müller et al., 2018).

Multi-year simulations of a CCM (nudged to ERA-Interim reanalysis meteorological fields) show the impact that the various types of PSCs (Box 3.1 in WMO (2014)) have on Antarctic chlorine activation and

ozone loss (Kirner et al., 2015a). In these simulations, in high southern latitudes, heterogeneous chemistry on liquid particles accounts for more than 90% of ozone depletion, with reactions on ice particles adding less than 5% of further ozone depletion and NAT particles less than 1%, although NAT particles play an essential role in denitrification. Simulations of HNO_3, ClO, and ozone agree closely with observations from MLS (Kirner et al., 2015a).

Polar ozone depletion simulations based on the WACCM model for the year 2011 indicate that total ozone depletion in both hemispheres is dependent on low temperatures (below 192 K) and associated heterogeneous chemistry on polar stratospheric cloud particles (Solomon et al., 2015). Reactions limited to temperatures above 192 K, or on binary (sulfate/water) liquid aerosols, yield little simulated polar ozone depletion in this model in either hemisphere. The simulated ozone loss is sensitive to sulfate, which provides additional surface area for heterogeneous reactions (Tabazadeh et al., 2002); enhancing stratospheric sulfate by a factor of three increases ozone loss by up to 20 Dobson Units (DU) in the Antarctic and 15 DU in the Arctic. These assumed enhanced sulfate levels are similar to those observed following recent relatively small volcanic eruptions since 2005. Ozone losses in the model are strongly sensitive to temperature, with a test case cooler by 2 K producing as much as 30 DU additional ozone loss in the Antarctic and 40 DU in the Arctic. The modeled result compares with an earlier analysis of observations that calculated the mean dependence on stratospheric temperature of Arctic ozone loss as 15.6 DU K^{-1} (Rex et al., 2006).

Moreover, Solomon et al. (2015) corroborate earlier findings (Jaeglé et al., 1997) that in the edge region of the Antarctic vortex, transport of $ClONO_2$ from lower latitudes to higher latitudes as well as latitudinal excursions of air parcels in and out of sunlight during winter enhances $ClONO_2$ and HOCl available for reaction with HCl and hence net chlorine activation. The onset of chlorine activation by heterogeneous processes is mostly limited by the amount of available $ClONO_2$, as confirmed by a recent combination of CALIOP PSC and MLS HCl and ClO observations with model simulations (Nakajima et al., 2016).

Recent studies focus on a quantitative analysis of the chemical reactions involved in polar ozone depletion in the stratosphere (for specific winters) and of the relevant reaction pathways and cycles (Wohltmann et al., 2017; Müller et al., 2018). Wohltmann et al. (2017), based on NASA's Jet Propulsion Laboratory (JPL) 2011 recommendation (Sander et al., 2011), find that the ClO dimer cycle contributes about 50% to the vortex-averaged ozone loss at 54 hPa in both hemispheres, while the BrO–ClO cycle contributes about 40%. Further, in the Southern Hemisphere, there is a clear shift from chlorine activation by the $ClONO_2$ + HCl reaction in early winter to activation by the HOCl + HCl reaction later in winter (Wohltmann et al., 2017; Müller et al., 2018). The HOCl + HCl reaction accounts for about 70% of the activation of Cl in the Southern Hemisphere, while it accounts for 30% of the activation in the Northern Hemisphere (Wohltmann et al., 2017). In the core of the Antarctic vortex, in the lowermost stratosphere, high levels of active chlorine are maintained by effective chemical cycles (HCl null-cycles) where the formation of HCl is balanced by immediate reactivation, which allows active chlorine levels to be maintained and thus rapid ozone destruction to occur. For the observed almost complete activation of stratospheric chlorine in the lower stratosphere, the production of HOCl via HO_2 + ClO, with the HO_2 resulting from photolysis of CH_2O, is essential (Müller et al., 2018).

In the dark core of the polar vortex MLS observations show a much faster depletion of HCl than simulated by current state-of-the-art models (ATLAS, CLaMS, WACCM, and TOMCAT/SLIMCAT) (Wohltmann et al., 2017; Grooß et al., 2018). This points to some unknown process that is currently not fully represented. There is only a minor impact of about 2% on the overall ozone column loss over the course of Antarctic winter and spring, however, because the HCl discrepancy and the associated underestimation of chlorine activation occur in early winter, when ozone loss rates are slow.

Reaction Kinetics

Canty et al. (2016) showed that the most recent recommendations for the kinetics that govern the partitioning of ClO and ClOOCl (put forth by the JPL panel) (Burkholder et al., 2015) are in extremely good agreement with the atmospheric observations of ClO and ClOOCl. The most important difference with respect to calculations that rely on older recommendations is

the temperature at which loss of ozone by the ClOOCl catalytic cycle terminates. The current recommendation (Burkholder et al., 2015) suggests that ClOOCl is less stable than previously assumed, resulting in an approximate 2 K downward shift in the termination temperature of polar ozone loss due to the ClOOCl catalytic cycle (Canty et al., 2016).

4.3.3 Very Short-Lived Halogenated Substances

Recent observations show that the atmospheric concentration of dichloromethane (CH_2Cl_2)—an ozone-depleting gas not controlled by the Montreal Protocol—is increasing (Leedham Elvidge et al., 2015; Hossaini et al., 2017; **Chapter 1** of this Assessment). The future evolution of atmospheric dichloromethane is uncertain, but for the present day (2015) the simulated contribution of dichloromethane to total inorganic chlorine in the polar lower stratosphere (100 hPa) is about 3% (Hossaini et al., 2017). Using atmospheric model simulations, Hossaini et al. (2017) show that the largest ozone decreases attributable to dichloromethane are simulated in the Southern Hemisphere. The impact of dichloromethane in these simulations is modest at the present time, with springtime zonal mean column ozone in the Southern Hemisphere up to 3%, or 6 DU, lower in simulations in which dichloromethane is considered (Hossaini et al., 2017).

Beyond dichloromethane, a number of very short-lived substances (VSLSs; for example, 1,2-Dichloroethane, $C_2H_4Cl_2$) have also been detected in Earth's atmosphere, although atmospheric measurements of these compounds are sparse (Hossaini et al., 2015a). While the major contribution to stratospheric chlorine from chlorine-containing VSLSs comes from dichloromethane, these other VSLSs also contribute. The additional chlorine loading from all chlorine-containing VSLSs in 2013 amounted to about 100 ppt (Hossaini et al., 2015a).

It is also important to account for the contribution of bromine-containing VSLSs to the stratospheric halogen loading (e.g., Frieler et al., 2006). Recent CCM simulations of the evolution of the Antarctic ozone hole show a significant additional reduction of the total ozone column over the polar cap and better agreement with observations, when brominated VSLSs are considered (**Figure 4-11**, Braesicke et al., 2013; Yang et al., 2014; Sinnhuber and Meul, 2015; Oman et al., 2016; Fernandez et al., 2017). For instance, Sinnhuber and Meul (2015) found that due to the inclusion of VSLSs, up to 25% more ozone was destroyed locally in the southern polar lower stratosphere (60°–90°S) in October in the period 1979 to 1995, leading to a regional reduction of total column ozone by about 10% (October) due to bromine-containing VSLSs. Compared to OMI satellite measurements, Oman et al. (2016) obtained better agreement in the very low ozone concentrations in the deep Antarctic lower stratospheric polar vortex during late September to early October from the late 1990s to the early 2000s when bromine from natural VSLSs was considered in their model. At the time of maximum chlorine loading around the year 2000, the 5 ppt of very short-lived Br_y increased the ozone hole area by about 40% (5 million km^2) and enhanced the ozone mass deficit by about 75% (8 million tons) (Fernandez et al., 2017, **Figure 4-11**). Although the strongest impact of bromine-containing VSLSs is in the Antarctic, there is also an impact on Arctic ozone levels in spring (e.g., Yang et al., 2014). However, it should be noted that the impact of bromine on stratospheric ozone occurs through the ClO/BrO–ClO chemical cycle and thus is only strong for enhanced stratospheric chlorine levels.

4.3.4 Polar Dynamical Processes

4.3.4.1 Dynamical Control of Polar Ozone

Year-to-year variability of stratospheric polar ozone is controlled by dynamical and chemical processes. Both are coupled to temperature changes which, in turn, are strongly influenced by wave activity (WMO, 2014). Recent studies of the dynamical contribution to temperature trends and ozone variability in Arctic spring essentially confirmed the important role of dynamics (Bohlinger et al., 2014; Bednarz et al., 2016; Ivy et al., 2016; Strahan et al., 2016). Ozonesonde measurements over Belgrano (Antarctica) show, for example, that the largest ozone depletion occurs in the coldest years (55–60% decrease of total ozone column in spring in the years 2000, 2003, and 2006), while the ozone loss in warm winters is smaller (20% in 2002 due to the Southern Hemisphere (SH) major sudden stratospheric warming) (Parrondo et al., 2014).

Planetary wave driving of the polar stratosphere is generally stronger and more variable in Northern

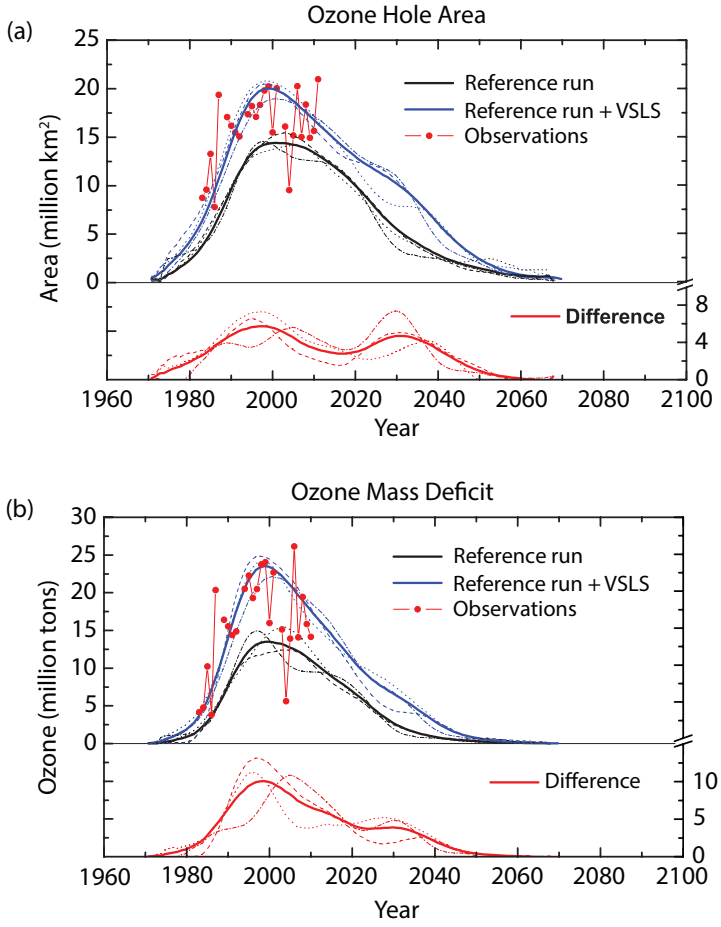

Figure 4-11. Temporal evolution of (a) the Antarctic ozone hole area and (b) ozone mass deficit for model experiments with the Community Atmosphere Model with Chemistry (CAM) without brominated VSLSs (black, reference) and with brominated VSLSs (blue, reference + VSLS) on the left axis, as well as the difference between runs (red) on the right axis. Solid thick lines show the ensemble mean for each experiment, while the dashed, dotted, and dashed-dotted thin lines correspond to each of the three independent simulations for each run. Red dots in the upper panels show observations. From Fernandez et al. (2017).

Hemisphere (NH) than in SH winter, leading to a warmer Arctic polar vortex and less chemical ozone depletion (see **Figures 4-1, 4-4, and 4-5**). In contrast, in austral winter and spring, Antarctic lower stratospheric temperatures are low enough for continuing heterogeneous ozone depletion, as the Antarctic vortex is much less disturbed by wave forcing (WMO, 2014; Solomon et al., 2014). The inter-hemispheric differences in the relationship between wave activity and the spring-to-fall ozone ratio are illustrated in **Figure 4-12** (update of Weber et al., 2011 and Figure 3-13 in WMO, 2014). **Figure 4-12** shows the compact linear relationship between the mean winter eddy heat flux at 100 hPa and the spring-to-fall high-latitude ozone ratio, combining data from both hemispheres. The winter eddy heat flux is consistently lower in the SH than in the NH. As a result, chemical ozone loss dominates in the SH lower stratosphere, and ozone values are lower in spring than in fall (except for 2002 and 2017). In contrast, the larger NH eddy heat flux leads to enhanced transport of ozone throughout the winter. As shown in **Figure 4-12**, this relationship held for all Antarctic and Arctic winters since the last Assessment, including the year 2015 (with the eruption of the Chilean volcano Calbuco enhancing Antarctic ozone depletion (see **Section 4.2.3.1**) and the northern winter 2015/2016 (see **Section 4.2.4.1**).

4.3.4.2 Refined Understanding of Dynamical Variability

The mechanisms involved in the generation, propagation, and dissipation of planetary waves are well known from theoretical, observational, and modeling approaches. Nevertheless, our understanding of the processes that determine the degree and interannual variability of wave driving of the polar stratosphere is still incomplete (WMO, 2014). Investigating the sources of interannual variability of wave activity in the stratosphere is still an intense area of research. The following sections report on advances since the last Assessment.

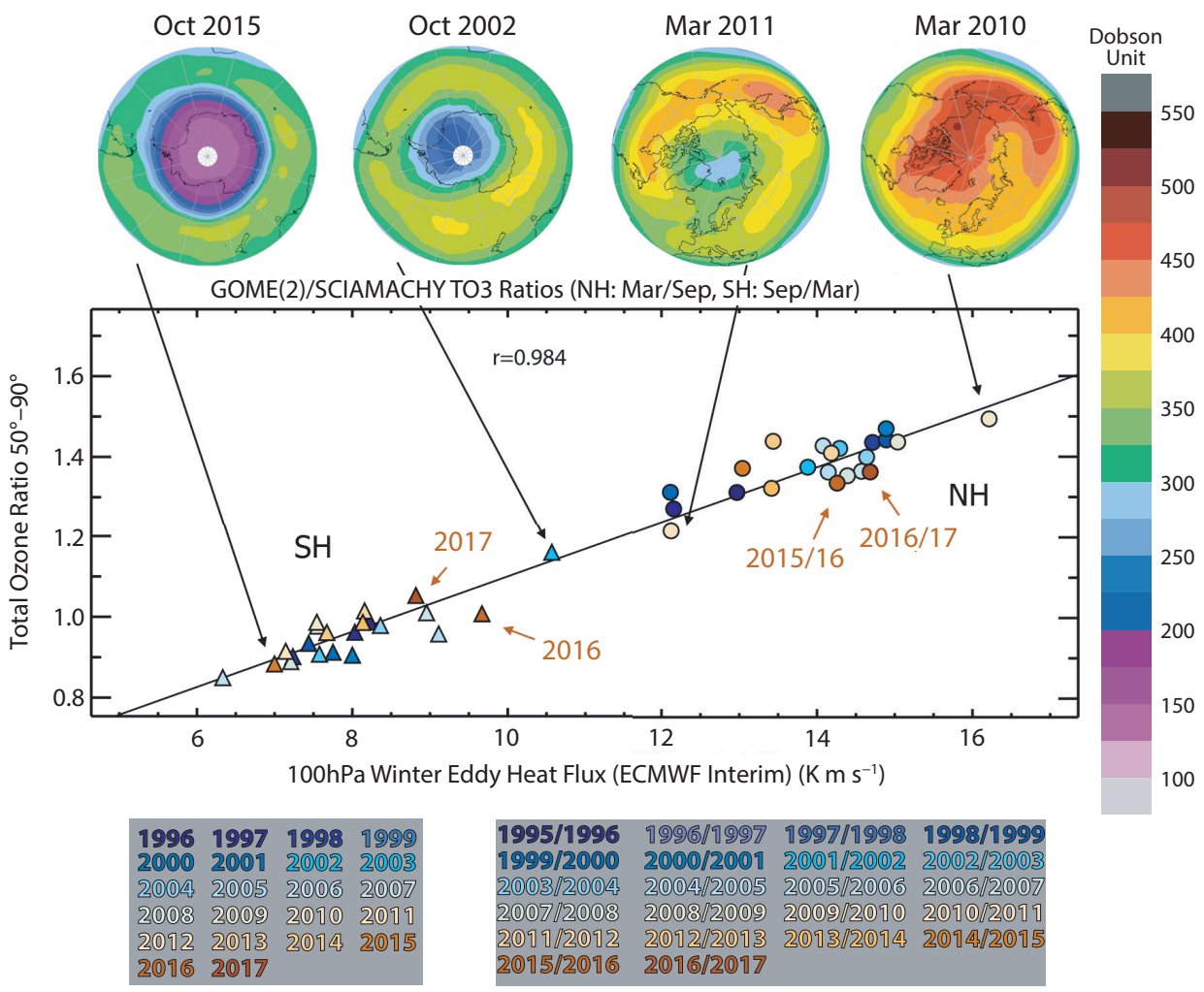

Figure 4-12. Spring-to-autumn ratio of observed high latitude total ozone (>50º latitude) as a function of the absolute extratropical winter mean eddy heat flux (September to March in the Northern Hemisphere and March to September in the Southern Hemisphere) derived from ECMWF ERA-Interim data. Data from the Southern Hemisphere are shown as triangles (September over March ozone ratios) and from the Northern Hemisphere as solid circles (March over September ratios). Polar total ozone distributions for select years are shown at the top. Updated from Weber et al. (2011).

Sources of Dynamical Variability: SSTs and ENSO

Since van Loon and Labitzke (1987), it is well known that variations in sea surface temperatures (SSTs) lead to anomalous stratospheric polar vortices, affecting stratospheric polar ozone. Recent studies have refined previous work by addressing in more detail the underlying mechanisms linking SST anomalies to stratospheric polar vortex variability, the role of the location of SST anomalies and differences in the impact of SSTs on the Arctic and Antarctic polar vortices and on stratospheric ozone.

SST anomalies generate anomalous upward wave flux into the stratosphere. Hence, increasing global SSTs and their latitudinal gradients modulate the polar vortices through an enhancement of the Brewer-Dobson circulation in both hemispheres. While globally uniform SST changes have a stronger impact on the Southern Hemisphere, changes in the SST gradients affect the Arctic vortex more significantly. This asymmetry is due to differences in the properties and transmission of the waves in both hemispheres (Hu et al., 2014).

Moreover, depending on the longitudinal position of the SST anomalies, they can either enhance or weaken upward wave propagation into the stratosphere through positive or negative interference with the climatological wave patterns. Hemispheric differences in the extratropical impact of regional tropical SST anomalies have been linked to differences in transient eddy forcing and stationary wave activity between the hemispheres (Li et al., 2010). Thus, higher SSTs in either the tropical Eastern Pacific Ocean (e.g., Calvo et al., 2017) or the North Atlantic (Omrani et al., 2014), or lower SSTs in either the North Pacific (e.g. Hurwitz et al., 2012) or the Indian Ocean (Fletcher and Kushner, 2011) lead to a weaker Arctic polar vortex. Using satellite observations and reanalysis data, Tian et al. (2017) reported a high correlation between SSTs in the East Asian marginal seas and lower stratospheric ozone over Antarctica in austral spring, with high SSTs reducing planetary wave activity in the SH, strengthening the stratospheric polar vortex, and thereby enhancing chemical ozone loss (with the opposite effects for low SSTs). According to their model simulations, ~17% of the decline of Antarctic lower stratospheric ozone between 1955 and 2005 may be associated with increasing SSTs over the marginal seas of East Asia.

Recent studies of the El Niño–Southern Oscillation (ENSO) highlighted the role of the location of the strongest SST anomalies (i.e., in the Eastern Pacific [EP] or the central Pacific [CP]) for the effects of ENSO on polar ozone. 'Canonical' EP El Niño events tend to weaken the polar vortex (e.g., Calvo et al., 2017 and references therein) and enhance stratospheric column ozone at high latitudes (e.g., Cagnazzo et al., 2009), while during La Niña events (characterized by negative SST anomalies in the central-eastern Pacific area), a stronger and colder polar Arctic vortex is observed (Iza et al., 2016), implying a reduced polar total ozone column. Compared to canonical El Niño events, CP El Niño events are more effective in the Antarctic where they lead to higher stratospheric temperatures and ozone in the lower stratosphere during austral summer and autumn (Zubiaurre and Calvo, 2012; Evtushevsky et al., 2015). However, the effects of CP El Niño on the Arctic stratosphere are still under debate (Hurwitz et al., 2014).

Dynamical Variability in NH Stratospheric Winters

Sudden stratospheric warmings (SSWs) in northern winter are induced by anomalously strong upward wave propagation from the troposphere and dissipation in the middle and high latitudes of the stratosphere. They weaken the polar vortex, warm the polar stratosphere, and enhance the Brewer-Dobson circulation (BDC) (e.g., Andrews et al., 1987; Charlton and Polvani, 2007). Since the previous Assessment, a growing number of studies investigated the impact of SSWs on polar processes and polar ozone. The enhanced temperature and BDC around the SSW date lead to a reduction of ozone loss and more ozone transported towards the pole (e.g., Strahan et al., 2016; Manney et al., 2015b; Damiani et al., 2014; Tao et al., 2015). In addition, meridional mixing increases during and after SSWs although its impact on ozone is not clear due to large case-to-case variability (Tao et al., 2015; Damiani et al., 2014; Manney et al., 2015a; Manney and Lawrence, 2016).

By comparing simulations with a CTM driven with observed meteorological conditions with and without heterogeneous chemistry, Strahan et al. (2016) quantified the chemical ozone depletion over the Arctic cap for the recent past (2005–2015). They showed that the linear relationship between the chemical ozone loss rate and the number of days cold enough for PSC particle formation within the polar vortex, found in earlier studies (Rex et al., 2004, 2006; Tilmes et al., 2003), still holds. While enhanced chemical ozone loss takes place in an undisturbed, cold, and stable polar vortex, the occurrence of a major SSW in mid-winter limits the number of cold days. As a result, ozone depletion in winters with a stable and cold polar vortex is roughly three times greater than in winters with a major SSW before mid-February. With five cold Arctic winters (2005, 2007, 2008, 2011, and 2014) and six winters with SSWs occurring in the period 2005–2015, a large part of the interannual variability of Arctic ozone over this period is explained (correlation of 0.97 between the maximum seasonal Arctic cap column ozone depletion and the number of cold days) (Strahan et al., 2016). Ozone loss in cold Arctic winters can additionally be amplified by high water vapor mixing ratios in the lower stratosphere, further increasing the probability of PSC formation and effective heterogeneous chlorine activation, as derived by Khosrawi et al. (2016) from satellite observations.

Particularly strong SSWs may perturb the mesosphere for many weeks. These events are characterized by an elevated stratopause which forms at pressure levels as high as 0.5 Pa (~70 km) about 10–14 days after the peak of the SSW. During the recovery phase of such elevated stratopause events, observations show a strong descent of polar mesospheric NO_x-rich air into the stratosphere (e.g., Pérot et al., 2014; Orsolini et al., 2017), inducing polar Arctic upper stratospheric ozone loss.

Recently, Siskind et al. (2016) proposed a new mechanism by which dynamical variability in northern spring may affect polar ozone in the following summer. In winters with strong mesospheric descent that are followed by dynamically quiet spring seasons (as in boreal winter 2009), relatively low values of CH_4 and high values of ClO may persist in the upper stratosphere throughout the summer. In 2009, these variations caused up to a 5% reduction in upper stratospheric ozone throughout the summer and early fall.

Downward Planetary Wave Reflection

As discussed in the previous section, the upward propagation and dissipation of planetary waves is *the* important driver of the BDC in the boreal winter stratosphere and largely determines the dynamical resupply of Arctic ozone in winter and spring. However, the overall effect of the planetary wave forcing on Arctic ozone levels in midwinter and spring not only depends on the tropospheric planetary wave sources but also on the stratospheric conditions for wave propagation, as highlighted in a recent CCM study by Lubis et al. (2017). Downward planetary wave reflection may occur in the stratosphere when upward pulses of wave activity decelerate the flow in the upper stratosphere, forming a downward-reflecting surface that redirects waves back to the troposphere (e.g., Harnik and Lindzen, 2001). These types of events lead to a weaker BDC and a colder polar vortex. Thus, there is a direct effect by planetary wave reflection on ozone due to transport, such that less ozone is advected towards the polar region, and an indirect effect due to the induced lower temperatures in the polar vortex, which enhance heterogeneous chemical ozone loss (Lubis et al., 2017).

4.3.5 Other Factors Affecting Polar Ozone

4.3.5.1 Solar Variability by Energetic Particle Precipitation

In addition to the impact on global ozone by decadal variations in solar ultraviolet irradiance (see **Chapter 3.2.1.1**), polar ozone can be destroyed by energetic particle precipitation (EPP) resulting in total ozone loss up to 10–20 DU after strong solar proton events (SPEs) (Vogel et al., 2008). EPP is strongly linked to solar activity either directly by coronal mass ejections (CMEs) producing sporadically large fluxes of solar energetic particles or indirectly by the quasi-continuous impact of the solar wind on Earth's magnetosphere resulting in precipitation of energetic electrons (see e.g., the review by Mironova et al., 2015). The presence of EPP affects the ionization levels in the middle and upper polar atmosphere, leading to significant changes of the chemical composition including ozone (see e.g., the review by Sinnhuber et al., 2012).

Solar proton events caused by CMEs are particularly frequent around the maximum of the solar cycle. A recent intercomparison study demonstrated the overall ability of specialized atmospheric models to reproduce the direct EPP effect by solar protons after the 2003 "Halloween" SPE in late October and early November 2003 (Funke et al., 2011). This event was characterized by short-term (days) mesospheric ozone depletions up to 70%, followed by longer-lasting (weeks to months) depletions of up to 35% in the upper stratosphere. After the "Halloween" event, which has been discussed in detail in WMO (2006), SPE-related composition changes of smaller magnitude have also been observed and modeled in other occasions, namely in November 2004 (Hocke, 2017), January 2005 (Jackman et al., 2011; Verkhoglyadova et al., 2015), as well as in January and March 2012 (von Clarmann et al., 2013; Jackman et al., 2014; Päivärinta et al., 2016). A statistical investigation of average changes in ozone from sonde measurements following 191 SPEs from 1989 to 2016 was carried out by Denton et al. (2018). Their results indicate that SPEs are linked to a ~5–10% decrease in ozone at ~20 km altitude during the polar winter. The greatest decrease occurs ~10–20 days following SPEs with ozone depleted for ~30 days on average.

Energetic electron precipitation is associated with geomagnetic storms and occurs mainly in the polar

auroral and sub-auroral regions with an intensity being largest about two years after the maximum of the solar cycle. Precipitation from mid-energy and from auroral electrons affects the mesosphere (50–100 km) and the lower thermosphere (95–120 km), respectively. The NO_x produced by EPP at these altitudes is long-lived during polar winter and transported down into the stratosphere to altitudes well below 30 km. Satellite observations have provided clear evidence of this EPP indirect effect (IE) occurring in every polar winter with a magnitude modulated by the solar cycle (e.g., Randall et al., 2007; Hendrickx et al., 2015; Funke et al., 2016). The EPP-generated NO_y contributes to the polar winter NO_y column at 20–70 km by 10–40% in the Southern Hemisphere (SH) (see **Figure 4-13**, top panel) (Funke et al., 2014). Stronger wave activity in Arctic winters is responsible for the generally smaller and more variable contributions in the Northern Hemisphere (up to 30%). Recently, observational evidence of polar ozone losses due to the EPP IE has

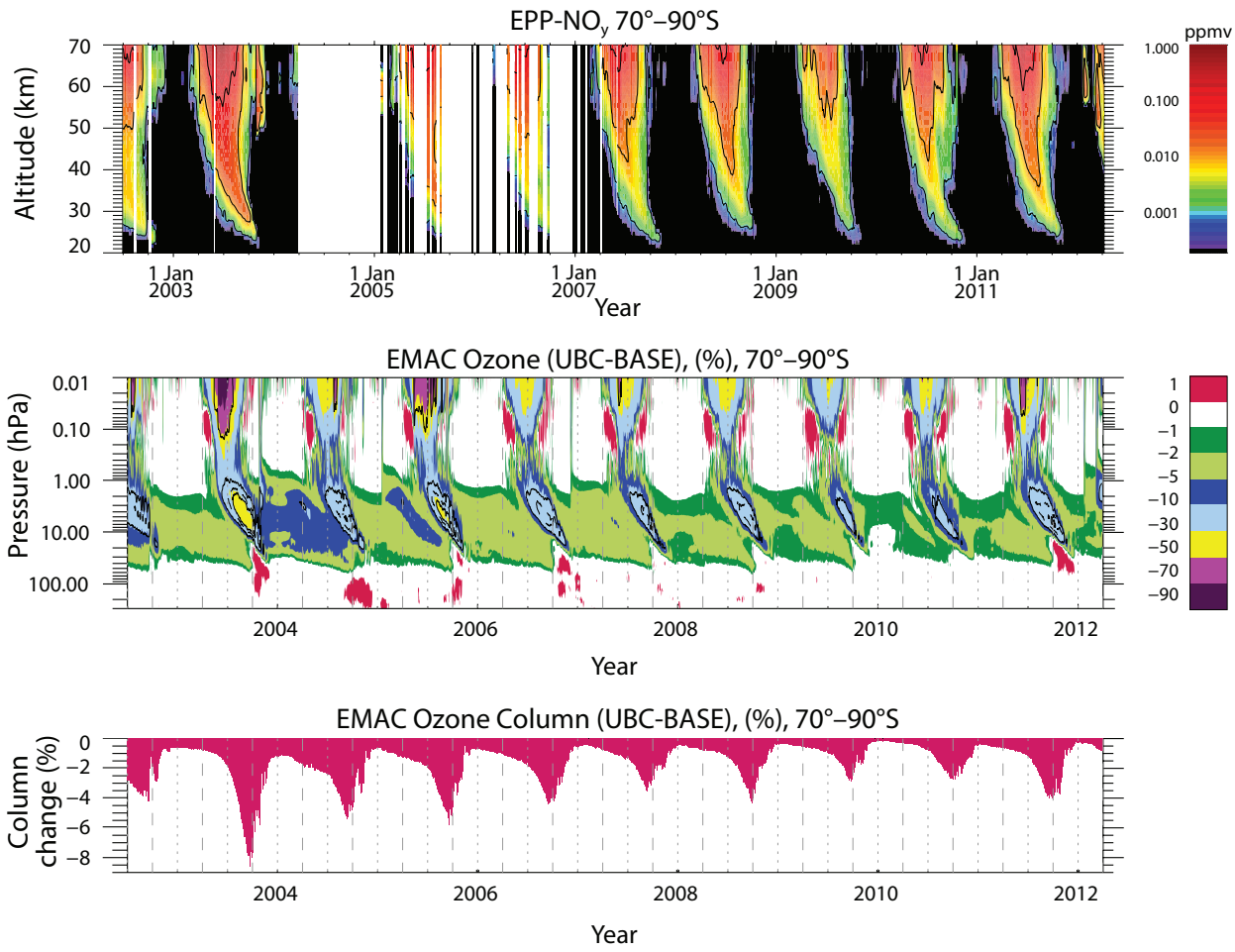

Figure 4-13. (*top*) Temporal evolution of the NO_y contribution produced by energetic particle precipitation (EPP-NO_y) (in ppmv) at 70°–90°S taken by the Michelson Interferometer for Passive Atmospheric Sounding (MIPAS) on board the Envisat satellite during 2002–2012. The contribution of EPP-NO_y has been discriminated from that produced by N_2O oxidation using a tracer correlation method based on MIPAS CH_4 and CO observations. (Adapted from Funke et al., 2014). (*middle and bottom*) Ozone loss due to EPP as a function of pressure level (*middle*) and for the total ozone column (*bottom*) at southern high latitudes (70°–90°S). Shown is the percentage difference between EMAC model simulations with and without EPP impact. The EPP effect is prescribed as an upper boundary condition of NO_y based on MIPAS observations; solar proton events (e.g., in October/November 2003 or January 2005) are prescribed by modeled ionization rates. Adapted from Sinnhuber et al. (2018).

been provided: SH polar stratospheric ozone loss due to the EPP IE peaks around 30–40 km in late winter with an average magnitude of about 10–15% (Fytterer et al., 2015; Damiani et al., 2016). Chemistry–climate models accounting for the EPP IE are able to reproduce the observed effects reasonably well. Forced by EPP-induced NO_y anomalies from satellite data between 2002 and 2012, Sinnhuber et al. (2018) show a recurring average decrease in Antarctic total column ozone around 4% in each winter/spring (ranging between 2% and 3% in 2009 and 2010, and 8% in 2003; see **Figure 4-13,** middle and bottom panel, adapted from Sinnhuber et al., 2018). Although the decrease in total column ozone by EPP-generated NO_y is less than one-tenth of the halogen-induced ozone depletion in the Antarctic polar vortex (see Figure 2-29 in WMO, 2010), the EPP effect needs to be considered in models to simulate realistic total ozone columns in polar winter. However, most CCMI models do not yet incorporate the effects of EPP-generated NO_y on polar ozone loss.

4.3.5.2 Volcanic Eruptions

Sulfate aerosols increase in the stratosphere after volcanic eruptions, providing surfaces on which heterogeneous chemical reactions occur favoring ozone loss (Hofmann and Solomon, 1989). In addition, volcanic aerosols also reduce polar ozone by an indirect dynamical mechanism through radiative heating of the lower stratosphere which increases the equator-to-pole temperature gradient. This leads to a strengthening of the polar vortex—either by thermal wind balance (Kodera, 1995) or reduced planetary wave forcing (Bittner et al., 2016)—and thus to more ozone loss.

While some climate models are able to reproduce the robust response of the polar vortex to volcanic eruptions (Pitari et al., 2016; Muthers et al., 2015; Raible et al., 2016), others are not (Driscoll et al., 2012; Charlton-Perez et al., 2013; Toohey et al., 2014), or their response depends on the size of the eruption (Bittner et al., 2016). The reasons for these discrepancies are still not well understood. Some models tend to overestimate the warming of the tropical stratosphere and thus magnify the polar dynamical response (Muthers et al., 2015). Moreover, the polar vortex response seems to be very sensitive to the spatio-temporal distribution of the volcanic forcing (Toohey et al., 2014) and also to the choice of the ozone climatology in climate models without interactive chemistry (Muthers et al., 2014).

While no major volcanic eruptions comparable in size to Mt. Pinatubo have occurred since 1991, satellite measurements revealed further injections of volcanic SO_2 into the stratosphere by a number of moderate eruptions at different latitudes during the past decade (WMO, 2011; Carn et al., 2016). Solomon et al. (2016) showed that including the SO_2 emissions from these moderate eruptions in specified-dynamics CCM simulations enlarged the size of the modeled Antarctic ozone hole in September and led to better agreement with the observed ozone hole. Moreover, they found about a 10% reduction of the modeled post-2000 healing of the Antarctic ozone hole in September as a result of the chemical effects of increased volcanic activity in the latter part of 2000–2014. Likewise, observations from ozonesondes and the Aura MLS suggest that stratospheric volcanic particles from the 2015 eruption of the Chilean volcano Calbuco enhanced Antarctic ozone depletion and contributed to the record-large Antarctic ozone hole in October 2015 (Stone et al., 2017) (see also **Section 4.2.3.1**). This ozone loss after volcanic eruptions is driven by heterogeneous chemical processes associated with SO_2 emissions, while radiative and dynamical feedbacks only play a minor role (Ivy et al., 2017).

A further potential impact of explosive volcanic eruptions on stratospheric ozone is the direct injection of halogens into the stratosphere. Recent developments in measurement technology allowed for improved estimates of halogen ejections from large historical eruptions (Kutterolf et al., 2015). As these substances are diluted on their transport from the troposphere to the stratosphere through scavenging by hydrometeors (Tabazadeh and Turco, 1993), estimates of the injection efficiency into the stratosphere vary widely for individual eruptions. Nevertheless, direct injections of significant quantities of volcanic halogens have recently been confirmed by remote sensing: MLS recorded stratospheric $HCl:SO_2$ ratios of 0.01–0.03 for 14 eruptions spanning the years 2005 to 2014 (Carn et al., 2016). Based on petrological constraints, Cadoux et al. (2015) found that the Late Bronze Age 'Minoan' eruption of the Santorini volcano released far more halogens than sulfur. Even if only 2% of these halogens had reached the stratosphere, they would have

resulted in reductions in ozone columns of 20% to >90% at northern high latitudes.

Recent Assessments have not considered the impact of the volcanic halogen loading on stratospheric ozone partly because of the large uncertainties in its magnitude and also because this process was determined to be small compared to anthropogenic halogen loading after the eruptions of El Chichón (in 1982) and Mt. Pinatubo (in 1991). However, volcanic halogens are expected to become more relevant in the future as anthropogenic halogens decline. The response of the total ozone column to the injection of SO_2 results from two chemical regimes causing opposite ozone changes: (1) in the lower stratosphere (pressures >30 hPa), heterogeneous chemistry on sulfate aerosol surfaces leads to chlorine activation and ozone depletion and (2) in the upper stratosphere (pressures <30 hPa), catalytic ozone depletion in the NO_x cycle is suppressed (Tie and Brasseur, 1995). Hence, in an atmosphere with low chlorine levels, such as in the era before industrial halogen production, upper stratospheric chemistry dominates and the total polar ozone column is expected to increase after volcanic eruptions (WMO, 2014; Muthers et al, 2015). Similarly, in the future, when anthropogenic halogen is expected to decrease, major volcanic eruptions that inject SO_2 into the stratosphere may cause an ozone increase (e.g., Naik et al., 2017). However, Klobas et al. (2017) found that in a future medium Representative Concentration Pathway RCP-6.0 GHG scenario there is still significant net loss of total column ozone after volcanic SO_2 emissions after mid-century. With increasing GHG concentrations, the post-volcanic chemical ozone depletion weakens due to stratospheric cooling and increased methane concentrations (Klobas et al., 2017; Naik et al., 2017). Klobas et al. (2017) further show that in a future low-halogen environment, the presence in the stratosphere of bromine from natural, very short-lived biogenic compounds is critically important for determining whether future eruptions will lead to ozone depletion. The additional injection of volcanic halogens would induce substantial ozone reductions, particularly in polar regions. Projecting how future volcanic eruptions might affect stratospheric polar ozone remains highly uncertain due to the complex interactions between volcanic aerosols, rising GHG concentrations and VSLSs.

4.4 RECOVERY OF POLAR OZONE

4.4.1 Polar Ozone Recovery in Previous Assessments

WMO (2007) defined three stages of current and future stratospheric ozone recovery: (1) a slowing in the rate of ozone decline, (2) the onset of ozone increases above the previous minimum values (so-called "turnaround") due to declining EESC, and (3) full recovery from ODSs. WMO (2007) concluded that, while stabilization of Antarctic ozone levels had been observed at a similar time as the expected peak of EESC, due to the influence of both saturation of depletion and anomalously high temperatures, the attribution was inconclusive and it was therefore not possible to state that either the first or second stages of recovery had yet occurred. WMO (2007) also included predictions of a slow recovery of Antarctic total column ozone, with an increase in springtime ozone of 5–10% between 2000 and 2020, or 0.25–0.5% yr^{-1} (approximately 0.5–1 DU yr^{-1}) over that period.

WMO (2011) concluded that the leveling off of Antarctic stratospheric ozone since the late 1990s could be attributed to the slight decline in Antarctic stratospheric ODSs, based on the analysis of Yang et al. (2008).

WMO (2014) discussed recovery of Antarctic springtime stratospheric ozone in more detail. Further studies of both vertically resolved and total column ozone had been published since WMO (2011), generally making use of multiple linear regression methods to account for non-chemical effects. It was concluded that Antarctic total column ozone appeared to have started to increase since reaching a minimum at the beginning of the 21st century and that the rate of increase appeared consistent with declining ODSs. The definitive conclusion that Antarctic stratospheric ozone was increasing due to declining ODSs could not yet be reached, however, due to uncertainties in measurements and statistical methods.

Compared to the Antarctic, the Arctic shows larger interannual variability in springtime ozone and smaller ozone depletion, and detection of changes in ozone due to decreases in EESC are therefore expected to take longer than in the Antarctic. WMO (2007) reported that no slowing of the decline in Arctic stratospheric ozone had yet been found. WMO

(2011) and WMO (2014) both reported little progress in assessing Arctic stratospheric ozone recovery since WMO (2007).

4.4.2 Long-Term Antarctic Ozone Trend

4.4.2.1 Onset of Antarctic Ozone Depletion

As noted in previous Assessments, the general choice of 1980 as the reference year for ozone levels should not be taken to mean that there was no anthropogenic ozone depletion in Antarctica prior to that year. Comparing simulations from 17 CCMVal-2 models with total column ozone measurements from four long-term Dobson sites in the Antarctic (Faraday, Halley, South Pole, and Syowa) combined with measurements from multiple space-based instruments (Bodeker et al., 2005), it was estimated that about half of the ozone loss attributable to halogens between 1960 and 2000 actually took place before 1980 (Langematz et al., 2016). Updated results of this study for more years of observations and new CCMI model simulations are shown in **Figure 4-14**. The observed halogen-induced, pre-1980 Antarctic spring total ozone depletion reaches about 54% of that in the 1960–2000 period, comparable in size to the previous estimate. Similar to the CCMVal-2 models, the CCMI models slightly underestimate the observed estimate, with a comparable spread in both model groups.

4.4.2.2 Onset of Antarctic Ozone Recovery

Since WMO (2014), several studies have taken advantage of the increasing length of record to identify parameters that quantify various aspects of ozone loss, which show a positive trend in ozone (i.e. a decrease in ozone depletion) since the year 2000. Different sources of data have been used to derive these parameters, such as ozonesondes or ground-based data from the global Dobson and Brewer networks. Merged multi-year ozone time series were generated from different satellite instruments, which allowed the quantification of long-term trends in total column ozone and vertical ozone profiles before and after the turnaround of Antarctic EESC. More details of the applied ozone data sets are given in the respective studies

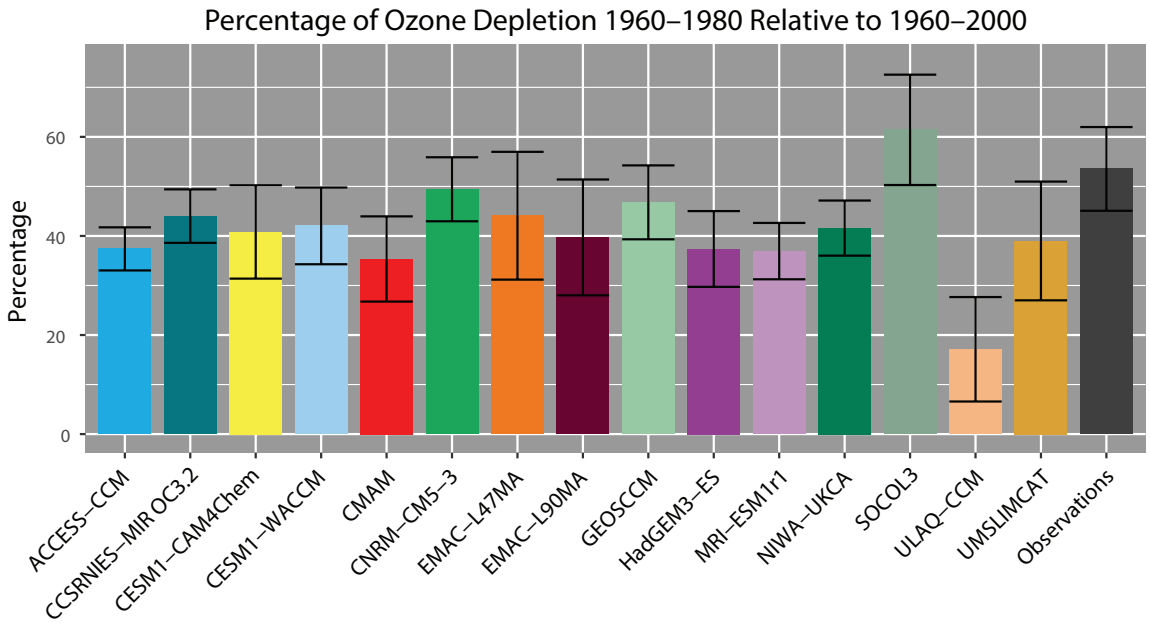

Figure 4-14. Halogen-induced Antarctic ozone depletion in September to November for the period 1960–1980 in % of the depletion for the period 1960–2000 in CCMI simulations and observations. Uncertainties of 1σ were derived by applying error propagation rules. For the analysis, the extended observational data base until 2016 (Bodeker et al., 2005) has been used. Adapted from Langematz et al. (2016).

listed in **Table 4-1**. From these ozone observations, long-term changes in Antarctic ozone were derived by applying various mathematical methods that provide estimates of trends in a number of ozone parameters (e.g., total column ozone, ozone within the particular height range at which depletion has previously been greatest, or metrics used to describe the severity of the Antarctic ozone hole) for specific Antarctic locations (e.g., Antarctic ground-based or ozonesonde stations or polar cap (60°–90°S) average) and season (e.g., September, October, or September to November average) and trend periods (i.e., different starting and finishing years). **Box 4-1** describes in more detail the methods applied to calculate Antarctic ozone trends.

Although the recent studies have differed in their approaches, they have found broadly consistent results. **Table 4-1** gives an overview of some of the identified trends discussed in the following subsections, including the ranges of uncertainty. It should be noted that the table only gives a subset of results, with most of the studies reported on having also considered additional or differently defined parameters and variations of method such as filtering criteria. There is consensus among all studies that, particularly in the month of September, several metrics of Antarctic ozone have shown reductions of depletion in the years following the peak in EESC. In contrast, in October, no significant trends in metrics of Antarctic ozone have been found to this time.

Individual studies find positive trends in Antarctic total column ozone in September that are significant at the 90% or 95% confidence levels (e.g., Solomon et al. 2016; Kuttipurath and Nair, 2017), while other metrics do not yield trends significant at the 2σ level. Apart from the impact of dynamical variability, uncertainties in derived trends arise from the formulation of the regression model, the use of different proxies, and the time period of the trend (Knibbe et al., 2014; de Laat et al., 2015; Chipperfield et al., 2017; Weber at al., 2018). Other factors not incorporated in the purely statistical uncertainty range include possible drifts in the observational data sets (Hubert et al., 2016), the procedures used to merge and homogenize data records from different instruments (e.g., Hassler et al., 2014; Frith et al., 2017), or the representativeness of sparse ground-based data particularly in light of changes to the structure of the vortex over time (Hassler et al., 2011a).

Total Column Ozone

Total column ozone over Antarctica in springtime has increased since 2000 at a mean rate estimated to be between 5 and 10% decade^{-1}, approximately equivalent to 1–2 DU yr^{-1} (Knibbe et al., 2014; Solomon et al., 2016; Kuttipurath and Nair, 2017; Chipperfield et al., 2017; Weber et al., 2018; Pazmiño et al., 2018).

Solomon et al. (2016) found a positive trend in total column ozone in the month of September over the period 2000–2014 as measured by ozonesondes at South Pole of 2.5 ± 1.5 DU yr^{-1}, and SBUV measurements over the polar cap (as available) of 2.5 ± 1.6 DU yr^{-1}, with both ranges at the 90% confidence level. These results are in good agreement with Pazmiño et al. (2018) who derived total column ozone trends inside the Antarctic polar vortex ranging between 1.85 and 2.67 DU yr^{-1} depending on the methods and data sets over the 2001–2016 period. Their trends are statistically significant at the 2σ level. Kuttippurath and Nair (2017) found a positive trend in September to November total column ozone of 1.72 to 1.80 ± 0.80% yr^{-1} (95% confidence level), depending on how the vortex is defined, over the period 2001–2013. The value of the calculated trend was not greatly sensitive to the choice of proxies.

Knibbe et al. (2014) derived a range of positive total column ozone trends depending on the inflection year in their piecewise linear trend (PWLT) analysis. Using 2001 (i.e., the year with maximum EESC over the SH polar cap), they found an increase of 3.1 ± 5.8 DU yr^{-1} for the period 2001–2010. The trend was, therefore, not statistically significant at the 95% confidence level.

More recently, Chipperfield et al. (2017) and Weber et al. (2018) both derived independent linear trends (ILTs) for September in Antarctica. Chipperfield et al. (2017) calculated the September Antarctic (60°–90°S) trend from 2000 to 2015 to be 4.7 ± 9.1% decade^{-1} using NASA SBUV data, while Weber et al. (2018), using five merged data sets from satellite and ground-based observations, found the 2000–2016 trend in September across the five data sets ranged between 8 to 10% decade^{-1} with a 2σ uncertainty of 7%. By contrast, the trend in October was only 3% decade^{-1} and not statistically significant (**Figure 4-15**). The fact that these two studies used almost the same data sets and similar methods but determined different results

Table 4-1. Trends in a selection of metrics of Antarctic ozone in spring since 2000 (the year with maximum halogen loading), derived from various data sets and using a variety of analysis methods. **Box 4-1** gives descriptions of the methods used. Note that only a subset of the results for the polar regions of each study are shown, each of which also considered additional parameters not shown here.

Parameter	Data Source	Trend	Confidence Level	Time Period	Method	Reference
TOTAL COLUMN OZONE						
Total column ozone September–November Antarctic	MSR + SCIAMACHY	3.1 ± 5.8 DU year^{-1}	±2σ	2001–2010	MLR (PWLT)	Knibbe et al. (2014)
Total column ozone September South Pole	Ozonesondes	2.5 ± 1.5 DU year^{-1}	90%	2000–2014	Linear trend excluding 2002	Solomon et al. (2016)
Total column ozone September, south of 63°S	SBUV	2.5 ± 1.6 DU year^{-1}				
Total column ozone locations of Antarctic stations September–November	TOMS/OMI	1.72-1.80 ± 0.8 % year^{-1}	95%	2001–2013	MLR (PWLT) with vortex filtering	Kuttipurath and Nair (2017)
Total column ozone September, 60°–90°S	NASA SBUV	4.7 ± 9.1 % decade^{-1}	±2σ	2000–2015	MLR (ILT)	Chipperfield et al. (2017)
Total column ozone September, 60°–90°S	Merged satellite data and WOUDC	8.1–10.1 ± 7 % decade^{-1}	±2σ	2000–2016	MLR (ILT)	Weber et al. (2018)
Total column ozone 15 September–15 October Antarctic vortex	MSR-2	1.42 ± 0.92 DU year^{-1}	±2σ	2001–2017	MLR (PWT) with vortex filtering	Pazmiño et al. (2018)
VERTICALLY RESOLVED OZONE						
Ozone mixing ratio September–November Antarctic vortex	Ozonesondes	Up to 8 % year^{-1}, significant between 325 and 550 K levels	95%	2001–2013	MLR (PWLT) with vortex filtering	Kuttipurath and Nair (2017)
Ozone partial column September South Pole, Syowa	Ozonesondes	"Clear increase" from 100 to 50 hPa	90%	2000–2015	Linear trend excluding 2002	Solomon et al. (2016)
OZONE HOLE METRICS						
Ozone hole area late September in cold years	AURA-MLS	Smaller in 2008, 2011 due to decreased Cl_y	—	2004–2012	Linear relationship	Strahan et al. (2014)
Ozone hole area September	TOMS/OMI	–4.5 ± 4.1 million km^2	90%	2000–2015	Linear trend excluding 2002	Solomon et al. (2016)
Ozone hole mass deficit between days 220 and 280	MSR-2 +GOME-2	–0.77 ± 0.17 Mt year^{-1}	±2σ	2000–2015	Linear trend 6 warmest years filtered	de Laat et al. (2017)
Ozone hole mass deficit 15 September–15 October	MSR-2	–0.68 ± 0.37 Mt year^{-1}	±2σ	2001–2017	MLR (PWT) with vortex filtering	Pazmiño et al. (2018)

Box 4-1. Methods Applied to Calculate Polar Ozone Trends

- ***Linear Trend***

  Linear trends since the year 2000 were used by Solomon et al. (2016), with the extreme year of 2002 filtered out. Similarly, de Laat et al. (2017) calculated a linear trend since 2000, after removing the six warmest years of the 1979–2015 record (1986, 1988, 2002, 2004, 2010, and 2012).

- ***MLR (Multiple Linear Regression)***

  Multiple linear regression is the most commonly used method to calculate the Antarctic ozone trend remaining after removing the influence of known sources of variability, such as eddy heat flux, solar variability, the Quasi-Biennial Oscillation (QBO), El Niño–Southern Oscillation (ENSO), and stratospheric aerosol loading. The significance of the resulting trend is sensitive to the choice of proxies used to represent physical processes, and the choices of spatial and temporal averaging and time period (de Laat et al., 2015). In previous Assessments, EESC was often used as a regressor variable.

- ***MLR with PWLT (Piecewise Linear Trends)***

  Following Kuttippurath et al. (2015), who warned that the fit of EESC to ozone time series was determined mostly by the years prior to turnaround, and therefore could result in an inaccurate recovery trend, fits to EESC are not used in this Assessment. Regression using PWLT instead fits two linear trends to the ozone time series before and after an appropriate "turnaround" year, usually either 2000 or 2001. The trends are constrained to give a common value at the turnaround year. PWLT was used by Knibbe et al. (2014).

- ***MLR with ILT (Independent Linear Trends)***

  Independent linear trends differ from PWLT in that the two linear trends are not constrained to meet at a common value at the turnaround year. This introduces an additional degree of freedom to the regression. Both Chipperfield et al. (2017) and Weber at al. (2018) used ILT.

- ***MLR with PWT (Piecewise Trends)***

  The "modified PWLT" model used by Pazmiño et al. (2018) is similar to ILT, but instead joins the two linear trends with a parabolic curve. This allows an overall improved regression result, as EESC and ozone show a non-linear growth rate around the period of the EESC peak.

reflects the uncertainty of the multiple linear regression method—in this case, the results show some sensitivity to the length of the time period and the treatment of the proxies.

Vertically Resolved Ozone

WMO (2014) reported the results of Hassler et al. (2011b) showing that ozone loss rates in springtime (measured by ozonesondes at South Pole between 100 and 40 hPa) had reached a maximum in the period 1991–1995 and had subsequently stabilized but had not shown any significant reduction between 2001 and 2010. The additional years of observational data from ozonesondes (Solomon et al., 2016; Kuttipurath and Nair, 2017) and Aura MLS (Strahan and Douglass, 2018) do now show evidence that Antarctic ozone within this height range has significantly increased since the year 2000.

Solomon et al. (2016) studied ozonesonde measurements from Syowa and South Pole stations in the month of September. They found a statistically significant increase in ozone over the period 2000–2015

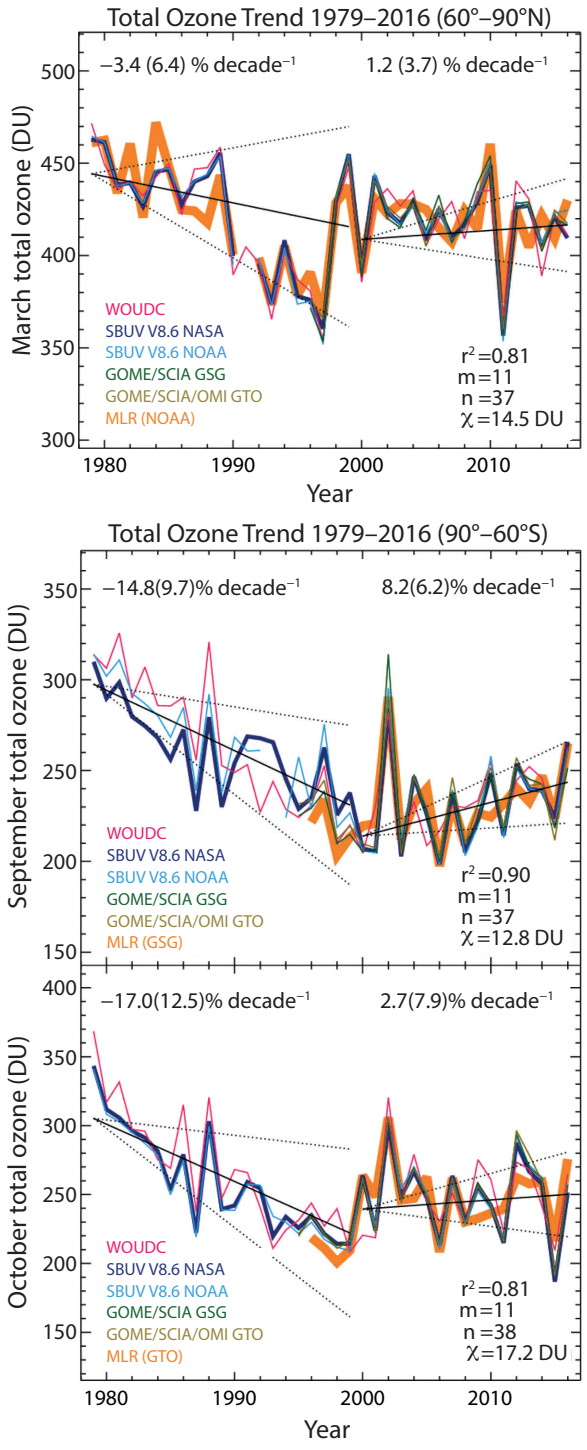

Figure 4-15. Total ozone time series for (*top panel*) the Arctic (60°–90°N) in the month of March and (*bottom two panels*) for Antarctica (60°–90°S) in the months of September and October, derived from five long-term observational data sets: WOUDC (based on the GAW network of ground-based Dobson and Brewer instruments), SBUV 8.6 processed by NASA, SBUV 8.6 processed by NOAA, GOME-SCIAMACHY-GOME-2(GSG) and GOME-type Total Ozone (GTO). In each panel, one data set has been chosen as labelled to show the results of applying a multiple linear regression with independent linear trends analysis (orange). Regressor terms include the solar cycle, QBO, ENSO, volcanic aerosol, and the strength of the Brewer-Dobson circulation. From Weber et al. (2018).

between 100 and 50 hPa, approximately half the size of the decrease measured in Syowa at this height between 1980 and 2000 **(Figure 4-16)**. Kuttipurath and Nair (2017) also found positive trends since 2001 reversing the pre-2000 vertically resolved trend using ozone profiles from ozonesonde stations distributed across Antarctica during the period 1979–2013 filtered according to their location as inside or outside of the Antarctic vortex at each altitude. For 2001–2013, they found the largest trends of up to 8% yr^{-1} around 15 km, with trends being significant at the 95% confidence level between approximately 12 and 22 km. Using simple linear trends without any dynamical or aerosol proxies gave similar results but increased the uncertainty of the trend, such that the trend was no longer significant over some of the height range.

Ozone Hole Metrics

Three metrics that have been widely used for many years to report on the state of the ozone hole from year to year are shown in **Figure 4-6**—the daily ozone hole area averaged from 21 to 30 September, the average of daily minimum ozone values from 21 September to 16 October, and the daily ozone mass deficit (OMD) averaged from 21 to 30 September. A fit of Antarctic EESC to each metric is also shown. It is apparent that all three metrics show a clear stabilization after the year 2000 when Antarctic EESC is calculated to have peaked, with the OMD showing both the greatest apparent turnaround since that date but also the largest variability. Note that in this figure, the fit has not taken into account dynamical variability, most evident for all three metrics in the year 2002 when the Antarctic vortex experienced an unprecedented major sudden stratospheric warming. Negative trends (that is, towards a smaller ozone hole) can now be seen in ozone hole area (Strahan et

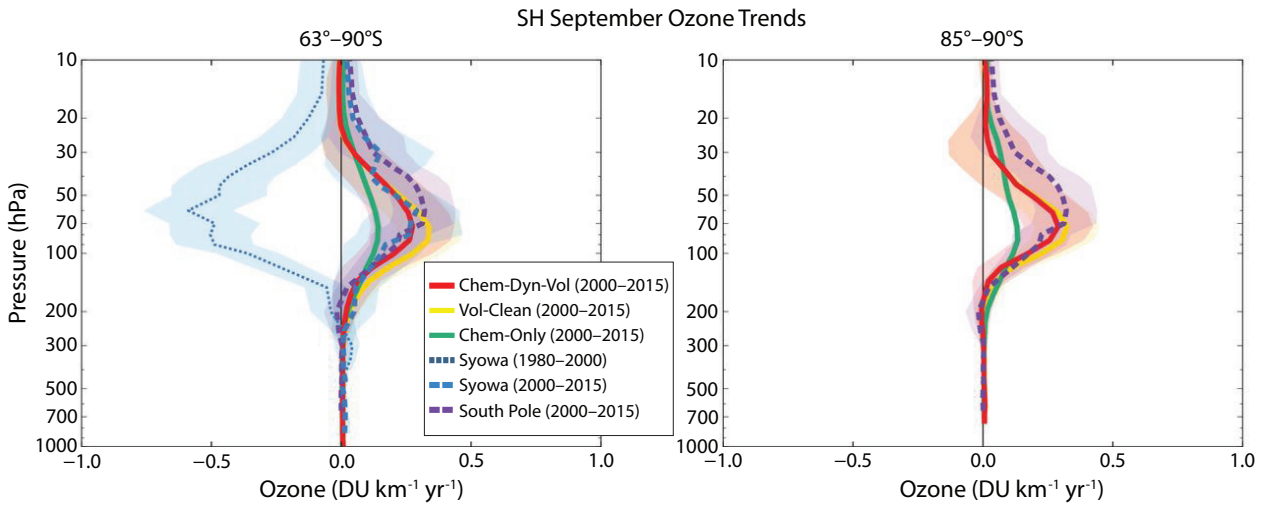

Figure 4-16. Trends in ozonesonde data from Syowa (69°S, 39.58°E) and South Pole stations with years as marked, with shading indicating the 90% confidence interval. Overlaid are model results from the WACCM model for regions 60°–90°S (*left*) and 85°–90°S (*right*) forced with different combinations of halogen changes ("chem"), specified dynamics ("dyn"), and injection of aerosols from volcanic eruptions ("vol"). (From Solomon, S., D.J. Ivy, D. Kinnison, M.J. Mills, R.R. Neely III, and A. Schmidt (2016), Emergence of healing in the Antarctice ozone layer, *Science*, *353* (6296), 269-274. Reprinted with permission from AAAS.)

al., 2014; Solomon et al., 2016) and ozone hole mass deficit (de Laat et al., 2017) once temperature fluctuations have been taken into account. The closeness with which particular ozone hole metrics follow the evolution of EESC varies with different choices of threshold and period of the year, due to saturation effects and, as already noted, the increased influence of dynamics in October compared to September (Solomon et al., 2016; Pazmiño et al., 2018).

Strahan et al. (2014) found that, comparing the ozone hole area in the very cold years of 2006, 2008, and 2011, the progressive reduction in size was proportional to declining EESC inferred from Aura MLS observations. Solomon et al. (2016) considered the size of the Antarctic ozone hole in September of each year, derived from TOMS/OMI data. From 2000 to 2015, the area decreased by 4.5 ± 4.1 million km^2.

The OMD between days 220 and 280 (from early August to early October) of each year was considered by de Laat et al. (2017) as derived from total column ozone measurements from multiple satellite instruments. Including all years in the trend, the decrease from 2000 to 2015 was 0.52 ± 0.50 Mt yr^{-1}. When excluding the six warmest years (1986, 1988, 2002, 2004, 2010, and 2012) from the record in order to remove the largest fluctuations caused by meteorological variability, the OMD decreased by 0.77 ± 0.17 Mt yr^{-1} (2σ). From 2000 to 2015, OMD defined in this way was estimated to have decreased about 30% from its peak value. Similar values were calculated using MLR with PWT (**Box 4-1**) by Pazmiño et al. (2018), who found a negative trend of OMD in September of 0.86 ± 0.36 Mt yr^{-1} since 2001, or 0.65 ± 0.33 Mt yr^{-1} if averaged over the period of maximum depletion, 15 September to 15 October.

Attribution to Decline in EESC

Attributing the trends in Antarctic ozone discussed in the previous sections to a decline in stratospheric halogen abundances is challenging, as the trend in EESC is small compared to the large variability in Cl_y due to transport, as derived from Aura MLS measurements between 2004 and 2012 (Strahan et al., 2014). Nevertheless, Strahan and Douglass (2018) using a longer Aura MLS data set until 2016, showed that vortex-averaged ozone loss (defined as the observed changes in partial column ozone between 261 and 12 hPa from July to mid-September) decreased over the 12-year data record because of the decline in lower stratospheric Cl_y levels. By analyzing ozone changes

over this seasonal average, dynamical contributions to ozone change are minimized.

Further evidence of a response of Antarctic ozone to declining ODSs was given by Solomon et al. (2016) by comparing measurements with CCM sensitivity simulations with different specified forcings. They showed (using model runs that held the dynamical conditions, temperatures, and volcanic aerosols constant at 1999 levels) about half of the lower stratospheric ozone increase in September observed between 2000 and 2014 was due to halogen decrease, with the remainder attributed to changes in dynamics and temperature (**Figure 4-16**). Likewise, the model results suggest that about half of the total column increase in September observed over that period is due to declining ODS levels (~ +1.3 DU yr^{-1}). The ozone hole was estimated to have decreased by 3.5 ± 0.3 million km^2 as the result of decreasing chlorine and bromine.

Further, Solomon et al. (2017) analyzed the seasonality of modeled and observed trends in Antarctic stratospheric ozone and stratospheric temperatures. The changes observed prior to 2000 were followed by oppositely signed changes after 2000 very similarly patterned in terms of season and altitude. These "mirrored" changes were largely able to be replicated by CCM runs only when forced with measured ODS levels, with a relatively small role being played by unforced dynamical changes. This finding is supported by de Laat et al. (2017) who found in their analysis of OMD in multi-sensor reanalysis (MSR) data that the ratio of pre- and post-2000 trends in OMD matched those in Antarctic EESC, seconded by regression results suggesting long-term changes in PSC volume and pre-winter ozone levels had played only minimal roles.

Modeling results (Solomon et al., 2017; Randel et al., 2017) suggest that observed changes in Antarctic ozone have significantly contributed to the observed cooling in Antarctic stratospheric springtime temperature from 1979 to the late 1990s and the subsequent warming trend to the present time. A component of the temperature variability discussed in the context of detecting ozone recovery should therefore be considered a feedback from EESC changes rather than being purely unforced.

4.4.2.3 Summary

While in the prior Assessment only two to three studies claimed to have found early signs of Antarctic ozone recovery, a number of studies has been presented since then. These used various new merged data sets and observations, including four more years since WMO (2014), as well as chemistry–climate model simulations to attribute the observed changes.

It is noteworthy that independent of the data set, time period, and analysis method, all studies derive trends in different metrics of Antarctic ozone of the same overall sign; i.e., they all show increasing total column ozone and ozone in the lower stratosphere, decreasing ozone hole area, and decreasing ozone mass deficit since about 2000 in Antarctic springtime. Some trends are statistically significant at the 2σ level, while others are either barely significant or not significant for various reasons, with differences arising for example from the applied regression model or the time period. However, it was found that the significance of the derived trends rises for the month of September when dynamical activity of the Antarctic polar vortex is small and chemical ozone depletion not saturated as in October. Particularly in the month of September, several metrics of Antarctic ozone have shown significant reductions of depletion in the years following the peak in EESC. By employing model simulations or other means, it has been shown that a portion of the positive trend in ozone can now be attributed to declining ODS levels. Therefore, it can now be concluded that the early signs of the second stage of Antarctic ozone recovery are becoming apparent.

4.4.3 Long-Term Arctic Ozone Trend

As stated in previous Assessments, detection of ozone recovery in the Arctic is much more difficult than the Antarctic, chiefly because of the much larger dynamical variability. Knibbe et al. (2014) analyzed spatial variations in monthly total column ozone for the period 1979–2012 in the Arctic but did not find any trend. Solomon et al. (2016) did not find statistically significant trends in springtime Arctic SBUV data (63°–90°N) for the period 2000–2014, with their model results suggesting the small positive trend expected from EESC decline is currently overwhelmed by dynamical effects. The study of Weber et al. (2018) described above found trends in the Arctic in March

were less than 1% decade^{-1} and not significant (**Figure 4-15**).

4.4.4 Benefits Achieved by the Montreal Protocol

By comparing model simulations using an uncontrolled growth of ODSs (unaffected by the Montreal Protocol) with simulations using ODS mixing ratios controlled by the Montreal Protocol, it is possible to identify how polar ozone would have developed in a "world avoided" with continuously growing ODS abundances. Moreover, the extent to which the polar ozone layer has already (in the recent past) benefited from the Montreal Protocol can be derived. CCM simulations assuming either a total chlorine loading of 9 ppbv for ~2025 or a growth rate of 3% yr^{-1} (leading to 9 ppbv in 2019) showed that uncontrolled growth in the emissions of ODSs would lead to ozone depletion in the coming decades much larger than projected for a controlled chlorine loading (Morgenstern et al., 2008; Newman et al., 2009; WMO, 2011; Garcia et al., 2012).

Chipperfield et al. (2015) used a state-of-the-art 3D chemistry transport model to investigate a "world avoided" scenario, comparing a simulation based on observed atmospheric ODS loading to one in which continued growth in ODS production of 3% yr^{-1} after 1987 is assumed (**Figure 4-17**). In Arctic winter 2010/2011, when the OMI satellite instrument shows a local ozone column of around 230 DU, the integration without Montreal Protocol regulation indicates a greatly reduced ozone column below 120 DU (**Figure 4-17e**). On 26 March 2011, a region of relatively low column ozone (250–275 DU) emerges in the observations (**Figure 4-17a**) and the model run with observed ODSs (**Figure 4-17b**). With the "world avoided" scenario, however, a further dramatic decrease in column ozone by up to 130 DU over a wide region of the Arctic occurs. Without the Montreal Protocol, a deep Arctic ozone hole would have developed in 2011 (**Figure 4-17c**). The Antarctic ozone hole would have been 40% larger by 2013 (with enhanced loss at subpolar latitudes) and longer-lived each year. Smaller Arctic ozone holes would have become a regular occurrence as chemical ozone depletion would have a stronger effect on Arctic ozone in spring than dynamic variability.

4.5 FUTURE CHANGES IN POLAR OZONE

This section discusses the future evolution of polar ozone as projected by new chemistry–climate model (CCM) simulations coordinated within the IGAC/SPARC Chemistry-Climate Model Initiative CCMI (Eyring et al., 2013a). The CCMI model data set provides an update of previous ozone projections obtained from the second phase of the SPARC Chemistry-Climate Model Validation (CCMVal, referred to as CCMVal-2; SPARC CCMVal, 2010) activity that formed the basis of projections of future ozone for the prior two Assessments (WMO, 2011; 2014).

4.5.1 New Ozone Projections from Chemistry–Climate Models

As a result of continuing global CCM activities, new model simulations have been produced. The majority of CCMs that participated in CCMI had already been part of CCMVal-2; many of these models have been further refined since the earlier activity. Improvements of some of the CCMI models compared to their CCMVal-2 versions include

- more detailed chemistry schemes, with enhanced tropospheric chemistry, a more consistent representation of sulfate surface area densities, and the consideration of the effects of naturally produced very short-lived (bromine) substances (VSLSs) on ozone depletion, and
- interactive coupling of the atmosphere-only CCMs to deep-ocean models, hence improving the representation of climate feedbacks in particular (as in 'classical' Coupled Model Intercomparison Project Phase 5 (CMIP5)-type climate models).

A detailed overview of the applied CCMs including model expansions and improvements since CCMVal-2 is given in Morgenstern et al. (2017).

The performance of the previous CCM generation that provided the ozone projections for the prior two Assessments has been evaluated in detail within the SPARC CCMVal activity. SPARC CCMVal (2010) compared the quality of the dynamics and transport, as well as of the radiation and chemistry schemes, and offered a useful baseline for evaluating the results of later model studies. So far, a similar coordinated

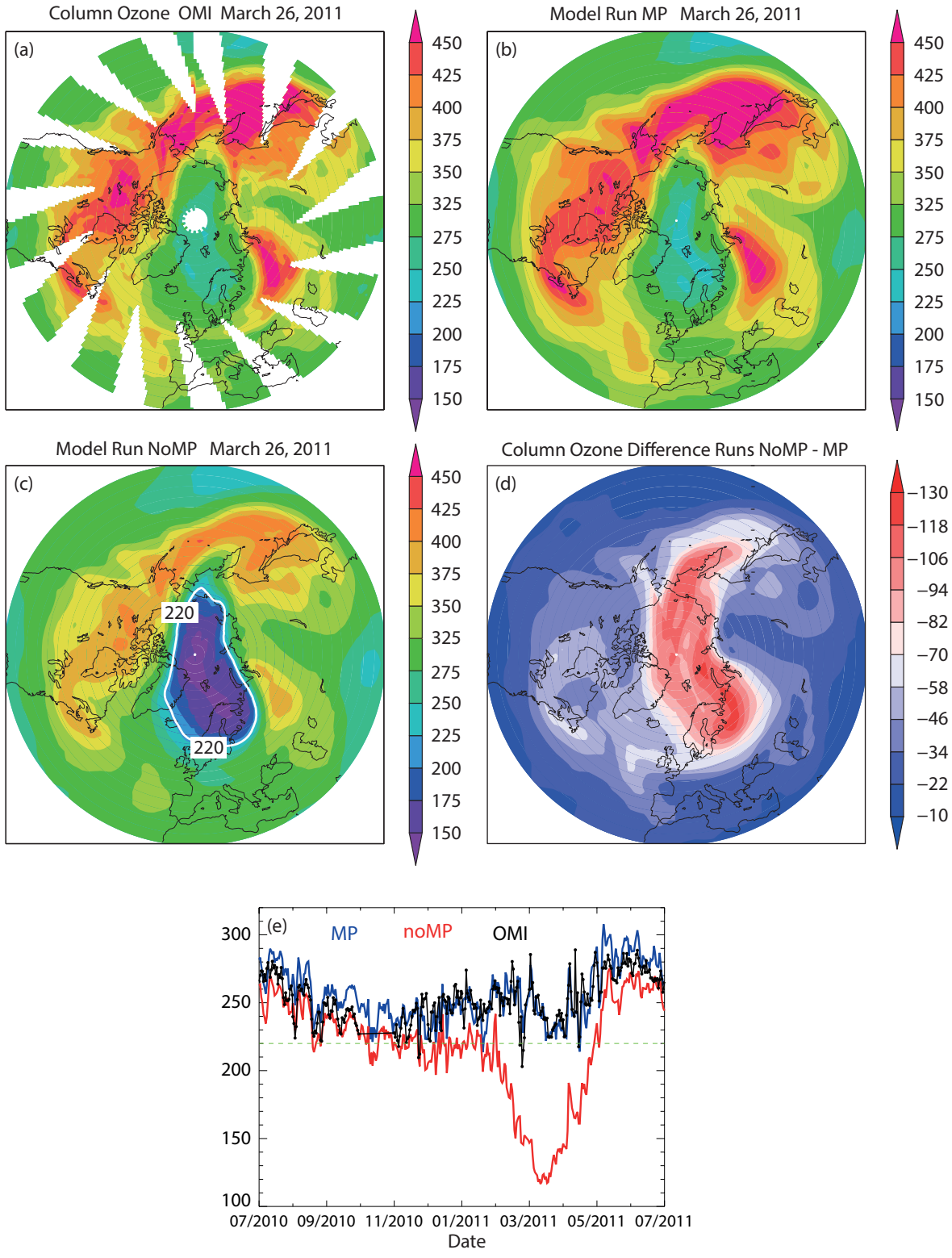

Figure 4-17. Evolution of column ozone in the Arctic from satellite observations and model simulations for winter 2010/2011. Column ozone (DU) on 26 March 2011 (a) observed by OMI, (b) from model run with ODSs controlled by the Montreal Protocol (MP), and (c) from model run with uncontrolled ODSs (NoMP) (with the 220 DU contour indicated in white). (d) Difference in column ozone between runs NoMP and MP. (e) The daily minimum ozone column in the Arctic region (latitude >45°N) from mid-2010 to mid-2011 as observed by the Ozone Monitoring Instrument (OMI) (black points), along with equivalent model results from run MP (blue) and run NoMP (red). From Chipperfield et al. (2015).

evaluation has not been completed for the current CCM versions, though a large number of analyses of the CCMI models focusing on different topics is underway (e.g., Wales et al., 2018; Dietmüller et al., 2018) A comprehensive comparison of ozone return dates in the CCMI, CMIP5, and CCMVal-2 simulations is presented in Dhomse et al. (2018).

A suite of CCMI simulations has been performed by the modeling groups using a standard set of specific forcings according to the recommendations in Eyring et al. (2013a); the relevant simulations and forcings for this Assessment are summarized in **Box 3-2**, "Modeling past and future changes in ozone: Model heritage and application". The most probable projections of the future evolution of polar ozone rely on the reference simulations (REF-C2) that are driven by an assumed decline of ODSs (WMO, 2011), the effects of brominated VSLSs, and a concurrent increase in GHG concentrations according to the RCP-6.0 scenario (Meinshausen et al., 2011). Sensitivity (SEN) simulations address the uncertainty of polar ozone recovery induced by different GHG scenarios and the attribution of ozone recovery to future changes in ODSs and GHGs.

As a novel aspect of CCMI, CCM simulations with specified dynamics (SD) have been performed for the historical period (1960–2010). The setup of these REF-C1SD simulations is specified in **Box 3-2.** The

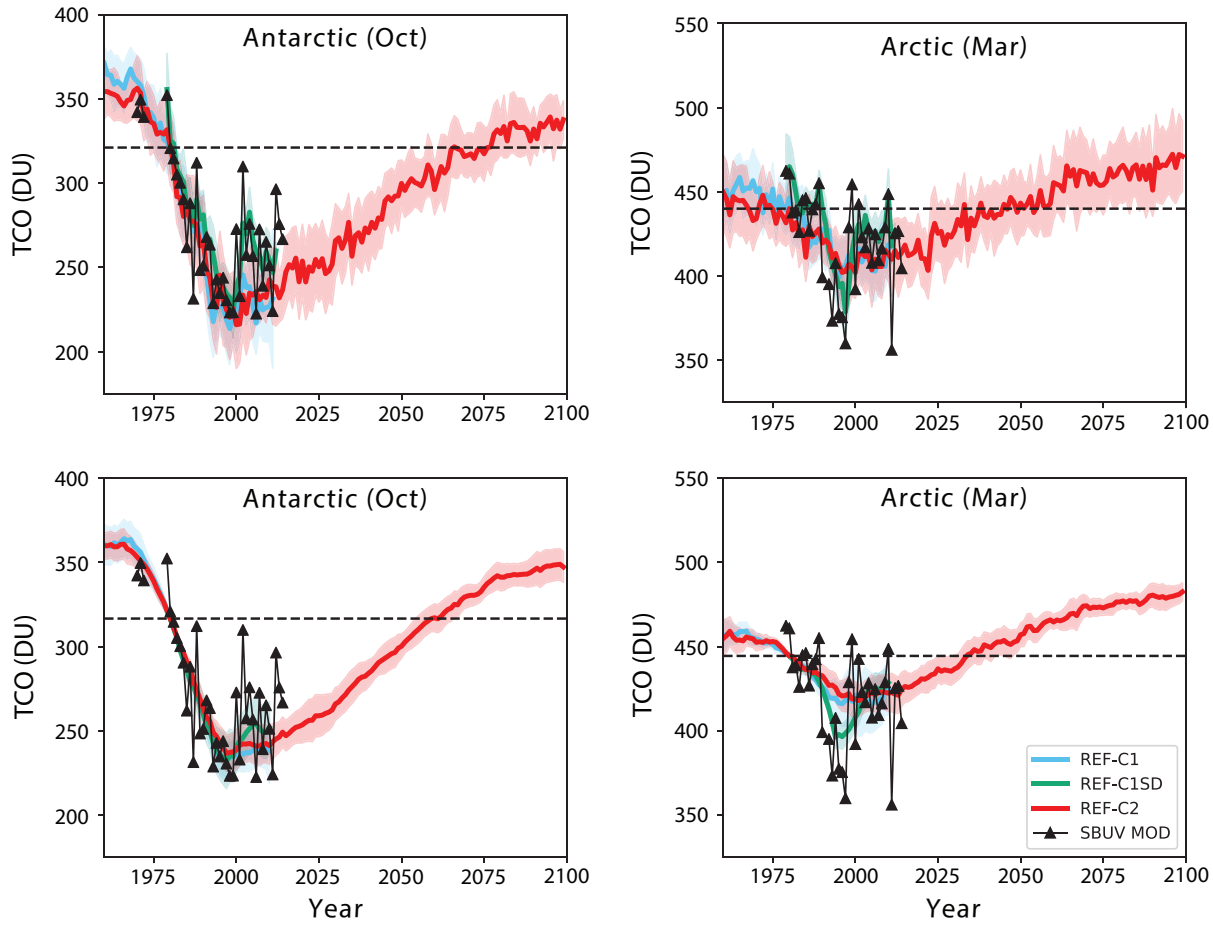

Figure 4-18. Multi-model mean (MMM1S) total column ozone time series (in Dobson Units, DU) from CCMI REF-C1 (light blue), REF-C1SD (green) and REF-C2 (red) simulations for the (*left*) SH polar (October) and (*right*) NH polar (March) regions. The dashed black lines show the 1980 reference value for each latitude band. The *top row* shows the unadjusted modeled values and the *bottom row* shows the time series adjusted with respect to mean 1980–1984 observations. Also shown are the merged SBUV observations. From Dhomse et al. (2018).

dynamics in the REF-C1SD simulations are adjusted ("nudged") towards observations or reanalysis data that represent the observed dynamical behavior of the atmosphere. Through the nudging, the model dynamics in the REF-C1SD simulations are forced to closely follow observed dynamical variability from year to year. These simulations thus provide realistic variability in the transport of chemical compounds and temperatures, in contrast to free-running CCMs that develop their own internal dynamical variability. The REF-C1SD runs therefore allow for a more detailed evaluation of the chemical processes (e.g., Solomon et al., 2015). A comparison of the REF-C1SD results with those from free-running REF-C1 simulations also helps to identify inaccuracies in the representation of dynamical processes in CCMs.

Figure 4-18 presents the multi-model mean (MMM1S) total column ozone time series from the REF-C1 (light blue) and REF-C1SD (green) simulations. MMM1S results represent the mean of the models that lie within one standard deviation (1σ) of the multi-model mean (MMM). Time series are shown for the unadjusted multi-model means (MMM1S) of the REF-C1, REF-C1SD, and REF-C2 simulations (top row) and the same MMM1S adjusted with respect to the mean 1980–1984 observations (bottom row) in Antarctic October (left) and Arctic March (right) (for more details see Dhomse et al., 2018). The top panels demonstrate that, as expected, the REF-C1SD simulations (i.e., in which the models are nudged towards analyzed meteorology) better reproduce the observed evolution of total column ozone than the REF-C1 simulations (i.e., the free-running CCMs). Both sets of simulations show the decline of the total ozone column until about the year 2000 in spring of the Northern and Southern Hemispheres. The REF-C1SD runs, however, better capture the observed year-to-year variability. Due to the averaging of individual model results, enhanced total ozone variability is suppressed in the MMM1S of the REF-C1SD simulations, as for example in the Arctic around the turn of the century and in the Antarctic during the following decade. Nevertheless, with constrained dynamics, the CCMs perform well in simulating the ozone evolution in the Antarctic and Arctic, giving confidence that the basic chemical processes and the ozone response to long-term ODS changes are understood.

4.5.2 Long-Term Projections of Polar Ozone

This section focuses on the future evolution of Antarctic and Arctic polar ozone projected by state-of-the-art CCMs following the best estimates of future decline in ODSs and increase in GHG concentrations. For this purpose, the CCMI REF-C2 simulations are analyzed for which the medium RCP-6.0 GHG scenario has been prescribed. Apart from refinements of the models, the experimental setup differs from the projections shown in WMO (2011) and WMO (2014) due to updates in the ODS and GHG scenarios (see also **Box-3-3**, "Ozone Return Dates") and the consideration of brominated VSLSs. The potential implications of these changes on the ozone return to historical values will be discussed in **Section 4.5.4**.

4.5.2.1 Future Antarctic Spring Total Column Ozone

Figure 4-18 (left) shows the future evolution of total column ozone (TCO) in the Antarctic (60°–90°S) in October for the multi-model mean of the REF-C2 simulations (red lines in **Figure 4-18**) from 20 CCMs (Dhomse et al., 2018). In the past (1960–2010), the multi-model mean (MMM1S) TCO shows good agreement with observations including the strong decrease of Antarctic ozone in the 1980s and early 1990s. A broad TCO minimum occurs around the year 2000. It is about 80 DU lower than the 1980 value, confirming the results presented in WMO (2011). In the future, the ozone hole will recover and a return of TCO to values of the year 1980 is expected to occur shortly after mid-century (between 2055 and 2066). Compared to the last Assessments (WMO, 2011, 2014), the current estimate is postponed by about 10 years. The previous earliest and latest projected return dates of Antarctic TCO (referring to the 1980 level) in October are also delayed by about 5 years (see also **Figure 4-22**). Possible reasons for these discrepancies are discussed in **Section 4.5.4**.

4.5.2.2 Future Arctic Spring Total Column Ozone

The temporal evolution of Arctic spring TCO derived from the CCMI simulations is presented for March in **Figure 4-18** (right). It shows the TCO MMM1S (60°–90°N) until 2100 derived from the REF-C2

simulations (red lines in **Figure 4-18**) of 20 CCMs (Dhomse et al., 2018). Again, model results representing the past are indicating qualitative agreement with observations concerning the long-term behavior, although the strong decrease of TCO in the 1990s, particularly in the years after the eruption of Pinatubo, is underestimated by the MMM1S. In the future, a return to TCO values of 1980 is expected before mid-century (between 2025 and 2043). Hence, the new projections suggest a return date for Arctic spring TCO that is delayed by 4 years compared to the CCMVal-2 estimate (WMO, 2011; 2014) (see also **Figure 4-22**). The range of potential TCO return dates is broader in the CCMI models, extending from 2025 (as for the CCMVal-2 models) to 2043, i.e., 8 years later than the CCMVal-2 models.

4.5.3 Factors Controlling Future Polar Ozone

4.5.3.1 Changing Roles of ODSs and GHGs

Whereas ODSs are expected to continue to decrease due to the controls of the Montreal Protocol, GHG concentrations are expected to continue to rise. Hence, the relative effects of ODSs and GHGs on polar ozone will change with time. For the most likely scenario of future ODS and GHG changes (i.e., REF-C2) the models project a return of TCO to historical values in the coming decades (see **Figure 4-18**). In this section, CCMI sensitivity simulations with separated forcings are discussed in order to disentangle the individual impacts of the ODS and GHG changes on the evolution of ozone.

In simulations with constant ODSs between 1960 and 2100 and growing GHG abundances (i.e., SEN-C2-fODS simulations), Antarctic total column ozone (TCO) in October shows only a small, non-significant positive long-term trend with weak year-to-year variations (**Figure 4-19**, top panel). A slight ozone increase after the middle of the 21st century results from stratospheric cooling forced by rising GHG

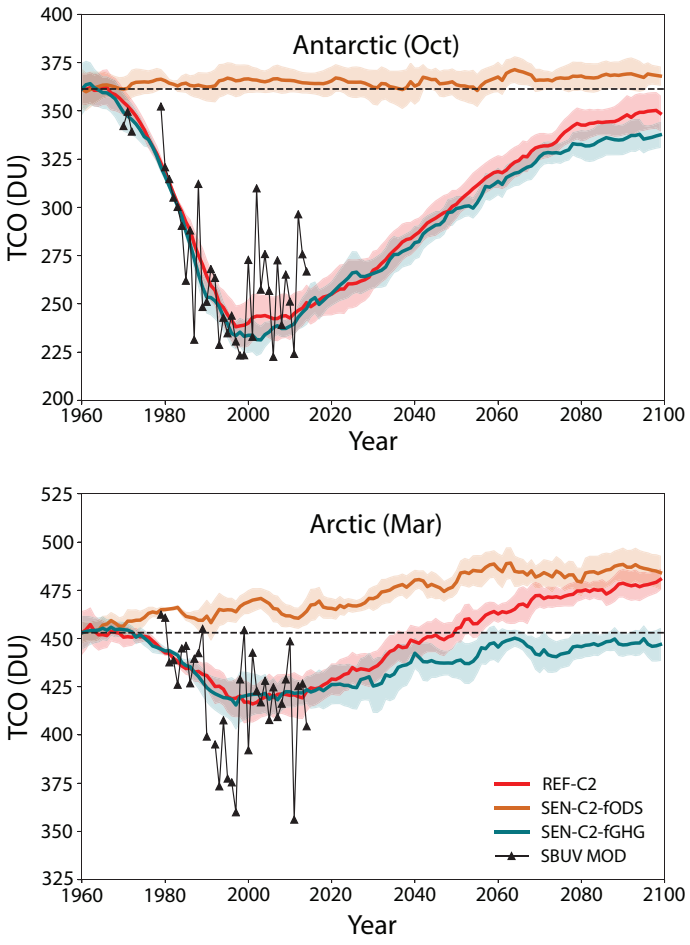

Figure 4-19. Temporal evolution of multi-model means (MMM1S) of total column ozone (in Dobson Units, DU) derived from REF-C2 (red), SEN-C2-fODS (brown), and SEN-C2-fGHG (green) CCMI scenario calculations for Antarctic spring (October, *top panel*) and Arctic spring (March, *bottom panel*). SEN-C2-fODS simulations use fixed ODS levels of the year 1960, while SEN-C2-fGHG simulations use fixed GHG levels of the year 1960. Black triangles indicate observations derived from SBUV MOD data. The black dashed lines denote the 1960 reference values for each region. Adapted from Dhomse et al. (2018).

concentrations. When GHGs are held constant at their 1960 values but ODSs vary according to the prescribed reference scenario (i.e., SEN-C2-fGHG simulations), the evolution of TCO closely follows that of the REF-C2 reference simulation. After the middle of the century, the GHG effect in the REF-C2 simulations accelerates Antarctic ozone recovery and leads to about 10 DU higher TCO around 2100 than with constant 1960 GHG concentrations. Hence, the evolution of the ODSs exerts the dominant influence on Antarctic TCO change modulated by a minor effect of GHGs in the second half of the century. Although the GHG effect strengthens Antarctic ozone recovery from ODSs, the 1960 baseline value will not be reached by the year 2100.

In Arctic spring, TCO gradually increases with time in the SEN-C2-fODS simulation with constant 1960 ODS levels (**Figure 4-19**, bottom panel). This ozone increase is caused by rising GHG concentrations which (a) cool the stratosphere, thereby reducing chemical gas-phase ozone depletion and (b) strengthen the Brewer-Dobson circulation (BDC) leading to a growing poleward and downward transport of ozone in Arctic spring (e.g., Oman et al., 2010; Oberländer et al., 2013). When prescribing GHG values for the 1960s (i.e., in SEN-C2-fGHG) throughout the whole projection, TCO closely follows the values of the REF-C2 reference simulation until about 2020. Afterwards, TCO in the simulation with constant 1960 GHG concentrations gradually approaches its 1960 values until the end of the 21st century, in contrast to the reference simulation where the rising GHG abundances induce an additional ozone increase, as described above. Hence, as in the Antarctic, the ODSs have been the primary driver of observed Arctic TCO trends in the past. However, in contrast to Antarctica, changes in GHGs will exert the dominant control over Arctic ozone distributions by the late 21st century. As demonstrated in CCM sensitivity studies with specified single or combined forcings (Rieder et al., 2014; Douglass et al., 2014; Kirner et al., 2015b; see also **Section 4.5.3.2**), past ODS changes mainly affected Arctic lower stratospheric ozone, while changes of GHG concentrations mainly affect the upper stratosphere. In addition, the growing GHG abundances in the REF-C2 scenario drive a stronger transport of ozone into the Arctic stratosphere. In total, whereas the decline in ODSs allows TCO to recover towards its 1960 baseline in the Arctic, the concurrent increase in GHGs induces not only an earlier return of Arctic TCO to its 1960 baseline value (in the 2040s for the REF-C2 MMM1S) but also a further TCO increase by about 20 DU by the end of the century.

These results reinforce the major findings of Eyring et al. (2010a) which were based on similar sensitivity simulations from a limited number of CCMVal-2 models. The additional CCMI simulations thus enhance the confidence in the models' responses to changing ODS and GHG concentrations.

4.5.3.2 Dynamic Variability in Arctic Spring

Particularly in the Arctic, CCM results show that the role of dynamical processes for determining springtime ozone will increase in the future. Individual CCM simulations indicate that even after 2040, when Arctic ozone is expected to have increased due to the effects of declining ODSs and rising GHGs, early springtime Arctic total column ozone can episodically drop by about 50 to 100 DU below the long-term mean for that period, reaching stratospheric ozone values characteristic of the near-present-day average ozone level (e.g., Langematz et al., 2014; Bednarz et al., 2016). This is due to the large year-to-year variability of the Arctic polar vortex. In the presence of a very cold, strong, and persistent polar vortex in late winter and early spring (as observed during March of 1997, 2011, and 2015), enhanced formation of polar stratospheric clouds (PSCs), and elevated halogen-induced ozone losses well above the long-term mean continue to occur. Together with reduced poleward transport of ozone, these factors contribute to the low total column ozone values as for instance measured in spring 1997.

For the future, CCM studies project a significant cooling trend in the Arctic winter mid- and upper stratosphere due to enhanced GHG concentrations (e.g., Oberländer et al., 2013; Rieder et al., 2014). There is, however, less confidence in the projected temperature trends in the Arctic lower stratosphere (e.g., Langematz et al., 2014; Rieder et al., 2014; Bednarz et al., 2016). Langematz et al. (2014) found in their CCM study that rising GHG concentrations lead to a cooling of the Arctic lower stratosphere in early winter.

However, their model did not show any significant temperature changes in late winter or spring. Neither was a statistically significant increase in the volume of PSCs (V_{PSC}), a temperature-dependent metric that is linearly correlated with wintertime chemical ozone loss (Rex et al., 2004), found throughout the 21st century. Nevertheless, CCM projections suggest the possibility that in the presence of a cold and strong polar vortex higher V_{PSC} and halogen-induced ozone losses may occur in individual Arctic winter/spring seasons until the middle of the 21st century (Langematz et al., 2014) or even into the second part of the century (Bednarz et al., 2016).

4.5.3.3 The Role of GHG Scenarios

As discussed in the previous sections, rising GHG concentrations influence the future recovery of stratospheric polar ozone. Ozone is not only affected by carbon dioxide (CO_2) through cooling of the upper stratosphere and modifying ozone transport but also by the GHGs methane (CH_4) and nitrous oxide (N_2O) through both radiative and chemical effects (Chapter 2 in WMO, 2014). Therefore, a projection of the return of ozone to a historical baseline will depend on the specific GHG scenario. Three different climate change scenarios (representative concentration pathways, RCPs, Meinshausen et al., 2011), i.e. RCP-4.5, RCP-6.0 (= REF-C2), and RCP-8.5 have been discussed in Dhomse et al. (2018). Note that the modest RCP-2.6 scenario was not included in the analysis because the number of model realizations for this scenario was too low. In **Figure 4-20** the total column ozone (TCO) (top row) as well as the partial column ozone (PCO) for the upper (second row) and lower stratosphere (third row) and the troposphere (bottom row) are presented for the subset of CCMI models that carried out simulations with different RCPs.

In Antarctic spring (October) (left column in **Figure 4-20**) slight differences between the RCPs begin to emerge in the upper stratosphere (US) and the troposphere in the middle of the century. In the US, ozone directly responds to the RCP scenario with the smallest ozone increase in the RCP-4.5 scenario and the largest ozone increase in RCP-8.5. In the RCP-8.5 scenario, the GHG-induced cooling is most pronounced, and subsequently, the temperature-dependent reduction in chemical ozone depletion strongest. All RCP scenarios project higher US partial ozone columns by the end of the century than existed in the US before the start of ODS-induced ozone depletion. In the troposphere, the assumed strong increase in CH_4 of the RCP-8.5 scenario will enhance ozone production more than in the other scenarios. No significant differences between the RCPs appear, however, in the lower stratosphere (LS). The projected warming of the Antarctic LS in spring, particularly in the first half of the 21st century when the ozone hole starts to diminish (see **Figure 5-8** in Chapter 5 of this Assessment), more than offsets a potential GHG-induced cooling (leading to heterogeneous ozone depletion). When integrated over the layers, TCO in Antarctic spring does not reveal significant differences between the GHG scenarios throughout the century. In the US, where ozone differences by the RCPs are most pronounced, PCO returns earlier to its 1980 values than TCO. However, differences in the US PCO return dates between the RCPs are not significant. As discussed in the previous section, ODSs are the dominant driver of ozone recovery in the South Polar lower stratosphere, even with more extreme future GHG abundance.

In Arctic spring, the effects of the extreme RCP-8.5 scenario become progressively more important for TCO and the stratospheric and tropospheric PCOs in the second half of the century (**Figure 4-20**, right column). While the stratospheric cooling in the RCP-8.5 scenario drives the stronger increase of US PCOs, the LS ozone growth is related to the projected strengthening of the Brewer-Dobson circulation with enhanced ozone transport into the LS. Tropospheric ozone increase is strongest in the RCP-8.5 scenario due to steadily rising levels of atmospheric CH_4 that reach 3.7 ppm by the end of the century. Adding the ozone changes in the different atmospheric layers yields higher TCO for the RCP-8.5 scenario compared to the more moderate scenarios. In the second half of the 21st century, the impact of GHGs is the dominant driver of stratospheric ozone changes. For all GHG scenarios, a "super-recovery" of Arctic spring TCO (i.e., an ozone increase above its concentrations in the 1960s and 1970s, when anthropogenic ozone depletion started) is projected. By 2100, the Arctic springtime stratospheric ozone column is expected to exceed 1960–1980 average values by about 35 DU for RCP-4.5 and about 50 DU for RCP-8.5 (Dhomse et al., 2018).

The different hemispheric sensitivity of future polar TCO to the climate change scenario was also found

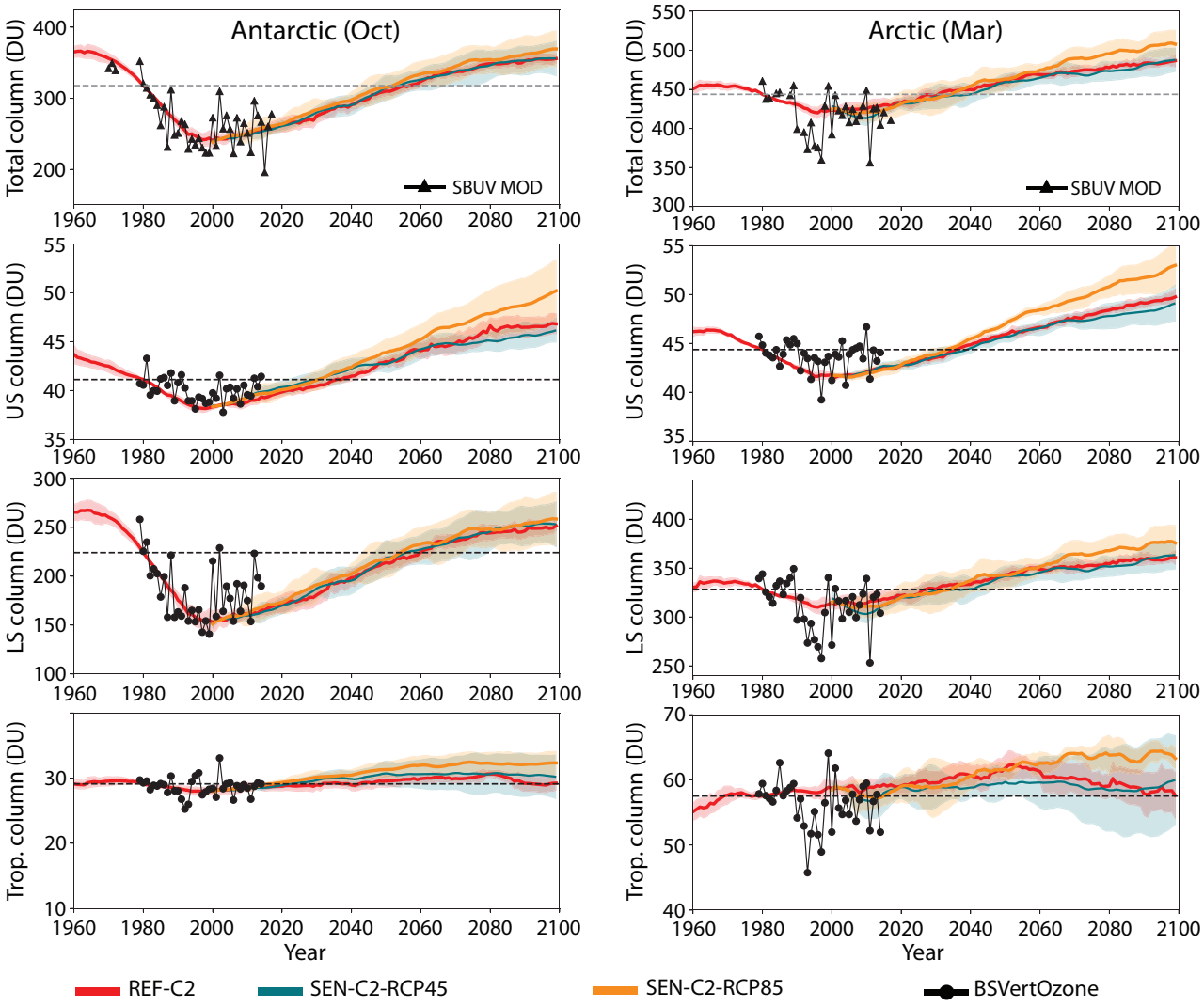

Figure 4-20. (*top*) Evolution of total column ozone (in Dobson Units, DU) MMM1S for the CCMI REF-C2 simulation (red lines) and the CCMI RCP scenario simulations SEN-C2-RCP45 (blue-green lines) and SEN-C2-RCP85 (orange lines). The REF-C2 simulation uses the RCP-6.0 scenario. Also shown are the partial ozone columns for the upper stratosphere (*second row*), the lower stratosphere (*third row*) and the troposphere (*bottom*). For comparison the respective total and partial ozone columns are shown. The black dashed lines denote the 1980 reference values for each region and layer. Adapted from Dhomse et al. (2018).

in analyses of the CMIP5 model subset with interactive chemistry (e.g., Eyring et al., 2013b), as well as in the ACCMIP model ensemble (Iglesias-Suarez et al., 2016). In the CCMI projections, however, the influence of the RCPs on TCO starts later in the century, and the TCO spread between RCPs is smaller than for the CMIP5 models in both hemispheres.

The RCP scenarios consist of projected concentration changes for a number of GHGs (most importantly CO_2, CH_4, and N_2O), which all have similar radiative effects, but differ in their chemical effects on ozone. As discussed previously, during the latter half of the 21st century, as ODS concentrations are expected to decline, GHGs become more relevant for ozone. Model studies indicate that in particular the future CO_2, N_2O, and CH_4 will have significant impacts on global total ozone (e.g., Fleming et al., 2011). The quantification of the net impact of these gases on future polar ozone is complicated by competing effects: Increasing N_2O concentrations will produce more NO_y and enhance ozone depletion, thereby reducing

the ozone increase due to CO_2-induced cooling and increases in CH_4 (Oman et al., 2010; Revell et al., 2012). However, ozone depletion by NO_y is less effective with decreasing temperature in the middle and upper stratosphere (Rosenfield and Douglass, 1998). In addition, chemical feedback processes reduce the efficiency of increasing N_2O to deplete ozone, as with increasing CO_2, less NO_y is produced (e.g., Portmann et al., 2012; Stolarski et al., 2015). Nevertheless, Revell et al. (2015) show that the ozone depletion potential (ODP) of N_2O for the year 2100 varies under different scenarios and is mostly larger than for the year 2000. Butler et al. (2016) describe how mitigation strategies may be adapted to the evolution of the individual gases: if reductions of CO_2 and CH_4 concentrations to RCP-2.6 levels (a low emissions scenario) could be achieved by the end of the 21st century, no super-recovery of stratospheric ozone is expected and N_2O mitigation would become important to avoid further ozone depletion. On the other hand, if CO_2 and N_2O were reduced to RCP-2.6 levels but CH_4 concentrations increased, stratospheric ozone would increase toward historical levels and large increases in global tropospheric ozone would be expected.

4.5.3.4 The Role of VSLSs

Since the last Assessment, considerable progress has been made in implementing the effects of bromine-containing very short-lived substances (VSLSs) on ozone (see also **Section 4.3.3**) into CCMs. Model simulations show clear signatures of brominated VSLSs in stratospheric ozone (e.g., Hossaini et al., 2015a; Sinnhuber and Meul, 2015; Oman et al., 2016; Fernandez et al., 2017; Falk et al., 2017). Brominated VSLSs are projected to affect the Antarctic ozone hole area and depth until about the middle of the century (Fernandez et al., 2017). As the abundance of long-lived halogens declines, the relative importance of brominated VSLSs regarding ozone reduction is predicted to increase in the coming decades and surpass ozone destruction by chlorine by about 2070 (Fernandez et al., 2017). However, as the depletion of stratospheric ozone due to brominated VSLSs depends also on the availability of chlorine, the impact of bromine on stratospheric ozone will continuously fade. Therefore, Fernandez et al. (2017) do not find a significant change in the return date of Antarctic ozone to 1980 values. This result is in contrast to model projections by Yang et al. (2014) and Oman et al. (2016) which show that active bromine from VSLSs is expected to delay the return of TCO to historical values by about 6–8 years (Yang et al., 2014) to a decade (Oman et al., 2016). The differences between these projections may be due to the applied models, the number of model realizations, or the specifications of future VSLSs. Hence more model studies are needed for a robust projection of the effect of brominated VSLSs on the Antarctic ozone return date.

As discussed in WMO (2014), increasing emissions of synthetic, chlorine-containing VSLSs, in particular dichloromethane (CH_2Cl_2), represent another, more recently detected component of VSLSs that affects polar ozone. Recent observations indicate that the atmospheric concentration of dichloromethane (which is not controlled by the Montreal Protocol) is growing (see **Chapter 1** for further details). Using CTM and CCM simulations, Hossaini et al. (2017) showed that the impact of dichloromethane on stratospheric ozone has clearly increased in recent years from a relative ozone decrease by dichloromethane of 3 DU in 2010 to 6 DU in 2016. Assuming a continuous increase of dichloromethane in coming decades at the mean rate observed over the 2004–2014 period, they found a delay of the return of Antarctic ozone to the 1980 baseline by nearly 20 years compared to a simulation without CH_2Cl_2 abundance (**Figure 4-21**). A sustained future increase in atmospheric concentrations of dichloromethane would therefore further slow the recovery of the Antarctic ozone hole. The future evolution of dichloromethane is however uncertain, given its recent decline in growth rate between 2014 and 2016 (see **Chapter 1**).

While the above cited studies have clearly shown that brominated and chlorinated VSLSs have a significant impact on stratospheric polar ozone, their consequences for the return dates of polar ozone to historical baseline values will depend on the future abundances of VSLSs in the atmosphere and are therefore uncertain, as addressed in more detail in **Section 4.5.4.2**.

4.5.4 Uncertainty in Polar Ozone Projections

Future ozone projections are affected by uncertainty due to internal variability of the atmosphere, structural

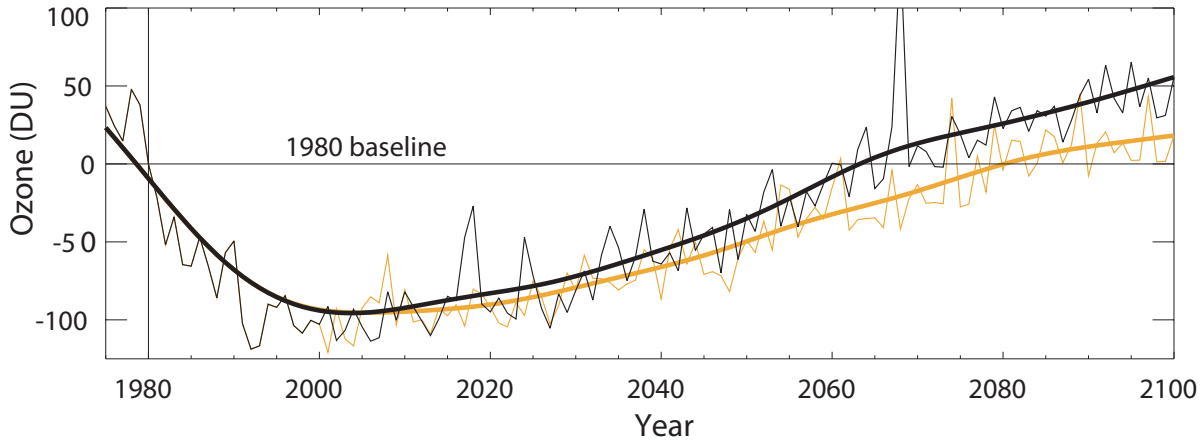

Figure 4-21. Future impact of growth in dichloromethane (CH_2Cl_2) on Antarctic column ozone and ozone trend derived from a CCM study. Results are shown for two UMSLIMCAT simulations: one run without CH_2Cl_2 and another where surface CH_2Cl_2 concentrations continue to increase at the mean rate observed over the 2004–2014 period. The figure shows the temporal evolution of October mean Antarctic stratospheric ozone column (in Dobson Units, DU) relative to 1980. While interannual variability is large, the two ozone time series are statistically different at the 95% significance level according to a Student's t-test (P_{value} = 0.02). Ozone returns to the 1980 baseline in the year 2064 (without CH_2Cl_2; black line) and in 2081 (with CH_2Cl_2; gold line). Adapted from Hossaini et al. (2017).

uncertainty due to differences between models and uncertainty in the future scenarios for ODSs and GHGs (see also **Box 3-3**). The role of internal dynamical variability in particular for Arctic polar ozone has been addressed in **Section 4.3.4**. In the following, the aspect of model uncertainty will be revisited for the new CCMI model simulations (**Section 4.5.4.1**) and the new ozone return dates will be discussed in the context of the ODS and GHG scenarios used (**Section 4.5.4.2**).

4.5.4.1 Model Uncertainty

As discussed in **Section 4.5.1**, CCMs differ in their treatment of the relevant physical, dynamical, and chemical processes. The broad range of total column ozone projections in the new CCMI simulations could be a result of the enhanced complexity of the applied CCMs. Most of the models participating in CCMI have been improved since CCMVal-2, being now more physically based, with enhanced resolution and more frequently coupled to ocean models, which leads to enhanced diversity in model results (Morgenstern et al., 2017).

In particular, the responses in total column ozone of the CCMI models to anthropogenic forcings, such as changes in ODSs and GHGs, were found to be less consistent across the different CCMs than those of the ozone profiles (Morgenstern et al., 2018). The likely cause of this is lower-stratospheric transport and dynamical responses, such as in the Brewer-Dobson circulation, exhibiting substantial inter-model differences. Good agreement of CCM results was found in the middle and upper stratosphere. Obvious differences were identified particularly in the troposphere, possibly caused by differences in the formulation and complexity of the tropospheric chemistry modules used in the CCMs.

These conclusions are confirmed by Dhomse et al. (2018) who investigate ozone recovery of partial columns in the lower stratosphere (LS, from the tropopause up to 10 hPa) and in the upper stratosphere (US, at 10 hPa and lower pressures) from 14 individual CCMI models. In the LS, where ozone has a long photochemical lifetime, the adjusted results from the CCMs show clear differences among the models in the polar regions. This suggests issues with the descriptions of dynamical (transport) and chemical

(heterogeneous chemistry) processes due to temperature biases in the CCMs. For the upper stratosphere, ozone in the polar regions behaves more similarly in the different models, as dynamical processes are less important for ozone, while the feedback of temperature changes on ozone becomes more important (Haigh and Pyle, 1982).

A further source of uncertainty in the CCMI ozone projections lies in existing uncertainties of rate constants for the N_2O and CH_4 reactions, which have been reassessed recently (SPARC, 2013). The CCMI models generally used the kinetic rate constants recommended at the time of the simulations (Sander et al., 2011). However, using updated estimates of kinetic and photochemical parameters, Fleming et al. (2015) report that uncertainties in the commonly used recommendations for the rates of chemical loss processes of N_2O and CH_4 lead to a substantial range in model ozone, both for present day and long-term projections of future ozone recovery. For October SH polar ozone, the largest uncertainty is due to the Cl + CH_4 reaction, which impacts the amount of chlorine in reservoir versus radical forms, resulting in a total ozone range of ±6% for present day chlorine loading. However, this range will diminish to less than ±1% by 2100 as atmospheric chlorine decreases.

4.5.4.2 Uncertainty in Ozone Return Dates

The return date of total or stratospheric ozone to a historical baseline is an important indicator to assess the success of the Montreal Protocol and its Amendments and adjustments. Ozone return dates have been presented previously based on CCMVal-2 projections (Eyring et al., 2010a, b; WMO, 2011) and CMIP5 simulations using different GHG scenarios (Eyring et al., 2013b; WMO, 2014). Estimates of ozone return dates from the new CCMI simulations have been derived in Dhomse et al. (2018). This section compares the different estimates of ozone return dates and discusses reasons generating uncertainty in the derived dates. It is important to note that all model projections use prescribed scenarios for future abundances of ODSs assuming a future decline of ODSs according to the regulations of the Montreal Protocol. This section does not assess the uncertainty in ozone return dates arising from potential non-compliance with the Montreal Protocol. (For more information on this topic see **Chapter 6**). The return dates for polar total column ozone from the CCMVal-2 projections in WMO (2011) and from the CCMI REF-C2 simulations as well as their estimated ranges are shown in **Figure 4-22**.

To account for model uncertainty, it is a common approach to give ozone return dates in terms of their mean value plus uncertainty range. Three different measures of ozone return dates were provided by Dhomse et al. (2018) for the CCMI simulations: (1) the multi-model mean (MMM) with the 1σ standard deviation defining the model range of recovery dates, (2) the median with the 10th and 90th percentiles defining the range of recovery dates, and (3) the multi-model mean including only models within one standard deviation of the MMM (MMM1S) with the 1σ standard deviation of the MMM1S defining the model range of recovery dates. For both polar regions, the median and MMM1S approaches provide (near) identical return dates giving confidence in the derived results.

Sensitivity to ODS and GHG Scenarios

As shown in **Sections 4.5.2.1** and **4.5.2.2**, the return dates of polar total column ozone (TCO) to 1980 baseline values are delayed in the CCMI models (MMM1S) by 4 years in the Arctic and 10 years in the Antarctic compared to the CCMVal-2 models (SPARC CCMVal, 2010; WMO, 2011). This delay in polar ozone recovery can partially be ascribed to updates in the ODS and GHG scenarios prescribed to the CCMI reference simulations (for more details see **Box 3-3** and Dhomse et al., 2018). The change in the ODS scenario from the adjusted A1 scenario of WMO (2007) used in CCMVal-2 to the A1 scenario of WMO (2011) in CCMI caused a delayed decline in stratospheric halogen levels. In addition, the transition from the SRES-A1b GHG scenario used in CCMVal-2 to the RCP-6.0 scenario in CCMI reduces the chemically driven increase of ozone due to a slower rise of CO_2 and CH_4 in the RCP-6.0 scenario, explaining a further delay in TCO recovery in the CCMI models.

The expected effect of rising N_2O concentrations in the REF-C2 simulations (about 40% between 1960 and 2100) is to delay the ozone return date due to an enhanced production of NO_x and catalytic ozone depletion. However, while the return date of global and northern mid-latitude stratospheric column ozone is

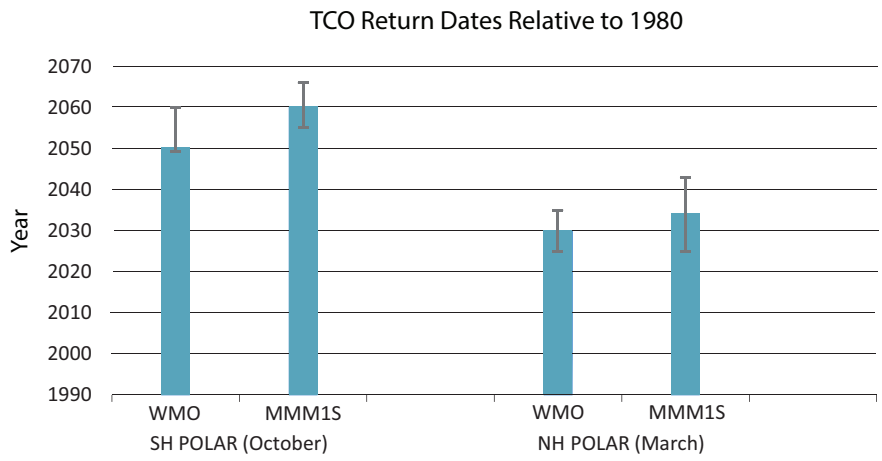

Figure 4-22. Estimated return years of total column ozone (TCO) to 1980 historical levels for the SH polar cap in October and the NH polar cap in March based on CCMVal-2 simulations (WMO) and on CCMI REF-C2 simulations (MMM1S). The estimated 1-σ uncertainties are shown with black vertical lines. Adapted from Dhomse et al. (2018).

significantly earlier in a scenario with fixed 1960 N_2O surface mixing ratios than in the REF-C2 simulations, it remains nearly unchanged in both polar areas (see Table 4 in Dhomse et al., 2018). Morgenstern et al. (2018) suggest that the negative effect of N_2O increases on ozone in the upper stratosphere might be compensated by a self-healing effect in the lower stratosphere initiated by the upper stratosphere ozone decline. However, the detailed processes leading to a zero response of the polar ozone return date to N_2O increases still need to be understood.

CH_4 concentrations increase in the RCP-6.0 scenario of the REF-C2 simulations by 57% between 1960 and their maximum in 2070, and by 128% between 1960 and 2100 in the RCP-8.5 scenario. Consistent with previous work (e.g., Revell et al., 2012), stratospheric ozone returns earlier in the CCMI simulations with rising CH_4 concentrations than in the constant-1960 scenario. This effect is stronger for the more extreme CH_4 increase in the RCP-8.5 scenario and stronger in Arctic spring (about 10 years) than in Antarctic spring (6 years). Note, however, that for the N_2O- and CH_4-sensitivity simulations only one realization by a limited number of models was available, reducing the robustness of the stated return dates.

Sensitivity to VSLSs

Section 4.5.3.4 revealed that both bromine- and chlorine-containing VSLSs have the potential to delay the return of the Antarctic ozone hole to historical values by somewhere between several years and up to three decades. Hence, the future evolution of the VSLS emissions represents a further source of uncertainty for the projection of the ozone return date. While the CCMVal-2 models generally did not include the effects of brominated VSLSs on ozone, most CCMI models took their effects into account. The additional ozone depletion by the VSLSs could therefore be a further contribution to the delay in CCMI TCO return dates (e.g., Oman et al., 2016).

The concentrations of the oceanic brominated VSLSs seem to have remained relatively stable over the past decades (see **Figure 1-16 in Chapter 1**). Based on this fact, most model studies assume a constant mixing ratio of brominated VSLSs of 5 ppt in simulations of past and future ozone. Based on present day, observed global oceanic and atmospheric concentrations (ERA-Interim) and historical and future data from three CMIP5 models, Ziska et al. (2017) derived, however, an increase of brominated VSLSs for the period 1979–2005. For the RCP-8.5 scenario, oceanic brominated VSLS emissions could increase by 30% from 2010 to 2100 (Tegtmeier et al., 2015; Ziska et al., 2017). In a transient CCM study using the RCP-6.0 GHG scenario and interactive VSLS emissions, an increase of the ocean–atmosphere flux of brominated VSLSs of about 8–10% by the end of the 21st century compared to present day was found (Falk et al., 2017). However, under the low chlorine loading at the end of the century, brominated VSLSs are projected to have less impact on total Antarctic stratospheric ozone depletion than in the present day (in agreement with studies using constant VSLS

mixing ratios) and may not act as a major source of future stratospheric ozone depletion (Falk et al., 2017). More CCM studies including the effects of climate change on VSLS emissions from the ocean need to be carried out to provide a robust estimate of the impact of future changes in brominated VSLSs on the return of polar ozone to historical values.

Chlorine-containing VSLSs are predominantly produced by industry. Among those, dichloromethane (CH_2Cl_2), has increased rapidly in recent years. Between 2000 and 2012, surface concentrations of CH_2Cl_2 increased at a global mean rate of almost 8% yr^{-1}, with the largest growth in South and Southeast Asia (Hossaini et al., 2015b; Oram et al., 2017). As discussed in **Section 4.5.3.4**, Hossaini et al. (2017) obtained a substantial delay of Antarctic ozone return, if the recently observed global mean CH_2Cl_2 growth rate of 2 ppt yr^{-1} continues. Whether such a growth rate would be likely to continue until the end of the century is arguable given the current global production capacity for CH_2Cl_2.

REFERENCES

Achtert, P., and M. Tesche, Assessing lidar-based classification schemes for polar stratospheric clouds based on 16 years of measurements at Esrange, Sweden, *J. Geophys. Res. Atmos.*, *119*, 1386–1405, doi:10.1002/2013JD020355, 2014.

Andrews, D.G., J.R. Holton, and C.B. Leovy, *Middle Atmosphere Dynamics*, vol. 40, 1st Edition, 489 pp., ISBN: 9780080211672, Academic Press, London, 1987.

Bednarz, E.M., A.C. Maycock, N.L. Abraham, P. Braesicke, O. Dessens, and J.A. Pyle, Future Arctic ozone recovery: The importance of chemistry and dynamics, *Atmos. Chem. Phys.*, *16*, 12159–12176, doi:10.5194/acp-16-12159-2016, 2016.

Bernhard, G., G. Manney, J.-U. Grooß, R. Müller, K. Lakkala, V. Fioletov, T. Koskela, A. Heikkilä, and B. Johnsen, Ozone and UV Radiation [in "State of the Climate in 2014"], *Bull. Am. Meteorol. Soc.*, *96* (7), S131–S133, doi:10.1175/2015BAMSStateof theClimate.1, 2015.

Bernhard, G., I. Ialongo, J.-U. Grooß, J. Hakkarainen, B. Johnsen, G.L. Manney, V. Fioletov, A. Heikkilä, and K. Lakkala, Ozone and UV Radiation [in "State of the Climate in 2015"], *Bull. Am. Meteorol. Soc.*, *97* (8), S152–S153, doi:10.1175/2016BAMS-Stateof theClimate.1, 2016.

Bernhard, G., V.E. Fioletov, J.-U. Grooß, I. Ialongo, B. Johnsen, K. Lakkala, G. Manney, and R. Müller, Ozone and UV radiation [in "State of the Climate in 2016"], *Bull. Am. Meteorol. Soc.*, *98*, S151–S154, doi:10.1175/2017BAMSStateoftheClimate.1, 2017.

Bittner, M., C. Timmreck, H. Schmidt, M. Toohey, and K. Krüger, The impact of wave-mean flow interaction on the Northern Hemisphere polar vortex after tropical volcanic eruptions, *J. Geophys. Res. Atmos.*, *121*, doi:10.1002/2015JD0244603, 2016.

Bodeker, G.E., H. Shiona, and H. Eskes, Indicators of Antarctic ozone depletion, *Atmos. Chem. Phys.*, *5*, 2603–2615, doi:10.5194/acp-5-2603-2005, 2005.

Bohlinger, P., B.-M. Sinnhuber, R. Ruhnke, and O. Kirner, Radiative and dynamical contributions to past and future Arctic stratospheric temperature trends, *Atmos. Chem. Phys.*, *14*, 1679–1688, doi:10.5194/acp-14-1679-2014, 2014.

Braesicke, P., J. Keeble, X. Yang, G. Stiller, S. Kellmann, N.L. Abraham, A. Archibald P. Telford, and J.A. Pyle, Circulation anomalies in the Southern Hemisphere and ozone changes, *Atmos. Chem. Phys.*, *13*, 10,677–10,688, doi:10.5194/acp-13-10677-2013, 2013.

Brooks, S.D., D. Baumgardner, B. Gandrud, J.E. Dye, M.J. Northway, D.W. Fahey, T.P. Bui, O.B. Toon, and M.A. Tolbert, Measurements of large stratospheric particles in the Arctic polar vortex, *J. Geophys. Res., 108* (D20), doi:10.1029/2002JD003278, 2003.

Burkholder, J.B., S.P. Sander, J. Abbatt, J.R. Barker, R.E. Huie, C.E. Kolb, M.J. Kurylo, V.L. Orkin, D.M. Wilmouth, and P.H. Wine, *Chemical kinetics and photochemical data for use in atmospheric studies, Evaluation No. 18*, JPL Publication 15-10, Jet Propulsion Laboratory, Pasadena, California, 2015. [Available at http://jpldataeval.jpl.nasa.gov.]

Butler, A.H., D.J. Seidel, S.C. Hardiman, N. Butchart, T. Birner, and A. Match, Defining sudden stratospheric warmings, *Bull. Amer. Meteorol. Soc., 96*, 1913–1928, doi:10.1175/BAMS-D-13-00173.1, 2015.

Butler, A.H., J.S. Daniel, R.W. Portmann, A.R. Ravishankara, P.J. Young, D.W. Fahey, and K.H. Rosenlof, Diverse policy implications for future ozone and surface UV in a changing climate, *Environ. Res. Lett.*, *11* (6), doi:10.1088/1748-9326/11/6/064017/meta, 2016.

Butler, A.H., J.P. Sjoberg, D.J. Seidel, and K.H. Rosenlof, A sudden stratospheric warming compendium, *Earth Syst. Sci. Data*, *9*, 63–76, doi:10.5194/essd-9-63-2017, 2017.

Cadoux, A., B. Scaillet, S. Bekki, C. Oppenheimer, and T.H. Druitt, Stratospheric Ozone destruction by the Bronze-Age Minoan eruption (Santorini Volcano, Greece), *Sci. Rep.*, *5*, 12243, doi:10.1038/srep12243, 2015.

Cagnazzo, C., E. Manzini, N. Calvo, A. Douglass, H. Akiyoshi, S. Bekki, M. Chipperfield, M. Dameris, M. Deushi, A.M. Fischer, H. Garny, A. Gettelman, M.A. Giorgetta, D. Plummer, E. Rozanov, T.G. Shepherd, K. Shibata, A. Stenke, H. Struthers, and W. Tian, Northern winter stratospheric temperature and ozone responses to ENSO inferred from an ensemble of Chemistry Climate Models, *Atmos. Chem. Phys.*, *9*, 8935–8948, doi:10.5194/acp-9-8935-2009, 2009.

Calvo, N., M. Iza, M.M. Hurwitz, E. Manzini, C. Peña-Ortiz, A.H. Butler, C. Cagnazzo, S. Ineson, and C.I. Garfinkel, Northern Hemisphere strato-

spheric pathway of different El Niño flavors in stratosphere resolving CMIP5 models, *J. Clim.*, –, 4351–4371, doi:10.1175/JCLI-D.16-0132.1, 2017.

Canty, T.P., R.J. Salawitch, and D.M. Wilmouth, The kinetics of the ClOOCl catalytic cycle, *J. Geophys. Res.*, *121*, 13 768–13 783, doi:10.1002/2016JD025710, 2016.

Carslaw, K.S., and T. Peter, Uncertainties in reactive uptake coefficients for solid stratospheric particles, 1. Surface chemistry, *Geophys. Res. Lett., 24* (14), 1743–1746, doi:10.1029/97GL01683, 1997.

Carn, S.A., L. Clarisse, and A.J. Prata, Multi-decadal satellite measurements of global volcanic degassing, *J. Volcanol. Geotherm. Res.*, *311*, 99–134, doi:10.1016/j.jvolgeores.2016.01.002, 2016.

Charlton, A.J., and L.M. Polvani, A new look at stratospheric sudden warmings, Part I: Climatology and modeling benchmarks, *J. Clim.*, *20*, 449–469, doi:10.1175/JCLI3996.1, 2007.

Charlton-Perez, A.J., M.P. Baldwin, T. Birner, R.X. Black, A.H. Butler, N. Calvo, N.A. Davis, E.P. Gerber, N. Gillett, S. Hardiman, J. Kim, K. Krüger, Y.-Y. Lee, E. Manzini, B.A. McDaniel, L. Polvani, T. Reichler, T.A. Shaw, M. Sigmond, S.-W. Son, M. Toohey, L. Wilcox, S. Yoden, B. Christiansen, F. Lott, D. Shindell, S. Yukimoto, S. Watanabe, On the lack of stratospheric dynamical variability in low-top versions of the CMIP5 models, *J. Geophys. Res. Atmos.*, *118*, 2494–2505, doi:10.1002/jgrd.50125, 2013.

Chipperfield, M.P., S.S. Dhomse, W. Feng, R.L. McKenzie, G.J.M. Velders, and J.A. Pyle, Quantifying the ozone and ultraviolet benefits already achieved by the Montreal Protocol. *Nat. Commun.*, *6*, 7233, doi:10.1038/ncomms8233, 2015.

Chipperfield, M., S. Bekki, S. Dhomse, N. Harris, B. Hassler, R. Hossaini, W. Steinbrecht, R. Thiéblemont, and M. Weber, Detecting recovery of the stratospheric ozone layer, *Nature*, *549*, 211–218, doi:10.1038/nature23681, 2017.

Curtius, J., R. Weigel, H.-J. Vössing, H. Wernli, A. Werner, C.-M. Volk, P. Konopka, M. Krebsbach, C. Schiller, A. Roiger, H. Schlager, V. Dreiling, and S. Borrmann, Observations of meteoric material and implications for aerosol nucleation in the winter Arctic lower stratosphere derived from in situ particle measurements, *Atmos. Chem. Phys.*, *5*, 3053–3069, doi:10.5194/acp-5-3053-2005, 2005.

Damiani, A., B. Funke, M. Lopez-Puertas, A. Gardini, T. von Clarmann, M.K. Santee, L. Froidevaux, and R.R. Cordero, Changes in the composition of the northern polar upper stratosphere in February 2009 after a sudden stratospheric warming, *J. Geophys. Res.*, *119*, 11,429–11,444, doi:10.1002/2014JD021698, 2014.

Damiani, A., B. Funke, M.L. Santee, R.R. Cordero, and S. Watanabe, Energetic particle precipitation: A major driver of the ozone budget in the Antarctic upper stratosphere, *Geophys. Res. Lett.*, *43* (7), 3554–3562, doi:10.1002/2016GL068279, 2016.

Dee, D.P., S.M. Uppala, A.J. Simmons, P. Berrisford, P. Poli, S. Kobayashi, U. Andrae, M.A. Balmaseda, G. Balsamo, P. Bauer, P. Bechtold, A.C.M. Beljaars, L. van de Berg, J. Bidlot, N. Bormann, C. Delsol, R. Dragani, M. Fuentes, A.J. Geer, L. Haimberger, S.B. Healy, H. Hersbach, E.V. Hólm, L. Isaksen, P. Kållberg, M. Köhler, M. Matricardi, A.P. McNally, B.M. Monge-Sanz, J.-J. Morcrette, B.-K. Park, C. Peubey, P. de Rosnay, C. Tavolato, J.-N. Thépaut, and F. Vitart, The ERA-Interim reanalysis: Configuration and performance of the data assimilation system, *Q. J. R. Meteorol. Soc.*, *137*, 553–597, doi:10.1002/qj.828, 2011.

de Laat, A.T.J., R.J. van der A, and M. van Weele, Tracing the second stage of ozone recovery in the Antarctic ozone-hole with a "big data" approach to multivariate regressions, *Atmos. Chem. Phys.*, *15* (1), 79–97, doi:10.5194/acp-15-79-2015, 2015.

de Laat, A.T.J., M. van Weele, and R.J. van der A, Onset of stratospheric ozone recovery in the Antarctic ozone hole in assimilated daily total ozone columns. *J. Geophys. Res. Atmos.*, *122,* 11,880–11,899, doi:10.1002/2016JD025723, 2017.

Denton, M.H., R. Kivi, T. Ulich, M.A. Clilverd, C.J. Rodger, and P. von der Gathen, Northern Hemisphere stratospheric ozone depletion caused by solar proton events: The role of the polar vortex, *Geophys. Res. Lett.*, *45*, 2115–2124, doi:10.1002/2017GL075966, 2018.

Dhomse, S., D. Kinnison, M.P. Chipperfield, I. Cionni, M. Hegglin, N.L. Abraham, H. Akiyoshi, A.T. Archibald, E.M. Bednarz, S. Bekki, P. Braesicke, N. Butchart, M. Dameris, M. Deushi, S. Frith, S.C. Hardiman, B. Hassler, L.W. Horowitz, R.-M. Hu, P. Jöckel, B. Josse, O. Kirner, S. Kremser, U. Langematz, J. Lewis, M. Marchand, M. Lin, E. Mancini, V. Marécal, M. Michou, O. Morgenstern, F.M.

O'Connor, L. Oman, G. Pitari, D.A. Plummer, J.A. Pyle, L.E. Revell, E. Rozanov, R. Schofield, A. Stenke, K. Stone, K. Sudo, S. Tilmes, D. Visioni, Y. Yamashita, and G. Zeng, Estimates of ozone return dates from Chemistry-Climate Model Initiative simulations, *Atmos. Chem. Phys.*, *18*, 8409–8438, doi:10.5194/acp-18-5408-218, 2018.

Dietmüller, S., R. Eichinger, H. Garny, T. Birner, H. Boenisch, G. Pitari, E. Mancini, D. Visioni, A. Stenke, L. Revell, E. Rozanov, D.A. Plummer, J. Scinocca, P. Jöckel, L. Oman, M. Deushi, S. Kiyotaka, D.E. Kinnison, R. Garcia, O. Morgenstern, G. Zeng, K.A. Stone, and R. Schofield, Quantifying the effect of mixing on the mean age of air in CCMVal-2 and CCMI-1 models, *Atmos. Chem. Phys.*, *18*, 6699–6720, doi:10.5194/acp-18-6699-2018, 2018.

Di Liberto, L., F. Cairo, F. Fierli, G. DiDonfrancesco, M. Viterbini, T. Deshler, and M. Snels, Observations of polar stratosperic clouds over McMurdo (77.85°S, 166.67°E) (2006-2010), *J. Geophys. Res. Atmos., 119 (9)*, 5528-5541, doi:10.1002/2013JD019892, 2014

Douglass, A.R., S.E. Strahan, L.D. Oman, and R.S. Stolarski, Understanding differences in chemistry climate model projections of stratospheric ozone, *J. Geophys. Res. Atmos.*, *119*, 4922–4939, doi:10.1002/2013JD021159, 2014.

Driscoll, S., A. Bozzo, L.J. Gray, A. Robock, and G. Stenchikov, Coupled Model Intercomparison Project 5 (CMIP5) simulations of climate following volcanic eruptions, *J. Geophys. Res.*, *117*, D17105, doi:10.1029/2012JD017607, 2012.

Ebert, M., R. Weigel, K. Kandler, G. Günther, S. Molleker, J.-U. Grooß, B. Vogel, S. Weinbruch, and S. Borrmann, Chemical analysis of refractory stratospheric aerosol particles collected within the arctic vortex and inside polar stratospheric clouds, *Atmos. Chem. Phys.*, *16* (13), 8405–8421, doi:10.5194/acp-16-8405-2016, 2016.

Evtushevsky, O.M., V.O. Kravchenko, L.L. Hood, and G.P. Milinevsky, Teleconnection between the central tropical Pacific and the Antarctic stratosphere: Spatial patterns and time lags, *Clim. Dyn.*, *44*, 1841–1855, doi:10.1007/s00382-014-2375-2, 2015.

Eyring, V., I. Cionni, G.E. Bodeker, A.J. Charlton-Perez, D.E. Kinnison, J.F. Scinocca, D.W. Waugh, H. Akiyoshi, S. Bekki, M.P. Chipperfield, M. Dameris, S. Dhomse, S.M. Frith, H. Garny, A. Gettelman, A. Kubin, U. Langematz, E. Mancini, M. Marchand, T. Nakamura, L.D. Oman, S. Pawson, G. Pitari, D.A. Plummer, E. Rozanov, T.G. Shepherd, K. Shibata, W. Tian, P. Braesicke, S.C. Hardiman, J.F. Lamarque, O. Morgenstern, J.A. Pyle, D. Smale, and Y. Yamashita, Multi-model assessment of stratospheric ozone return dates and ozone recovery in CCMVal-2 models, *Atmos. Chem. Phys.*, *10*, 9451–9472, doi:10.5194/acp-10-9451-2010, 2010a.

Eyring, V., I. Cionni, J.F. Lamarque, H. Akiyoshi, G.E. Bodeker, A.J. Charlton-Perez, S.M. Frith, A. Gettelman, D.E. Kinnison, T. Nakamura, L.D. Oman, S. Pawson, and Y. Yamashita, Sensitivity of 21st century stratospheric ozone to greenhouse gas scenarios, *Geophys. Res. Lett.*, *37*, L16807, doi:10.1029/2010GL044443, 2010b.

Eyring, V., J.-F. Lamarque, P. Hess, F. Arfeuille, K. Bowman, M.P. Chipperfield, B. Duncan, A. Fiore, A. Gettelman, M.A. Giorgetta, C. Granier, M. Hegglin, D. Kinnison, M. Kunze, U. Langematz, B. Luo, R. Martin, K. Matthes, P.A. Newman, T. Peter, A. Robock, T. Ryerson, A. Saiz-Lopez, R. Salawitch, M. Schultz, T.G. Shepherd, D. Shindell, J. Staehelin, S. Tegtmeier, L. Thomason, S. Tilmes, J.-P. Vernier, D.W. Waugh, and P.J. Young, Overview of IGAC/SPARC Chemistry-Climate Model Initiative (CCMI) community simulations in support of upcoming ozone and climate assessments, SPARC Newsletter, *40*, 48–66, 2013a.

Eyring, V., J.M. Arblaster, I. Cionni, J. Sedlácek, J. Perlwitz, P.J. Young, S. Bekki, D. Bergmann, P. Cameron-Smith, W.J. Collins, G. Faluvegi, K.-D. Gottschaldt, L.W. Horowitz, D.E. Kinnison, J.-F. Lamarque, D.R. Marsh, D. Saint-Martin, D.T. Shindell, K. Sudo, S. Szopa, and S. Watanabe, Long-term ozone changes and associated climate impacts in CMIP5 simulations, *J. Geophys. Res. Atmos.*, *118* (10), 5029–5060, doi:10.1002/jgrd.50316, 2013b.

Fahey, D.W., R.S. Gao, K.S. Carslaw, J. Kettleborough, P.J. Popp, M.J. Northway, J.C. Holecek, S.C. Ciciora, R.J. McLaughlin, T.L. Thompson, R.H. Winkler, D.G. Baumgardner, B. Gandrud, P.O. Wennberg, S. Dhaniyala, K. McKinley, T. Peter, R.J. Salawitch, T.P. Bui, J.W. Elkins, C.R. Webster, E.L. Atlas, H. Jost, J.C. Wilson, R.L. Herman, A. Kleinböhl, and M. von König, The detection of

large HNO_3-containing particles in the winter Arctic stratosphere, *Science*, *291*, 1026–1031, doi:10.1126/science.1057265, 2001.

Falk, S., B.-M. Sinnhuber, G. Krysztofiak, P. Jöckel, P. Graf, and S.T. Lennartz, Brominated VSLs and their influence on ozone under a changing climate, *Atmos. Chem. Phys.*, *17*, 11,313–11,329, doi:10.5194/acp-17-11313-2017, 2017.

Fernandez, R.P., D.E. Kinnison, J.-F. Lamarque, S. Tilmes, and A. Saiz-Lopez, Impact of biogenic very short-lived bromine on the Antarctic ozone hole during the 21st century, *Atmos. Chem. Phys.*, *17* (3), 1673–1688, doi:10.5194/acp-17-1673-2017, 2017.

Fleming E.L., C.H. Jackman, R.S. Stolarski, and A.R. Douglass, A model study of the impact of source gas changes on the stratosphere for 1850–2100, *Atmos. Chem. Phys., 11,* 8515–8541, doi:10.5194/acp-11-8515-2011, 2011.

Fleming, E.L., C. George, D.E. Heard, C.H. Jackman, M.J. Kurylo, W. Mellouki, V.L. Orkin, W.H. Swartz, T.J. Wallington, P.H. Wine, and J.B. Burkholder, The impact of current CH_4 and N_2O atmospheric loss process uncertainties on calculated ozone abundances and trends, *J. Geophys. Res.*, *120*, 5267–5293, doi:10.1002/2014JD022067, 2015.

Fletcher, C., and P. Kushner, The role of linear interference in the annular mode response to tropical SST forcing, *J. Clim*, *24*, 778–794, doi: 10.1175/2010JCLI3735.1, 2011.

Fogt, R.L., El Niño and Antarctica [in "State of the Climate in 2015"], *Bull. Am. Meteorol. Soc.*, *97* (8), S162, doi:10.1175/2016BAMSStateoftheClimate.1, 2016.

Frieler, K., M. Rex, R.J. Salawitch, T. Canty, M. Streibel, R.M. Stimpfle, K. Pfeilsticker, M. Dorf, D.K. Weisenstein, and S. Godin-Beekmann, Toward a better quantitative understanding of polar stratospheric ozone loss, *Geophys. Res. Lett.*, *33*, L10812, doi:10.1029/2005GL025466, 2006.

Frith, S.M., R.S. Stolarski, N.A. Kramarova, and R.D. McPeters, Estimating uncertainties in the SBUV Version 8.6 merged profile ozone data set, *Atmos. Chem. Phys.*, *17*, 14,695–14,707, doi:10.5194/acp-17-14695-2017, 2017.

Funke, B., A. Baumgaertner, M. Calisto, T. Egorova, C.H. Jackman, C.J. Kieser, A. Krivolutsky, M. López-Puertas, D.R. Marsh, T. Reddmann, E. Rozanov, S.-M. Salmi, M. Sinnhuber, G.P. Stiller, P.T. Verronen, S. Versick, T. von Clarmann, T.Y. Vyushkova, N. Wieters, and J.M. Wissing, Composition changes after the "Halloween" solar proton event: The High-Energy Particle Precipitation in the Atmosphere (HEPPA) model versus MIPAS data intercomparison study, *Atmos. Chem. Phys.*, *11*, 9089–9139, doi:10.5194/acp-11-9089-2011, 2011.

Funke, B., M. López-Puertas, G.P. Stiller, and T. von Clarmann, Mesospheric and stratospheric NO_y produced by energetic particle precipitation during 2002–2012, *J. Geophys. Res.*, *119*, doi:10.1002/2013JD021404, 2014.

Funke, B., M. López-Puertas, G.P. Stiller, S. Versick, and T. von Clarmann, A semi-empirical model for mesospheric and stratospheric NO_y produced by energetic particle precipitation, *Atmos. Chem. Phys.*, *16* (13), 8667–8693, doi:10.5194/acp-16-8667-2016, 2016.

Fytterer, T., M.G. Mlynczak, H. Nieder, K. Pérot, M. Sinnhuber, G. Stiller, and J. Urban, Energetic particle induced intra-seasonal variability of ozone inside the Antarctic polar vortex observed in satellite data, *Atmos. Chem. Phys.*, *15* (6), 3327–3338, doi:10.5194/acp-15-3327-2015, 2015.

Garcia, R.R., D.E. Kinnison, and D.R. Marsh, "World avoided" simulations with the Whole Atmosphere Community Climate Model, *J. Geophys. Res.*, *117*, D23303, doi:10.1029/2012JD018430, 2012.

Gelaro, R., W. McCarty, M.J. Suárez, R. Todling, A. Molod, L. Takacs, C.A. Randles, A. Darmenov, M.G. Bosilovich, R. Reichle, K. Wargan, L. Coy, R. Cullather, C. Draper, S. Akella, V. Buchard, A. Conaty, A.M. da Silva, W. Gu, G. Kim, R. Koster, R. Lucchesi, D. Merkova, J.E. Nielsen, G. Partyka, S. Pawson, W. Putman, M. Rienecker, S.D. Schubert, M. Sienkiewicz, and B. Zhao, The Modern-Era Retrospective Analysis for Research and Applications, Version 2 (MERRA-2), *J. Clim.*, 30, 5419–5454, doi: 10.1175/JCLI-D-16-0758.1, 2017.

Grooß, J.-U., R. Müller, R. Spang, I. Tritscher, T. Wegner, M.P. Chipperfield, W. Feng, D.E. Kinnison, and S. Madronich, On the discrepancy of HCl processing in the core of the wintertime polar vortices, *Atmos. Chem. Phys.*, *18*, 8647–8666, doi:10.5194/acp-18-8647-2018, 2018.

Haigh, J.D., and J. Pyle, Ozone perturbation experiments in a two-dimensional circulation model, *Q. J. R. Meteorol. Soc.*, *108* (457), 551–574,

doi:10.1002/qj.49710845705, 1982.

Haigh, J.D., and H.K. Roscoe, The final warming date of the Antarctic polar vortex and influences on its interannual variability, *J. Clim.*, *22*, 5809–5819, doi:10.1175/2009JCLI2865.1, 2009.

Harnik, N., and R.S. Lindzen, The effect of reflecting surfaces on the vertical structure and variability of stratospheric planetary waves, *J. Atmos. Sci.*, *58*, 2872–2894, doi:10.1175/1520-0469(2001)058<2872:TEORSO>2.0.CO;2, 2001.

Hassler, B., G.E. Bodeker, S. Solomon, and P.J. Young, Changes in the polar vortex: Effects on Antarctic total ozone observations at various stations, *Geophys. Res. Lett.*, *38* (1), L01805, doi:10.1029/2010GL045542, 2011a.

Hassler, B., J.S. Daniel, B.J. Johnson, S. Solomon, and S.J. Oltmans, An assessment of changing ozone loss rates at South Pole: Twenty-five years of ozonesonde measurements, *J. Geophys. Res.*, *116* (D22), D22301, doi:10.1029/2011JD016353, 2011b.

Hassler, B., I. Petropavlovskikh, J. Staehelin, T. August, P.K. Bhartia, C. Clerbaux, D. Degenstein, M.D. Mazière, B.M. Dinelli, A. Dudhia, G. Dufour, S.M. Frith, L. Froidevaux, S. Godin-Beekmann, J. Granville, N.R.P. Harris, K. Hoppel, D. Hubert, Y. Kasai, M.J. Kurylo, E. Kyrölä, J.-C. Lambert, P.F. Levelt, C.T. McElroy, R.D. McPeters, R. Munro, H. Nakajima, A. Parrish, P. Raspollini, E.E. Remsberg, K.H. Rosenlof, A. Rozanov, T. Sano, Y. Sasano, M. Shiotani, H.G.J. Smit, G. Stiller, J. Tamminen, D.W. Tarasick, J. Urban, R.J. van der A, J.P. Veefkind, C. Vigouroux, T. von Clarmann, C. von Savigny, K.A. Walker, M. Weber, J. Wild, and J.M. Zawodny, Past changes in the vertical distribution of ozone, Part 1: Measurement techniques, uncertainties and availability, *Atmos. Meas. Tech.*, *7*, 1395–1427, doi:10.5194/amt-7-1395-2014, 2014.

Hendrickx, K., L. Megner, J. Gumbel, D.E. Siskind, Y.J. Orsolini, H.N. Tyssøy, and M. Hervig, Observation of 27-day solar cycles in the production and mesospheric descent of EPP-produced NO, *J. Geophys. Res. Space Phys.*, *120* (10), 8978–8988, doi:10.1002/2015JA021441, 2015.

Hocke, K., Response of the middle atmosphere to the geomagnetic storm of November 2004, *J. Atmos. Terr. Phys.*, *154*, 86–91, doi: 10.1016/j.jastp.2016.12.013 2017.

Hofmann, D.J., and S. Solomon, Ozone destruction through heterogeneous chemistry following the eruption of El Chichón, *J. Geophys. Res.*, *94* (D4), 5029–5041, doi:10.1029/JD094iD04p05029, 1989.

Hoffmann, L., R. Spang, A. Orr, M.J. Alexander, L.A. Holt, and O. Stein, A decadal satellite record of gravity wave activity in the lower stratosphere to study polar stratospheric cloud formation, *Atmos. Chem. Phys.*, *17* (4), 2901–2920, doi:10.5194/acp-17-2901-2017, 2017.

Hossaini, R., M.P. Chipperfield, S.A. Montzka, A. Rap, S. Dhomse, and W. Feng, Efficiency of short-lived halogens at influencing climate through depletion of stratospheric ozone, *Nat. Geosci.*, *8*, 186–190, doi:10.1038/ngeo2363, 2015a.

Hossaini, R., M.P. Chipperfield, A. Saiz-Lopez, J.J. Harrison, R. von Glasow, R. Sommariva, E. Atlas, M. Navarro, S.A. Montzka, W. Feng, S. Dhomse, C. Harth, J. Mühle, C. Lunder, S. O'Doherty, D. Young, S. Reimann, M.K. Vollmer, P.B. Krummel, and P.F. Bernath, Growth in stratospheric chlorine from short-lived chemicals not controlled by the Montreal protocol, *Geophys. Res. Lett.*, *42* (11), 4573–4580, doi:10.1002/2015GL063783, 2015b.

Hossaini, R., M.P. Chipperfield, S.A. Montzka, A.A. Leeson, S.S. Dhomse, and J.A. Pyle, The increasing threat to stratospheric ozone from dichloromethane, *Nat. Comm.*, *8*, 186–190, doi:10.1038/ncomms15962, 2017.

Hu, D., W. Tian, F. Xie, J. Shu, and S. Dhomse, Effects of meridional sea surface temperature change on stratospheric temperature and circulation, *Adv. Atmos. Sci.*, *31*, 888–900, doi:10.007/s00376-013-3152-6, 2014.

Hubert, D., J.-C. Lambert, T. Verhoelst, J. Granville, A. Keppens, J.-L. Baray, A.E. Bourassa, U. Cortesi, D.A. Degenstein, L. Froidevaux, S. Godin-Beekmann, K.W. Hoppel, B.J. Johnson, E. Kyrölä, T. Leblanc, G. Lichtenberg, M. Marchand, C.T. McElroy, D. Murtagh, H. Nakane, T. Portafaix, R. Querel, J.M. Russell III, J. Salvador, H.G. Smit, K. Stebel, W. Steinbrecht, K.B. Strawbridge, R. Stübi, D.P.J. Swart, G. Taha, D.W. Tarasick, A.M. Thompson, J. Urban, J.A.E. van Gijsel, R. Van Malderen, P. von der Gathen, K.A. Walker, E. Wolfram, and J.M. Zawodny, Ground-based assessment of the bias and long-term stability of 14 limb and occultation ozone profile data records, *Atmos. Meas. Tech.*, *9*, 2497–2534, doi:10.5194/amt-9-2497-2016, 2016.

Huck, P.E., S. Tilmes, G.E. Bodeker, W.J. Randel, A.J.

McDonald, and H. Nakajima, An improved measure of ozone depletion in the Antarctic stratosphere, *J. Geophys. Res.*, *112*, D11104, doi:10.1029/2006JD007860, 2007.

Hurwitz, M., P. Newman, and C. Garfinkel, On the influence of the North Pacific sea surface temperatures on the Arctic winter climate, *J. Geophys. Res.*, *117*, D19110, doi:10.1029/2012JD017819, 2012.

Hurwitz, M.M., N. Calvo, C.I. Garfinkel, A.H. Butler, S. Ineson, C. Cagnazzo, E. Manzini, and C. Peña-Ortiz, Extra-tropical atmospheric response to ENSO in the CMIP5 models, *Clim. Dyn.*, *43*, doi:10.1007/s00382-014-2110-z, 2014.

Iannarelli, R., and M.J. Rossi, Heterogeneous kinetics of H_2O, HNO_3 and HCl on HNO_3 hydrates (α-NAT, β-NAT, NAD) in the range 175–200 K, *Atmos. Chem. Phys.*, *16* (18), 11,937–11,960, doi:10.5194/acp-16-11937-2016, 2016.

Iglesias-Suarez, F, P.J. Young, and O. Wild, Stratospheric ozone change and related climate impacts over 1850–2100 as modelled by the ACCMIP ensemble, *Atmos. Chem. Phys.*, *16*, 343–363, doi:10.5194/acp-16-343-2016, 2016.

Ivy, D.J., S. Solomon, and H.E. Rieder, Radiative and dynamical influences on polar stratospheric temperature trends, *J. Clim.*, *29* (13), 4927–4938, doi:10.1175/jcli-d-15-0503.1, 2016.

Ivy, D.J., S. Solomon, D. Kinnison, M.J. Mills, A. Schmidt, and R.R. Neely III, The influence of the Calbuco eruption on the 2015 Antarctic ozone hole in a fully coupled chemistry-climate model, *Geophys. Res. Lett.*, *44*, 2556–2561, doi:10.1002/2016GL071925, 2017.

Iza, M., N. Calvo, and E. Manzini, The stratospheric pathway of La Niña, *J. Clim.*, *29*, doi:10.1175/JCLI-D.16-0230.1, 2016.

Jackman, C.H., D.R. Marsh, F.M. Vitt, R.G. Roble, C.E. Randall, P.F. Bernath, B. Funke, M. López-Puertas, S. Versick, G.P. Stiller, A.J. Tylka, and E. L. Fleming, Northern Hemisphere atmospheric influence of the solar proton events and ground level enhancement in January 2005, *Atmos. Chem. Phys.*, *11*, 6153–6166, doi:10.5194/acp-11-6153-2011, 2011.

Jackman, C.H., C.E. Randall, V.L. Harvey, S. Wang, E.L. Fleming, M. López-Puertas, B. Funke, and P.F. Bernath, Middle atmospheric changes caused by the January and March 2012 solar proton events, *Atmos. Chem. Phys.*, *14* (2), 1025–1038, doi:10.5194/acp-14-1025-2014, 2014.

Jaeglé, L., C.R. Webster, R.D. May, D.C. Scott, R.M. Stimpfle, D.W. Kohn, P.O. Wennberg, T.F. Hanisco, R.C. Cohen, M.H. Proffitt, K.K. Kelly, J. Elkins, D. Baumgardner, J.E. Dye, J.C. Wilson, R.F. Pueschel, K.R. Chan, R.J. Salawitch, A.F. Tuck, S.J. Hovde, and Y.L. Yung, Evolution and stoichiometry of heterogeneous processing in the Antarctic stratosphere, *J. Geophys. Res.*, *10* (102), 13,235–13,253, doi:10.1029/97JD00935, 1997.

James, A.D., J.S.A. Brooke, T.P. Mangan, T.F. Whale, J.M.C. Plane, and B.J. Murray, Nucleation of nitric acid hydrates in polar stratospheric clouds by meteoric material, *Atmos. Chem. Phys.*, *18*, 4519–4531, doi:10.5194/acp-18-4519-2018, 2018.

Kalnay, E., M. Kanamitsu, R. Kistler, W. Collins, D. Deaven, L. Gandin, M. Iredell, S. Saha, G. White, J. Woollen, Y. Zhu, A. Leetmaa, R. Reynolds, M. Chelliah, W. Ebisuzaki, W. Higgins, J. Janowiak, K.C. Mo, C. Ropelewski, J. Wang, R. Jenne, and D. Joseph, The NCEP/NCAR 40-Year Reanalysis Project, *Bull. Am. Meteorol. Soc.*, *77*, 437–471, doi:10.1175/1520-0477(1996)077<0437:TNYRP>2.0.CO;2, 1996.

Kawa, S.R., P.A. Newman, L.R. Lait, M.R. Schoeberl, R.M. Stimpe, D.W. Kohn, C.R. Webster, R.D. May, D. Baumgardner, J.E. Dye, J.C. Wilson, K.R. Chan, and M. Loewenstein, Activation of chlorine in sulfate aerosol as inferred from aircraft observations, *J. Geophys. Res.*, *102* (D3), 3921–3933, doi:10.1029/96JD01992, 1997.

Khosrawi, F., J. Urban, S. Lossow, G. Stiller, K. Weigel, P. Braesicke, M.C. Pitts, A. Rozanov, J.P. Burrows, and D. Murtagh, Sensitivity of polar stratospheric cloud formation to changes in water vapour and temperature, *Atmos. Chem. Phys.*, *16*, 101–121, doi:10.5194/acp-16-101-2016, 2016.

Khosrawi, F., O. Kirner, B.-N. Sinnhuber, S. Johansson, M. Höpfner, M.L. Santee, L. Froidevaux, J. Ungermann, R. Ruhnke, W. Woiwode, H, Oelhaf, and P. Braesicke, Denitrification, dehydration and ozone loss during the 2015/2016 Artic winter, *Atmos. Chem. Phys.*, *17*, 12,893-12,910, doi:10.5194/acp-17-12893-2017, 2017.

Kirner, O., R. Müller, R. Ruhnke, and H. Fischer, Contribution of liquid, NAT and ice particles to chlorine activation and ozone depletion in Antarctic winter and spring, *Atmos. Chem. Phys.*, *15* (4), 2019–2030, doi:10.5194/acp-15-2019-2015,

2015a.

Kirner, O., R. Ruhnke, and B.-M. Sinnhuber, Chemistry-climate interactions of stratospheric and mesospheric ozone in EMAC long-term simulations with different boundary conditions for CO_2, CH_4, N_2O, and ODS, *Atmos. Ocean*, *53* (1), 140–152, doi:10.1080/07055900.2014.9807, 2015b.

Klekociuk, A.R., M.B. Tully, P.B. Krummel, H.P. Gies, S.P. Alexander, P.J. Fraser, S.I. Henderson, J. Javorniczky, J.D. Shanklin, R. Schofield, and K.A. Stone, The Antarctic ozone hole during 2013, *Aust. Meteorol. Ocean*, *65*, 247–266, 2015.

Klobas, J.E., D.M. Wilmouth, D.K. Weisenstein, J.G. Anderson, and R.J. Salawitch, Ozone depletion following future volcanic eruptions, *Geophys. Res. Lett*., *44*, doi:10.1002/2017GL073972, 2017.

Knibbe, J.S., R.J. van der A, and A.T. J. de Laat, Spatial regression analysis on 32 years of total column ozone data, *Atmos. Chem. Phys*., *14*, 8461–8482, doi:10.5194/acp-14-8461-2014, 2014.

Kodera, K., On the origin and nature of the interannual variability of the winter stratospheric circulation in the Northern Hemisphere, *J. Geophys. Res*., *100*, 14,077–14,087, 1995.

Kutterolf, S., T. Hansteen, A. Freundt, H. Wehrmann, K. Appel, K. Krüger, and W. Perez, Bromine and chlorine emissions from Plinian eruptions along the Central American volcanic arc: From source to atmosphere, *Earth Planet. Sci. Lett.*, *429,* 234–246, doi:10.1016/j.epsl.2015.07.064, 2015.

Kuttippurath, J., and P.J. Nair, The signs of Antarctic ozone recovery, *Sci. Rep.*, *7*, 585, doi:10.1038/s41598-017-00722-7, 2017.

Kuttippurath, J., G.E. Bodeker, H.K. Roscoe, and P.J. Nair, A cautionary note on the use of EESC-based regression analysis for ozone trend studies, *Geophys. Res. Lett*., *42*, 162–168, doi:10.1002/2014GL062142, 2015.

Labitzke, K.G., and H. van Loon, *The Stratosphere: Phenomena, History, and Relevance*, Springer-Verlag Berlin Heidelberg GmbH, New York, New York, doi:10.1007/978-3-642-58541-8, 1999.

Lambert, A., and M.L. Santee, Accuracy and precision of polar lower stratospheric temperatures from reanalyses evaluated from A-Train CALIOP and MLS, COSMIC GPS RO, and the equilibrium thermodynamics of supercooled ternary solutions and ice clouds, *Atmos. Chem. Phys*., *18*, 1945–1975, doi:10.5194/acp-18-1945-2018, 2018.

Lambert, A., M.L. Santee, and N.J. Livesey, Interannual variations of early winter Antarctic polar stratospheric cloud formation and nitric acid observed by CALIOP and MLS, *Atmos. Chem. Phys*., *16* (23), 15,219–15,246, doi:10.5194/acp-16-15219-2016, 2016.

Langematz, U., S. Meul, K. Grunow, E. Romanowsky, S. Oberländer, J. Abalichin, and A. Kubin, Future Arctic temperature and ozone: The role of stratospheric composition changes, *J. Geophys. Res. Atmos*., *119*, 2092–2112, doi:10.1002/2013JD021100, 2014.

Langematz, U., F. Schmidt, M. Kunze, G.E. Bodeker, and P. Braesicke, Antarctic ozone depletion between 1960 and 1980 in observations and chemistry-climate model simulations, *Atmos. Chem. Phys.*, *16* (24), 15,619–15,627, doi:10.5194/acp-16-15619-2016, 2016.

Lawrence, Z.D., and G.L. Manney, Characterizing stratospheric polar vortex variability with computer vision techniques, *J. Geophys. Res.*, *122*, doi:10.1002/2017JD027556, 2017.

Lawrence, Z.D., G.L. Manney, K. Minschwarner, M.L. Santee, and A. Lambert, Comparisons of polar processing diagnostics from 34 years of the ERA-Interim and MERRA reanalyses, *Atmos. Chem. Phys.*, *17*, 3873–3892, doi:10.5194/acp-15-3873-2015, 2015.

Leedham Elvidge, E.C., D.E. Oram, J.C. Laube, A.K. Baker, S.A. Montzka, S. Humphrey, D.A. O'Sullivan, and C.A.M. Brenninkmeijer, Increasing concentrations of dichloromethane, CH_2Cl_2, inferred from CARIBIC air samples collected 1998–2012, *Atmos. Chem. Phys*., *15* (4), 1939–1958, doi:10.5194/acp-15-1939-2015, 2015.

Li, S., J. Perlwitz, M.P. Hoerling, and X. Chen, Opposite annular responses on the Northern and Southern Hemispheres to Indian Ocean warming, *J. Clim*., *23*, 3720–3738, doi:10.1175/2010JCLI3410.1, 2010.

Long, C.S., M. Fujiwara, S. Davis, D.M. Mitchell, and C.J. Wright, Climatology and interannual variability of dynamic variables in multiple reanalyses evaluated by the SPARC Reanalysis Intercomparison Project (S-RIP), *Atmos. Chem. Phys.*, *17*, 14,593–14,629, doi:10.5194/acp-17-14593-2017, 2017.

Lubis, S.W., V. Silverman, K. Matthes, N. Harnik, N.-

E. Omrani, and S. Wahl, How does downward planetary wave coupling affect polar stratospheric ozone in the Arctic winter stratosphere?, *Atmos. Chem. Phys.*, *17*, 2437–2458, doi:10.5194/acp-17-2437-2017, 2017.

Manney, G.K., and Z.D. Lawrence, The major stratospheric final warming in 2016: Dispersal of vortex air and termination of Arctic chemical ozone loss, *Atmos. Chem. Phys.*, *16*, 15,371–15,396, doi:10.5194/acp-16-15371-2016, 2016.

Manney, G.K., Z.D. Lawrence, M.L. Santee, N.J. Livesey, A. Lambert, and M.C. Pitts, Polar processing in a split vortex: Arctic ozone loss in early winter 2012/2013, *Atmos. Chem. Phys.*, *15*, 5381–5403, doi:10.5194/acp-15-5381-2015, 2015a.

Manney, G.L., Z.D. Lawrence, M.L. Santee, W.G. Read, N.J. Livesey, A. Lambert, L. Froidevaux, H.C. Pumphrey, and M.J. Schwartz, A minor sudden stratospheric warming with a major impact: Transport and polar processing in the 2014/2015 Arctic winter, *Geophys. Res. Lett.*, *42*, 7808–7816, doi:10.1002/2015GL065864, 2015b.

Matthias, V., A. Dörnbrack, and G. Stober, The extraordinarily strong and cold polar vortex in the early northern winter 2015/2016, *Geophys. Res. Lett.*, *43*, 12,287–12,294, doi:10.1002/2016GL071676, 2016.

Meinshausen, M., S.J. Smith, K. Calvin, J.S. Daniel, M.L.T. Kainuma, J.-F. Lamarque, K. Matsumoto, S.A. Montzka, S.C.B. Raper, K. Riahi, A. Thomson, G.J.M. Velders, and D.P.P. van Vuuren, The RCP greenhouse gas concentrations and their extensions from 1765 to 2300, *Clim. Change*, *109* (1/2), 213-241, doi:10.1007/s10584-011-0156-z, 2011.

Mironova, I.A., K.L. Aplin, F. Arnold, G.A. Bazilevskaya, R.G. Harrison, A.A. Krivolutsky, K.A. Nicoll, E.V. Rozanov, E. Turunen, and I.G. Usoskin, Energetic particle influence on the Earth's atmosphere, *Space Sci. Rev.*, *194*, 1–96, doi:10.1007/s11214-015-0185-4, 2015.

Molleker, S., S. Borrmann, H. Schlager, B. Luo, W. Frey, M. Klingebiel, R. Weigel, M. Ebert, V. Mitev, R. Matthey, W. Woiwode, H. Oelhaf, A. Dörnbrack, G. Stratmann, J.-U. Grooß, G. Günther, B. Vogel, R. Müller, M. Krämer, J. Meyer, and F. Cairo, Microphysical properties of synoptic-scale polar stratospheric clouds: In situ measurements of unexpectedly large HNO_3-containing particles in the Arctic vortex, *Atmos. Chem. Phys.*, *14* (19), 10,785–10,801, doi:10.5194/acp-14-10785-2014, 2014.

Morgenstern, O., P. Braesicke, M.M. Hurwitz, F.M. O'Connor, A.C. Bushell, C.E. Johnson, and J.A. Pyle, The world avoided by the Montreal Protocol, *Geophys. Res. Lett.*, *35*, L16811, doi:10.1029/2008GL034590, 2008.

Morgenstern, O., M.I. Hegglin, E. Rozanov, F.M. O'Connor, N.L. Abraham, H. Akiyoshi, A.T. Archibald, S. Bekki, N. Butchart, M.P. Chipperfield, M. Deushi, S.S. Dhomse, R.R. Garcia, S.C. Hardiman, L.W. Horowitz, P. Jöckel, B. Josse, D. Kinnison, M. Lin, E. Mancini, M.E. Manyin, M. Marchand, V. Marécal, M. Michou, L.D. Oman, G. Pitari, D.A. Plummer, L.E. Revell, D. Saint-Martin, R. Schofield, A. Stenke, K. Stone, K. Sudo, T.Y. Tanaka, S. Tilmes, Y. Yamashita, K. Yoshida, and G. Zeng, Review of the global models used within phase 1 of the Chemistry–Climate Model Initiative (CCMI), *Geosci. Model Dev.*, *10*, 639–671, doi:10.5194/gmd-10-639-2017, 2017.

Morgenstern, O., K.A. Stone, R. Schofield, H. Akiyoshi, Y. Yamashita, D.E. Kinnison, R.R. Garcia, K. Sudo, D.A. Plummer, J. Scinocca, L.D. Oman, M.E. Manyin, G. Zeng, E. Rozanov, A. Stenke, L.E. Revell, G. Pitari, E. Mancini, G. Di Genova, D. Visioni, S.S. Dhomse, and M.P. Chipperfield, Ozone sensitivity to varying greenhouse gases and ozone-depleting substances in CCMI-1 simulations, *Atmos. Chem. Phys.*, *18*, 1091–1114, doi:10.5194/acp-18-1091-2018, 2018.

Müller, R., J.-U. Grooß, C. Lemmen, D. Heinze, M. Dameris, and G. Bodeker, Simple measures of ozone depletion in the polar stratosphere, *Atmos. Chem. Phys.*, *8*, 251–264, doi:10.5194/acp-8-251-2008, 2008.

Müller, R., J.-U. Grooß, A.M. Zafar, S. Robrecht, and R. Lehmann, The maintenance of elevated active chlorine levels in the Antarctic lower stratosphere through HCl null cycles, *Atmos. Chem. Phys.*, *18*, 2985–2997, doi:10.5194/acp-18-2985-2018, 2018.

Murphy, D.M., and B.L. Gary, Mesoscale temperature fluctuations and polar stratospheric clouds, *J. Atmos. Sci.*, *52* (10), 1753–1760, doi:10.1175/1520-0469(1995)<1753:mtfapd>2.0.co;2, 1995.

Muthers, S., J.G. Anet, C.C. Raible, S. Brönnimann, E. Rozanov, F. Arfeuille, T. Peter, A.I. Shapiro, J. Beer, F. Steinhilber, Y. Brugnara, and W. Schmutz,

Northern hemispheric winter warming pattern after tropical volcanic eruptions: Sensitivity to the ozone climatology, *J. Geophys. Res. Atmos.*, *119*, 1340–1355, doi:10.1002/2013JD020138, 2014.

Muthers, S., F. Arfeuille, C.C. Raibel, and E. Rozanov, The impacts of volcanic aerosol on stratospheric ozone and the Northern Hemisphere polar vortex: Separating radiative-dynamical changes from direct effects due to enhanced aerosol heterogeneous chemistry, *Atmos. Chem. Phys.*, *15*, 11,461–11,476, doi:10.5194/acp-15-11461-2015, 2015.

Naik V., L.W. Horowitz, M.D. Schwarzkopf, and M. Lin, Impact of volcanic aerosols on stratospheric ozone recovery, *J. Geophys. Res. Atmos.*, *122*, doi:10.1002/2016JD025808, 2017.

Nakajima, H., I. Wohltmann, T. Wegner, M. Takeda, M.C. Pitts, L.R. Poole, R. Lehmann, M.L. Santee, and M. Rex, Polar stratospheric cloud evolution and chlorine activation measured by CALIPSO and MLS, and modeled by ATLAS, *Atmos. Chem. Phys., 16*, 3311–3325, doi:10.5194/acp-16-3311-2016, 2016.

Nash, E.R., P.A. Newman, J.E. Rosenfield, and M.R. Schoeberl, An objective determination of the polar vortex using Ertel's potential vorticity, *J. Geophys. Res.*, *101*, 9471–9478, doi:10.1029/96JD00066, 1996.

Nash, E.R., S.E. Strahan, N. Kramarova, C.S. Long, M.C. Pitts, P.A. Newman, B. Johnson, M.L. Santee, I. Petropavlovskikh, and G.O. Braathen, Antarctic Ozone Hole [in "State of the Climate in 2015"], *Bull. Am. Meteorol. Soc.*, *97* (8), S188–S172, 2016.

Newman, P.A., and E.R. Nash, The unusual Southern Hemisphere stratosphere winter of 2002, *J. Atmos. Sci.*, *62*, 614-628, doi:10.1175/JAS-3323.1, 2005.

Newman, P.A., S.R. Kawa, and E.R. Nash, On the size of the Antarctic ozone hole, *Geophys. Res. Lett., 31*, L21104, doi:10.1029/2004GL020596, 2004.

Newman, P.A., E.R. Nash, S.R. Kawa, S.A. Montzka, and S.M. Schauffler, When will the Antarctic ozone hole recover?, *Geophys. Res. Lett.*, *33*, L12814, doi:10.1029/2005GL025232, 2006.

Newman, P.A., L.D. Oman, A.R. Douglass, E.L. Fleming, S.M. Frith, M.M. Hurwitz, S.R. Kawa, C.H. Jackman, N.A. Krotkov, E.R. Nash, J.E. Nielsen, S. Pawson, and G.J.M. Velders, What would have happened to the ozone layer if chlorofluorocarbons had not been regulated?, *Atmos. Chem. Phys.*, *9*, 2113–2128, doi:10.5194/acp-9-2113-2009, 2009.

Newman, P.A., E.R. Nash, S.E. Strahan, N. Kramarova, C.S. Long, M.C. Pitts, B. Johnson, M.L. Santee, I. Petropavlovskikh, and G.O. Braathen, Stratospheric Ozone [in "State of the Climate in 2014"], *Bull. Am. Meteorol. Soc.*, *96* (7), S165–S167, 2015.

Newman, P.A., E.R. Nash, S.E. Strahan, N. Kramarova, C.S. Long, M.C. Pitts, B. Johnson, M.L. Santee, I. Petropavlovskikh, and G.O. Braathen, 2016 Antarctic ozone [in "State of the Climate in 2016"], *Bull. Am. Meteorol. Soc.*, *98* (8), S169–S172, doi:10.1175/2017BAMSStateoftheClimate.1, 2017.

Oberländer, S., U. Langematz, and S. Meul, Unraveling impact factors for future changes in the Brewer-Dobson circulation, *J. Geophys. Res. Atmos.*, *118*, 10,296–10,312, doi:10.1002/jgrd.50775, 2013.

Oman, L.D., D.A. Plummer, D.W. Waugh, J. Austin, J.F. Scinocca, A.R. Douglass, R.J. Salawitch, T. Canty, H. Akiyoshi, S. Bekki, P. Braesicke, N. Butchart, M.P. Chipperfield, D. Cugnet, S. Dhomse, V. Eyring, S. Frith, S.C. Hardiman, D.E. Kinnison, J.-F. Lamarque, E. Mancini, M. Marchand, M. Michou, O. Morgenstern, T. Nakamura, J.E. Nielsen, D. Olivié, G. Pitari, J. Pyle, E. Rozanov, T.G. Shepherd, K. Shibata, R.S. Stolarski, H. Teyssèdre, W. Tian, Y. Yamashita, and J.R. Ziemke, Multimodel assessment of the factors driving stratospheric ozone evolution over the 21st century, *J. Geophys. Res. Atmos.*, *115*, D24306, doi:10.1029/2010JD014362, 2010.

Oman, L.D., A.R. Douglass, R.J. Salawitch, T.P. Canty, J.R. Ziemke, and M. Manyin, The effect of representing bromine from VSLs on the simulation and evolution of Antarctic ozone, *Geophys. Res. Lett.*, *43*, 9869–9876, doi:10.1002/2016GL070471, 2016.

Omrani, N.-E., N.S. Keenlyside, J. Bader, and E. Manzini, Stratosphere key for wintertime atmospheric response to warm Atlantic decadal conditions, *Clim. Dyn.*, *42*, 649–663, doi:10.1007/s00382-013-1860-3, 2014.

Oram, D.E., M.J. Ashford, J.C. Laube, L.J. Gooch, S. Humphrey, W.T. Surges, E. Leedham-Elvidge, G.L. Forster, N.R.P. Harris, M.I., Mead, A.A. Samah, S.M. Phang, C.-F. Ou-Yang, N.-H. Lin, J.-L. Wang, A.K. Baker, C.A.M. Brenninkmeijer, and D. Sherry, A growing threat to the ozone layer from

short-lived anthropogenic chlorocarbons, *Atmos. Chem. Phys.*, *17*, 11,929-11,941, doi:10.5194/acp-17-11929-2017, 2017.

Orr, A., J.S. Hosking, L. Homann, J. Keeble, S.M. Dean, H.K. Roscoe, N.L. Abraham, S. Vosper, and P. Braesicke, Inclusion of mountain wave-induced cooling for the formation of PSCs over the Antarctic Peninsula in a chemistry-climate model, *Atmos. Chem. Phys.*, *15* (2), 1071–1086, doi:10.5194/acp-15-1071-2015, 2015.

Orsolini, Y.J., V. Limpasuvan, K. Pérot, P. Espy, R. Hibbins, S. Lossow, K. Raaholt Larsson, and D. Murtagh, Modelling the descent of nitric oxide during the elevated stratopause event of January 2013, *J. Atmos. Terr. Sci.*, *155*, 50–61, doi:10.1016/j.jastp.2017.01.006, 2017.

Päivärinta, S.M., P.T. Verronen, B. Funke, A. Gardini, A. Seppälä, and M.E. Andersson, Transport versus energetic particle precipitation: Northern polar stratospheric NO_x and ozone in January–March 2012, *J. Geophys. Res. Atmos.*, *121* (10), 6085–6100, doi:10.1002/2015JD024217, 2016.

Parrondo, M.C., M. Gil, M. Yela, B.J. Johnson, and H.A. Ochoa, Antarctic ozone variability inside the polar vortex estimated from balloon measurements, *Atmos. Chem. Phys.*, *14* (1), 217–229, doi:10.5194/acp-14-217-2014, 2014.

Pazmiño, A., S. Godin-Beekmann, A. Hauchecorne, C. Claud, S. Khaykin, F. Goutail, E. Wolfram, J. Salvador, and E. Quel, Multiple symptoms of total ozone recovery inside the Antarctic vortex during austral spring, *Atmos. Chem. Phys., 18*, 7557–7572, doi:10.5194/acp-18-7557-2018, 2018.

Pérot, K., J. Urban, and D.P. Murtagh, Unusually strong nitric oxide descent in the Arctic middle atmosphere in early 2013 as observed by Odin/SMR, *Atmos. Chem. Phys.*, *14* (15), 8009–8015, doi:10.5194/acp-14-8009-2014, 2014.

Pitari, G., G. Di Genova, E. Mancini, D. Visioni, I. Gandolfi, and I. Cionni, Stratospheric aerosols from major volcanic eruptions: A Composition-Climate Model Study of the aerosol cloud dispersal and e-folding time, *Atmos.*, *7* (75), doi:10.3390/atmos7060075, 2016.

Pommereau, J.-P., F. Goutail, F. Lefèvre, A. Pazmiño, C. Adams, V. Dorokhov, P. Eriksen, R. Kivi, K. Stebel, X. Zhao, and M. van Roozendael, Why unprecedented ozone loss in the Arctic in 2011? Is it related to climate change?, *Atmos. Chem. Phys.*, *13*, 5299–5308, doi:10.5194/acp-13-5299-2013, 2013.

Portmann, R.W., J.S. Daniel, and A.R. Ravishankara, Stratospheric ozone depletion due to nitrous oxide: Influences of other gases, *Philos. Trans. Roy. Soc. B*, *367* (1593), 1256–1264, doi:10.1098/rstb.2011.0377, 2012.

Raible, C.C., S. Brönnimann, R. Auchmann, P. Brohan, T.L. Froelicher, H.-F. Graf, P. Jones, J. Luterbacher, S. Muthers, R. Neukom, A. Robock, S. Self, A. Sudrajat, C. Timmreck, and M. Wegmann, Tambora 1815 as a test case for high impact volcanic eruptions: Earth system effects, *WIREs Clim. Change*, *7*, 569–589, doi:10.1002/wcc.407, 2016.

Randall, C.E., V.L. Harvey, C.S. Singleton, S.M. Bailey, P.F. Bernath, M. Codrescu, H. Nakajima, and J.M. Russell, Energetic particle precipitation effects on the Southern Hemisphere stratosphere in 1992–2005, *J. Geophys. Res.*, *112*, D08308, doi:10.1029/2006JD007696, 2007.

Randel, W.J., L. Polvani, F. Wu, D.E. Kinnison, C.-Z. Zou, and C. Mears, Troposphere-stratosphere temperature trends derived from satellite data compared with ensemble simulations from WACCM, *J. Geophys. Res. Atmos.*, *122* (18), 9651-9667, doi: 10.1002/2017JD027158, 2017.

Revell, L.E., G.E. Bodeker, P.E. Huck, B.E. Williamson, and E. Rozanov, The sensitivity of stratospheric ozone changes through the 21st century to N_2O and CH_4, *Atmos. Chem. Phys.*, *12,* 11,309–11,317, doi:10.5194/acp-12-11309-2012, 2012.

Revell, L.E., F. Tummon, R.J. Salawitch, A. Stenke, and T. Peter, The changing ozone depletion potential of N_2O in a future climate, *Geophys. Res. Lett., 42*, 10,047–10,055, doi:10.1002/2015GL065702, 2015.

Rex, M., R.J. Salawitch, N.R.P. Harris, P. von der Gathen, G.O. Braathen, A. Schulz, H. Deckelmann, M. Chipperfield, B.-M. Sinnhuber, E. Reimer, R. Alfier, R. Bevilacqua, K. Hoppel, M. Fromm, J. Lumpe, H. Küllmann, A. Kleinböhl, H. Bremer, M. von König, K. Künzi, D. Toohey, H. Vömel, E. Richard, K. Aikin, H. Jost, J.B. Greenblatt, M. Loewenstein, J.R. Podolske, C.R. Webster, G.J. Flesch, D.C. Scott, R.L. Herman, J.W. Elkins, E.A. Ray, F.L. Moore, D.F. Hurst, P. Romashkin, G.C. Toon, B. Sen, J.J. Margitan, P. Wennberg, R. Neuber, M. Allart, B.R. Bojkov, H. Claude, J. Davies, W. Davies, H. De Backer, H. Dier, V. Dorokhov, H. Fast,

Y. Kondo, E. Kyrö, Z. Litynska, I.S. Mikkelsen, M.J. Molyneux, E. Moran, T. Nagai, H. Nakane, C. Parrondo, F. Ravegnani, P. Skrivankova, P. Viatte, and V. Yushkov, Chemical depletion of Arctic ozone in winter 1999/2000, *J. Geophys. Res.*, *107* (D20), doi:10.1029/2001JD000533, 2002.

Rex, M., R.J. Salawitch, P. von der Gathen, N.R.P. Harris, M.P. Chipperfield, and B. Naujokat, Arctic ozone loss and climate change, *Geophys. Res. Lett.*, *31*, L04116, doi:10.1029/2003GL018844, 2004.

Rex, M., R.J. Salawitch, H. Deckelmann, P. von der Gathen, N.R.P. Harris, M.P. Chipperfield, B. Naujokat, E. Reimer, M. Allaart, S.B. Andersen, R. Bevilacqua, G.O. Braathen, H. Claude, J. Davies, H. De Backer, H. Dier, V. Dorokhov, H. Fast, M. Gerding, S. Godin-Beekmann, K. Hoppel, B. Johnson, E. Kyrö, Z. Litynska, D. Moore, H. Nakane, M.C. Parrondo, A.D. Risley Jr., P. Skrivankova, R. Stübi, P. Viatte, V. Yushkov, and C. Zerefos, Arctic winter 2005: Implications for stratospheric ozone loss and climate change, *Geophys. Res. Lett.*, *33*, L23808, doi:10.1029/2006GL026731, 2006.

Rieder, H.E., and L.M. Polvani, Are recent Arctic ozone losses caused by increasing greenhouse gases?, *Geophys. Res. Lett.*, *40*, 4437–4441, doi:10.1002/grl.50835, 2013.

Rieder, H.E., L.M. Polvani, and S. Solomon, Distinguishing the impacts of ozone-depleting substances and well-mixed greenhouse gases on Arctic stratospheric ozone and temperature trends, *Geophys. Res. Lett.*, *41*, 2652–2660, doi:10.1002/2014GL059367, 2014.

Rosenfield, J.E., and A.R. Douglass, Doubled CO_2 effects on NO_y in a coupled 2-D model, *Geophys. Res. Lett., 25*, 4381–4384, doi:10.1029/1998GL900147, 1998.

Saha, S., S. Moorthi, H. Pan, X. Wu, J. Wang, S. Nadiga, P. Tripp, R. Kistler, J. Woollen, D. Behringer, H. Liu, D. Stokes, R. Grumbine, G. Gayno, J. Wang, Y. Hou, H. Chuang, H.H. Juang, J. Sela, M. Iredell, R. Treadon, D. Kleist, P. van Delst, D. Keyser, J. Derber, M. Ek, J. Meng, H. Wei, R. Yang, S. Lord, H. van den Dool, A. Kumar, W. Wang, C. Long, M. Chelliah, Y. Xue, B. Huang, J. Schemm, W. Ebisuzaki, R. Lin, P. Xie, M. Chen, S. Zhou, W. Higgins, C. Zou, Q. Liu, Y. Chen, Y. Han, L. Cucurull, R.W. Reynolds, G. Rutledge, and M. Goldberg, The NCEP Climate Forecast System Reanalysis, *Bull. Am. Meteorol. Soc.*, *91*, 1015–1058, doi:10.1175/2010BAMS3001.1, 2010.

Salawitch, R.J., S.C. Wofsy, and M.B. McElroy, Influence of polar stratospheric clouds on the depletion of Antarctic ozone, *Geophys. Res. Lett.*, *15*, 871–874, doi:10.1029/GL015i008p00871, 1988.

Salawitch, R.J., G.P. Gobbi, S.C. Wofsy, and M.B. McElroy, Denitrification in the Antarctic stratosphere, *Nature, 339*, 525–527, doi:10.1038/339525a0, 1989.

Sander, S.P., J. Abbatt, J.R. Barker, J.B. Burkholder, R.R. Friedl, D.M. Golden, R.E. Huie, C.E. Kolb, M.J. Kurylo, G.K. Moortgat, V.L. Orkin, and P.H. Wine, Chemical Kinetics and Photochemical Data for Use in Atmospheric Studies, Evaluation No. 17, *JPL Publication 10-6*, Jet Propulsion Laboratory, Pasadena, California. [available at: http://jpldataeval.jpl.nasa.gov], 2011.

Schütze, K., J.C. Wilson, S. Weinbruch, N. Benker, M. Ebert, G. Günther, R. Weigel, and S. Borrmann, Sub-micrometer refractory carbonaceous particles in the polar stratosphere, *Atmos. Chem. Phys.*, *17*, 12,475–12,493, doi:10.5194/acp-17-12475-2017, 2017.

Sinnhuber, B.-M., and S. Meul, Simulating the impact of emissions of brominated very short lived substances on past stratospheric ozone trends, *Geophys. Res. Lett.*, *42*, 2449–2456, doi:10.1002/2014GL062975, 2015.

Sinnhuber, M., H. Nieder, and N. Wieters, Energetic particle precipitation and the chemistry of the mesosphere / lower thermosphere, *Surv. Geophys.*, *33*, doi:10.1007/s10712-012-9201-3, 2012.

Sinnhuber, M., U. Berger, B. Funke, H. Nieder, T. Reddmann, G. Stiller, S. Versick, T. von Clarmann, and J.M. Wissing, NO_y production, ozone loss and changes in net radiative heating due to energetic particle precipitation in 2002–2010, *Atmos. Chem. Phys.*, *18*, 1115–1147, doi:10.5194/acp-18-1115-2018, 2018.

Siskind, D.E., GE. Nedoluha, F. Sassi, P. Rong, S.M. Bailey, M.E. Hervig, and C.E. Randall, Persistence of upper stratospheric wintertime tracer variability into the Arctic spring and summer, *Atmos. Chem. Phys.*, *16*, 7957–7967, doi:10.5194/acp-16-7957-2016, 2016.

Solomon, S., R.R. Garcia, F.S. Rowland, and D.J. Wuebbles, On the depletion of Antarctic ozone, *Nature*, *321*, 755–758, doi:10.1038/321755a0,

1986.

Solomon, S., J. Haskins, D.J. Ivy, and F. Min, Fundamental differences between Arctic and Antarctic ozone depletion, *Proc. Natl. Acad. Sci.*, *111* (17), 6220–6225, doi:10.1073/pnas.1319307111, 2014.

Solomon, S., D. Kinnison, J. Bandoro, and R. Garcia, Simulation of polar ozone depletion: An update, *J. Geophys. Res.*, *120*, 7958–7974, doi:10.1002/2015JD023365, 2015.

Solomon, S., D.J. Ivy, D. Kinnison, M.J. Mills, R.R. Neely III, and A. Schmidt, Emergence of healing in the Antarctic ozone layer, *Science*, *353* (6296), 269–274, doi:10.1126/science.aae0061, 2016.

Solomon, S., D. Ivy, M. Gupta, J. Bandoro, B. Santer, Q. Fu, P. Lin, R.R. Garcia, D. Kinnison, and M. Mills, Mirrored changes in Antarctic ozone and stratospheric temperature in the late 20th versus early 21st centuries, *J. Geophys. Res. Atmos.*, *122*, doi:10.1002/2017JD026719, 2017.

Spang, R., L. Hoffmann, M. Höpfner, S. Griessbach, R. Müller, M.C. Pitts, A.M.W. Orr, and M. Riese, A multi-wavelength classification method for polar stratospheric cloud types using infrared limb spectra, *Atmos. Meas. Tech.*, *9* (8), 3619–3639, doi:10.5194/amt-9-3619-2016, 2016.

Spang, R., L. Hoffmann, R. Müller, J.-U. Grooß, I. Tritscher, M. Höpfner, M. Pitts, A. Orr, and M. Riese, A climatology of polar stratospheric cloud composition between 2002 and 2012 based on MIPAS/Envisat observations, *Atmos. Chem. Phys.*, *18*, 5089–5113, doi:10.5194/acp-18-5089-2018, 2018.

SPARC CCMVal (Stratosphere-troposphere Processes And their Role in Climate), *SPARC Report on the Evaluation of Chemistry-Climate Models*, edited by V. Eyring, T.G. Shepherd, and D.W. Waugh, SPARC Report No. 5, WCRP-132, WMO/TD-No. 1526, 478 pp., [available at: http://www.atmosp.physics.utoronto.ca/SPARC/ccmval_final/index.php], 2010.

SPARC (Stratosphere-troposphere Processes And their Role in Climate), *SPARC Report on the Lifetimes of Stratospheric Ozone-Depleting Substances, Their Replacements, and Related Species*, edited by M.K.W. Ko, P.A. Newman, S. Reimann, S.E. Strahan, SPARC Report No. 6, WCRP-15/2013, 2013.

Stolarski, R., M. Schoeberl, P. Newman, R. McPeters, and A. Krueger, The 1989 Antarctic ozone hole as observed by TOMS, *Geophys. Res. Lett.*, *17* (9), 1267–1270, doi:10.1029/GL017i009p01267, 1990.

Stolarski, R.S., A.R. Douglass, L.D. Oman, and D. Waugh, Impact of future nitrous oxide and carbon dioxide emissions on the stratospheric ozone layer, *Environ. Res. Lett., 10* (3), doi:10.1088/1748-9326/10/3/03011, 2015.

Stone, K.A., S. Solomon, D.E. Kinnison, M.C. Pitts, L.R. Poole, M.J. Mills, A. Schmidt, R.R. Neely III, D. Ivy, M.J. Schwartz, B.J. Johnson, M.B. Tully, A.R. Klekociuk, G. König-Langlo, and S. Hagiya, Observing the impact of Calbuco volcanic aerosols on South Polar ozone depletion in 2015, *J. Geophys. Res.*, *122*, 11,862–11,879, doi:10.1002/2017JD026987, 2017.

Strahan, S.E., and A.R. Douglass, Decline in Antarctic ozone depletion and lower stratospheric chlorine determined from Aura Microwave Limb Sounder observations, *Geophys. Res. Lett.*, *45*, 382–390, doi:10.1002/2017GL074830, 2018.

Strahan, S.E., A.R. Douglass, P.A. Newman, and S.D. Steenrod, Inorganic chlorine variability in the Antarctic vortex and implications for ozone recovery, *J. Geophys. Res. Atmos.*, *119* (24), doi:10.1002/2014JD022295, 2014.

Strahan, S.E., A.R. Douglass, and S.D. Steenrod, Chemical and dynamical impacts of stratospheric sudden warmings on Arctic ozone variability, *J. Geophys. Res. Atmos.*, *121*, 11,836–11,851, doi:10.1002/2016JD025128, 2016.

Tabazadeh, A., and R.P. Turco, A model for heterogeneous chemical processes on the surfaces of ice and nitric acid trihydrate particles, *J. Geophys. Res.*, *98* (D7), 12727–12740, doi:10.1029/93JD00947, 1993.

Tabazadeh. A., K. Drdla, M.R. Schoeberl, P. Hamill, and O.B. Toon, Arctic "ozone hole" in a cold volcanic stratosphere, *Proc. Natl. Acad. Sci.*, *99* (5), 2609–2612; doi:10.1073/pnas.052518199, 2002.

Tao, M., P. Konopka, F. Ploeger, J.-U. Grooß, R. Müller, C.M. Volk, K.A. Walker, and M. Riese, Impact of the 2009 major sudden stratospheric warming on the composition of the stratosphere, *Atmos. Chem. Phys.*, *15*, 8695–8715, doi: 10.5194/acp-15-8695-2015, 2015.

Tegtmeier, S., F. Ziska, I. Pisso, B. Quack, G.J.M. Velders, X. Yang, and K. Krüger, Oceanic bromoform emissions weighted by their ozone depletion potential, *Atmos. Chem. Phys.*, *15*, 13,647–13,663,

doi:10.5194/acp-15-13647-2015, 2015.

Tian, W., Y. Li, F. Xie, J. Zhang, M.P. Chipperfield, W. Feng, Y. Hu, S. Zhao, X. Zhou, Y. Yang, and X. Ma, The relationship between lower-stratospheric ozone at southern high latitudes and sea surface temperature in the East Asian marginal seas in austral spring, *Atmos. Chem. Phys.*, *17*, 6705–6722, doi:10.5194/acp-17-6705-2017, 2017.

Tie, X.-X., and G. Brasseur, The response of stratospheric ozone to volcanic eruptions: Sensitivity to atmospheric chlorine loading, *Geophys. Res. Lett.*, *22 (22)*, 3035–3038, doi:10.1029/95GL03057, 1995.

Tilmes, S., R. Müller, J.-U. Grooß, M. Höpfner, G.C. Toon, and J.M. Russell III, Very early chlorine activation and ozone loss in the Arctic winter 2002–2003, *Geophys. Res. Lett.*, *30* (23), 2201–2205, doi:10.1029/2003GL018079, 2003.

Toohey, M., K. Krüger, M. Bittner, C. Timmreck, and H. Schmidt, The impact of volcanic aerosols on the Northern Hemisphere stratospheric polar vortex: Mechanisms and sensitivity forcing structure, *Atmos. Chem. Phys.*, *14*, 13,063–13,079, doi:10.5194/acp-14-13063-2014, 2014.

Uchino, O., R.D. Bojkov, D.S. Balis, K. Akagi, M. Hayashi, and R. Kajihara, Essential characteristics of the Antarctic-spring ozone decline: Update to 1998, *Geophys. Res. Lett.*, *26* (10), 1377–1380, doi:10.1029/1999GL900277, 1999.

van Loon, H., and K. Labitzke, The Southern Oscillation, Part V: The anomalies in the lower stratosphere of the Northern Hemisphere in winter and a comparison with the Quasi-Biennial Oscillation, *Mon. Wea. Rev., 115*, 357–369, doi:10.1175/1520-0493(1987)115<0357:TSOPVT>2.0.CO;2, 1987.

Verkhoglyadova, O.P., S. Wang, M.G. Mlynczak, L.A. Hunt, and G.P. Zank, Effects of two large solar energetic particle events on middle atmosphere nighttime odd hydrogen and ozone content: Aura/MLS and TIMED/SABER measurements, *J. Geophys. Res. Space Phys.*, *120* (1), 12–29, doi:10.1002/2014JA020609, 2015.

Vogel, B., P. Konopka, J.-U. Grooß, R. Müller, B. Funke, M. López-Puertas, T. Reddmann, G. Stiller, T. von Clarmann, and M. Riese, Model simulations of stratospheric ozone loss caused by enhanced mesospheric NOx during Arctic Winter 2003/2004, *Atmos. Chem. Phys.*, *8*, 5279–5293, doi:10.5194/acp-8-5279-2008, 2008.

von Clarmann, T., B. Funke, M. López-Puertas, S. Kellmann, A. Linden, G.P. Stiller, C.H. Jackman, and V.L. Harvey, The Solar proton events in 2012 as observed by MIPAS, *Geophys. Res. Lett.*, *40*, 1–5, doi:10.1002/grl.50119, 2013.

von Hobe, M., S. Bekki, S. Borrmann, F. Cairo, F. D'Amato, G. Di Donfrancesco, A. Dörnbrack, A. Ebersoldt, M. Ebert, C. Emde, I. Engel, M. Ern, W. Frey, S. Genco, S. Griessbach, J.-U. Grooß, T. Gulde, G. Günther, E. Hösen, L. Hoffmann, V. Homonnai, C.R. Hoyle, I.S.A. Isaksen, D.R. Jackson, I.M. Janosi, R.L. Jones, K. Kandler, C. Kalicinsky, A. Keil, S.M. Khaykin, F. Khosrawi, R. Kivi, J. Kuttippurath, J.C. Laube, F. Lefevre, R. Lehmann, S. Ludmann, B.P. Luo, M. Marchand, J. Meyer, V. Mitev, S. Molleker, R. Müller, H. Oelhaf, F. Olschewski, Y. Orsolini, T. Peter, K. Pfeilsticker, C. Piesch, M.C. Pitts, L.R. Poole, F.D. Pope, F. Ravegnani, M. Rex, M. Riese, T. Röckmann, B. Rognerud, A. Roiger, C. Rolf, M.L. Santee, M. Scheibe, C. Schiller, H. Schlager, M. Siciliani de Cumis, N. Sitnikov, O.A. Svde, R. Spang, N. Spelten, F. Stordal, O. Suminska-Ebersoldt, A. Ulanovski, J. Ungermann, S. Viciani, C.M. Volk, M. vom Scheidt, P. von der Gathen, K. Walker, T. Wegner, R. Weigel, S. Weinbruch, G. Wetzel, F.G. Wienhold, I. Wohltmann, W. Woiwode, I.A.K. Young, V. Yushkov, B. Zobrist, and F. Stroh, Reconciliation of essential process parameters for an enhanced predictability of Arctic stratospheric ozone loss and its climate interactions (RECONCILE): Activities and results, *Atmos. Chem. Phys.*, *13* (18), 9233–9268, doi:10.5194/acp-13-9233-2013, 2013.

Wales, P.A., R.J. Salawitch, J.M. Nicely, D.C. Anderson, T.P. Canty, S. Baidar, B. Dix, T.K. Koenig, R. Volkamer, D. Chen, L.G. Huey, D.J. Tanner, C.A. Cuevas, R.P. Fernandez, D.E. Kinnison, J.-F. Lamarque, A. Saiz-Lopez, E.L. Atlas, S.R. Hall, M.A. Navarro, L.L. Pan, S.M. Schauffler, M. Stell, S. Tilmes, K. Ullmann, A.J. Weinheimer, H. Akiyoshi, M.P. Chipperfield, M. Deushi, S.S. Dhomse, W. Feng, P. Graf, R. Hossaini, P. Jöckel, E. Mancini, M. Michou, O. Morgenstern, L.D. Oman, G. Pitari, D.A. Plummer, L.E. Revell, E. Rozanov, D. Saint-Martin, R. Schofield, A. Stenke, K.A. Stone, D. Visioni, Y. Yamashita, and G. Zeng, Stratospheric injection of brominated very short-lived

substances: Aircraft observations in the Western Pacific and representation in global models, *J. Geophys. Res.*, *123*, doi:10.1029/2017JD027978, 2018.

Weber, M., S. Dikty, J.P. Burrows, H. Garny, M. Dameris, A. Kubin, J. Abalichin, and U. Langematz, The Brewer-Dobson circulation and total ozone from seasonal to decadal time scales, *Atmos. Chem. Phys.*, *11*, 11,221–11,235, doi:10.5194/acp-11-11221-2011, 2011.

Weber, M., W. Steinbrecht, C. Roth, M. Coldewey-Egbers, R.J. van der A, D. Degenstein, V.E. Fioletov, S.M. Frith, L. Froidevaux, C.S. Long, D. Loyola, and J.D. Wild, Stratospheric Ozone, [in "State of the Climate in 2014"], *Bull. Amer. Meteorol. Soc.*, *96* (7), S44–S46, doi:10.1175/2015BAMSStateoftheClimate.1, 2015.

Weber, M., W. Steinbrecht, C. Roth, M. Coldewey-Egbers, D. Degenstein, Y.E. Fioletov, S.M. Frith, L. Froidevaux, J. de Laat, C.S. Long, D. Loyola, and J.D. Wild, Stratospheric Ozone, [in "State of the Climate in 2015"], *Bull. Amer. Meteorol. Soc.*, *97* (8), S49–S51, doi:10.1175/2016BAMSStateoftheClimate.1, 2016.

Weber M., W. Steinbrecht, S.M. Frith, O. Tweedy, M. Coldewey-Egbers, S. Davis, D. Degenstein, Y.E. Fioletov, L. Froidevaux, J. de Laat, C.S. Long, D. Loyola, C. Roth, and J.D. Wild, Stratospheric Ozone, [in "State of the Climate in 2016"], *Bull. Amer. Meteorol. Soc.*, *98* (8), S49–S51, doi:10.1175/2017BAMSStateoftheClimate.1, 2017.

Weber, M., M. Coldewey-Egbers, V.E. Fioletov, S. Frith, J.D. Wild, J.P. Burrows, C.S. Long, and D. Loyola, Total ozone trends from 1979 to 2016 derived from five merged observational datasets – the emergence into ozone recovery, *Atmos. Chem. Phys.*, *18*, 2097–2117, doi:10.5194/acp-18-2097-2018, 2018.

Wegner, T., M.C. Pitts, L.R. Poole, I. Tritscher, J.-U. Grooß, and H. Nakajima, Vortex-wide chlorine activation by a mesoscale PSC event in the Arctic winter of 2009/10, *Atmos. Chem. Phys.*, *16* (7), 4569–4577, doi:10.5194/acp-16-4569-2016, 2016.

Weigel, R., C.M. Volk, K. Kandler, E. Hösen, G. Günther, B. Vogel, J.-U. Grooß, S. Khaykin, G.V. Belyaev, and S. Borrmann, Enhancements of the refractory submicron aerosol fraction in the Arctic polar vortex: Feature or exception?, *Atmos. Chem. Phys.*, *14*, 12,319–12,342, doi:10.5194/acp-14-12319-2014, 2014.

Wetzel, G., H. Oelhaf, M. Birk, A. de Lange, A. Engel, F. Friedl-Vallon, O. Kirner, A. Kleinert, G. Maucher, H. Nordmeyer, J. Orphal, R. Ruhnke, B.-M. Sinnhuber, and P. Vogt, Partitioning and budget of inorganic and organic chlorine species observed by MIPAS-B and TELIS in the Arctic in March 2011, *Atmos. Chem. Phys.*, *15* (14), 8065–8076, doi:10.5194/acp-15-8065-2015, 2015.

WMO (World Meteorological Organization), *Scientific Assessment of Ozone Depletion: 2006*, Global Ozone Research and Monitoring Project–Report No. 50, 572 pp., Geneva, Switzerland, 2007.

WMO (World Meteorological Organization), *Scientific Assessment of Ozone Depletion: 2010*, Global Ozone Research and Monitoring Project–Report No. 52, 516 pp., Geneva, Switzerland, 2011.

WMO (World Meteorological Organization), *Scientific Assessment of Ozone Depletion: 2014,* Global Ozone Research and Monitoring Project Report–No. 55, 416 pp., Geneva, Switzerland, 2014

Wohltmann, I., T. Wegner, R. Müller, R. Lehmann, M. Rex, G.L. Manney, M.L. Santee, P. Bernath, O. Sumińska-Ebersoldt, F. Stroh, M. von Hobe, C.M. Volk, E. Hösen, F. Ravegnani, A. Ulanovsky, and V. Yushkov, Uncertainties in modelling heterogeneous chemistry and Arctic ozone depletion in the winter 2009/2010, *Atmos. Chem. Phys., 13*, 3909–3929, doi:10.5194/acp-13-3909-2013, 2013.

Wohltmann, I., R. Lehmann, and M. Rex, A quantitative analysis of the reactions involved in stratospheric ozone depletion in the polar vortex core, *Atmos. Chem. Phys.*, *17*, 10,535–10,563, doi:10.5194/acp-17-10535-2017, 2017.

Woiwode, W., M. Höpfner, L. Bi, M.C. Pitts, L.R. Poole, H. Oelhaf, S. Molleker, S. Borrmann, M. Klingebiel, G. Belyaev, A. Ebersoldt, S. Griessbach, J.-U. Grooß, T. Gulde, M. Krämer, G. Maucher, C. Piesch, C. Rolf, C. Sartorius, R. Spang, and J. Orphal, Spectroscopic evidence of large aspherical β-NAT particles involved in denitrification in the December 2011 Arctic stratosphere, *Atmos. Chem. Phys.*, *16* (14), 9505–9532, doi:10.5194/acp-16-9505-2016, 2016.

Yang, E.-S., D.M. Cunnold, M.J. Newchurch, R.J. Salawitch, M.P. McCormick, J.M. Russell III, J.M. Zawodny, and S.J. Oltmans, First stage of Antarctic ozone recovery, *J. Geophys. Res.*, *113*, D20308, doi:10.1029/2007JD009675, 2008.

Yang, X., N.L. Abraham, A.T. Archibald, P. Braesicke, J. Keeble, P.J. Telford, N.J. Warwick, and J.A. Pyle, How sensitive is the recovery of stratospheric ozone to changes in concentrations of very shortlived bromocarbons?, *Atmos. Chem. Phys.*, *14* (19), 10,431–10,438, doi:10.5194/acp-14-10431-2014, 2014.

Ziska, F., B. Quack, I. Stemmler, S. Tegtmeier, and K. Krüger, Future emissions of marine halogenated very short-lived substances under climate change, *J. Atmos. Chem.*, *74*, 245, doi:10.1007/s10874-016-9355-3, 2017.

Zhu, Y., O.B. Toon, A. Lambert, D.E. Kinnison, C. Bardeen, and M.C. Pitts, Development of a polar stratospheric cloud model within the Community Earth System Model: Assessment of 2010 Antarctic winter, *J. Geophys. Res.*, *122*, 10,418–10,438. doi:10.1002/2017JD027003, 2017a.

Zhu, Y., O.B. Toon, M.C. Pitts, A. Lambert, C. Bardeen, and D.E. Kinnison, Comparing simulated PSC optical properties with CALIPSO observations during the 2010 Antarctic winter, *J. Geophys. Res. Atmos.*, *122*, 1175–1202, doi:10.1002/2016JD025191, 2017b.

Zubiaurre, I., and N. Calvo, The ENSO Modoki signal in the stratosphere, *J. Geophys. Res. Atmos.*, *117,* D06109, doi:10.1029/2011JD016690, 2012